Stochastic resonance

Luca Gammaitoni

Dipartimento di Fisica, Università di Perugia, and Istituto Nazionale di Fisica Nucleare, Sezione di Perugia, VIRGO-Project, I-06100 Perugia, Italy

Peter Hänggi

Institut für Physik, Universität Augsburg, Lehrstuhl für Theoretische Physik I, D-86135 Augsburg, Germany

Peter Jung

Department of Physics and Astronomy, Ohio University, Athens, Ohio 45701

Fabio Marchesoni

Department of Physics, University of Illinois, Urbana, Illinois 61801 and Istituto Nazionale di Fisica della Materia, Università di Camerino, I-62032 Camerino, Italy

Over the last two decades, stochastic resonance has continuously attracted considerable attention. The term is given to a phenomenon that is manifest in nonlinear systems whereby generally feeble input information (such as a weak signal) can be be amplified and optimized by the assistance of noise. The effect requires three basic ingredients: (i) an energetic activation barrier or, more generally, a form of threshold; (ii) a weak coherent input (such as a periodic signal); (iii) a source of noise that is inherent in the system, or that adds to the coherent input. Given these features, the response of the system undergoes resonance-like behavior as a function of the noise level; hence the name stochastic resonance. The underlying mechanism is fairly simple and robust. As a consequence, stochastic resonance has been observed in a large variety of systems, including bistable ring lasers, semiconductor devices, chemical reactions, and mechanoreceptor cells in the tail fan of a crayfish. In this paper, the authors report, interpret, and extend much of the current understanding of the theory and physics of stochastic resonance. They introduce the readers to the basic features of stochastic resonance and its recent history. Definitions of the characteristic quantities that are important to quantify stochastic resonance, together with the most important tools necessary to actually compute those quantities, are presented. The essence of classical stochastic resonance theory is presented, and important applications of stochastic resonance in nonlinear optics, solid state devices, and neurophysiology are described and put into context with stochastic resonance theory. More elaborate and recent developments of stochastic resonance theory are discussed, ranging from fundamental quantum properties—being important at low temperatures—over spatiotemporal aspects in spatially distributed systems, to realizations in chaotic maps. In conclusion the authors summarize the achievements and attempt to indicate the most promising areas for future research in theory and experiment. [S0034-6861(98)00101-9]

CONTENTS

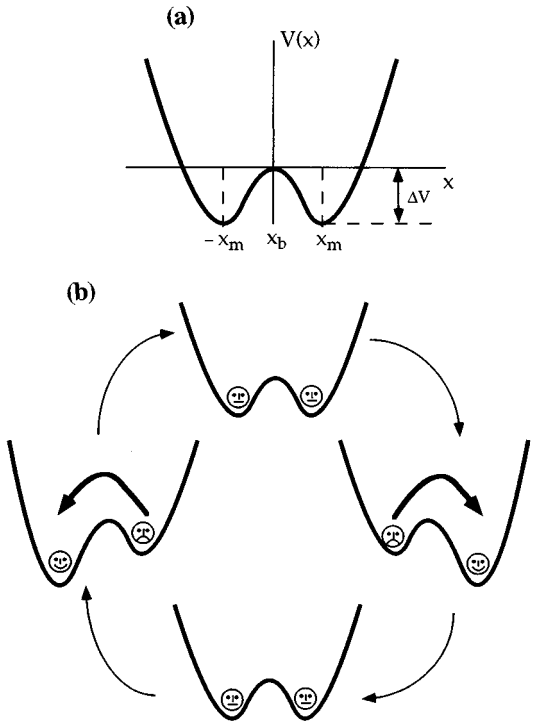

FIG. 1. Stochastic resonance in a symmetric double well. (a) Sketch of the double-well potential $V(x)=(1/4)bx^4-(1/2)ax^2$. The minima are located at $\pm x_m$, where $x_m=(a/b)^{1/2}$. These are separated by a potential barrier with the height given by $\Delta V=a^2/(4b)$. The barrier top is located at $x_b=0$. In the presence of periodic driving, the double-well potential $V(x,t)=V(x)-A_0x\cos(\Omega t)$ is tilted back and forth, thereby raising and lowering successively the potential barriers of the right and the left well, respectively, in an antisymmetric manner. This cyclic variation is shown in our cartoon (b). A suitable dose of noise (i.e., when the period of the driving approximately equals twice the noise-induced escape time) will make the "sad face" happy by allowing synchronized hopping to the globally stable state (strictly speaking, this holds true only in the statistical average).

I. INTRODUCTION

Users of modern communication devices are annoyed by any source of background hiss. Under certain circumstances, however, an extra dose of noise can in fact help rather than hinder the performance of some devices. There is now even a name for the phenomenon: *stochastic resonance*. It is presently creating a buzz in fields such as physics, chemistry, biomedical sciences, and engineering.

The mechanism of stochastic resonance is simple to explain. Consider a heavily damped particle of mass m and viscous friction γ, moving in a symmetric double-well potential $V(x)$ [see Fig. 1(a)]. The particle is subject to fluctuational forces that are, for example, induced by coupling to a heat bath. Such a model is archetypal for investigations in reaction-rate theory (Hänggi, Talkner, and Borkovec, 1990). The fluctuational forces cause transitions between the neighboring potential wells with a rate given by the famous Kramers rate (Kramers, 1940), i.e.,

$$r_K=\frac{\omega_0\omega_b}{2\pi\gamma}\exp\left(-\frac{\Delta V}{D}\right). \tag{1.1}$$

with $\omega_0^2=V''(x_m)/m$ being the squared angular frequency of the potential in the potential minima at $\pm x_m$, and $\omega_b^2=|V''(x_b)/m|$ the squared angular frequency at the top of the barrier, located at x_b; ΔV is the height of the potential barrier separating the two minima. The noise strength $D=k_BT$ is related to the temperature T.

If we apply a weak periodic forcing to the particle, the double-well potential is tilted asymmetrically up and down, periodically raising and lowering the potential barrier, as shown in Fig. 1(b). Although the periodic forcing is too weak to let the particle roll periodically from one potential well into the other one, noise-induced hopping between the potential wells can become synchronized with the weak periodic forcing. This statistical synchronization takes place when the average waiting time $T_K(D)=1/r_K$ between two noise-induced interwell transitions is comparable with *half* the period T_Ω of the periodic forcing. This yields the *time-scale matching condition* for stochastic resonance, i.e.,

$$2T_K(D)=T_\Omega\,. \tag{1.2}$$

In short, stochastic resonance in a symmetric double-well potential manifests itself by a synchronization of activated hopping events between the potential minima

with the weak periodic forcing (Gammaitoni, Marchesoni, *et al.*, 1989). For a given period of the forcing T_Ω, the time-scale matching condition can be fulfilled by tuning the noise level $D_{\max}$ to the value determined by Eq. (1.2).

The concept of stochastic resonance was originally put forward in the seminal papers by Benzi and collaborators (Benzi *et al.*, 1981, 1982, 1983) wherein they address the problem of the periodically recurrent ice ages. This very suggestion that stochastic resonance might rule the periodicity of the primary cycle of recurrent ice ages was raised independently by C. Nicolis and G. Nicolis (Nicolis, 1981, 1982, 1993; Nicolis and Nicolis, 1981). A statistical analysis of continental ice volume variations over the last 10^6 yr shows that the glaciation sequence has an average periodicity of about 10^5 yr. This conclusion is intriguing because the only comparable astronomical time scale in earth dynamics known so far is the modulation period of its orbital eccentricity caused by planetary gravitational perturbations. The ensuing variations of the solar energy influx (or solar constant) on the earth surface are exceedingly small, about 0.1%. The question climatologists (still) debate is whether a geodynamical model can be devised, capable of enhancing the climate sensitivity to such a small external periodic forcing. Stochastic resonance provides a simple, although not conclusive answer to this question (Matteucci, 1989, 1991; Winograd *et al.*, 1992; Imbrie *et al.*, 1993). In the model of Benzi *et al.* (1981, 1982, 1983), the global climate is represented by a double-well potential, where one minimum represents a small temperature corresponding to a largely ice-covered earth. The small modulation of the earth's orbital eccentricity is represented by a weak periodic forcing. Short-term climate fluctuations, such as the annual fluctuations in solar radiation, are modeled by Gaussian white noise. If the noise is tuned according to Eq. (1.2), synchronized hopping between the cold and warm climate could significantly enhance the response of the earth's climate to the weak perturbations caused by the earth's orbital eccentricity, according to arguments by Benzi *et al.* (1981, 1982).

A first experimental verification of the stochastic resonance phenomenon was obtained by Fauve and Heslot (1983), who studied the noise dependence of the spectral line of an ac-driven Schmitt trigger. The field then remained somewhat dormant until the modern age of stochastic resonance was ushered in by a key experiment in a bistable ring laser (McNamara, Wiesenfeld, and Roy, 1988). Soon after, prominent dynamical theories in the adiabatic limit (Gammaitoni, Marchesoni, Menichella-Saetta, and Santucci, 1989; McNamara and Wiesenfeld, 1989; Presilla, Marchesoni, and Gammaitoni, 1989; Hu *et al.*, 1990) and in the full nonadiabatic regime (Jung and Hänggi, 1989, 1990, 1991a) have been proposed. Moreover, descriptions in terms of the linear-response approximation have frequently been introduced to characterize stochastic resonance (Dykman *et al.*, 1990a, 1990b; Gammaitoni *et al.*, 1990; Dykman, Haken, *et al.*, 1993; Jung and Hänggi, 1991a; Hu, Haken, and Ning, 1992).

Over time, the notion of stochastic resonance has been widened to include a number of different mechanisms. The unifying feature of all these systems is the increased sensitivity to small perturbations at an optimal noise level. Under this widened notion of stochastic resonance, the first non-bistable systems discussed were excitable systems (Longtin, 1993). In contrast to bistable systems, excitable systems have only one stable state (the rest state), but possess a threshold to an excited state which is not stable and decays after a relatively long time (in comparison to the relaxation rate of small perturbations around the stable state) to the rest state. Soon afterwards, threshold detectors (see Sec. V.C, which presents cartoon versions of excitable systems) were discovered as a class of simple systems exhibiting stochastic resonance (Jung, 1994; Wiesenfeld *et al.* 1994; Gingl, Kiss, and Moss, 1995; Gammaitoni, 1995a; Jung, 1995). In the same spirit, stochastic-resonance-like features in purely autonomous systems have been reported (Hu, Ditzinger, *et al.*, 1993; Rappel and Strogatz, 1994).

The framework developed for excitable and threshold dynamical systems has paved the way for stochastic resonance applications in neurophysiology: stochastic resonance has been demonstrated in mechanoreceptor neurons located in the tail fan of crayfish (Douglass *et al.*, 1993) and in hair cells of crickets (Levin and Miller, 1996).

In the course of an ever-increasing flourishing of stochastic resonance, new applications with novel types of stochastic resonance have been discovered, and there seems to be no end in sight. Most recently, the notion of stochastic resonance has been extended into the domain of microscopic and mesoscopic physics by addressing the quantum analog of stochastic resonance (Löfstedt and Coppersmith, 1994a, 1994b; Grifoni and Hänggi, 1996a, 1996b) and also into the world of spatially extended, pattern-forming systems (spatiotemporal stochastic resonance) (Jung and Mayer-Kress, 1995; Löcher *et al.*, 1996; Marchesoni *et al.*, 1996; Wio, 1996; Castelpoggi and Wio, 1997; Vilar and Rubí, 1997). Other important extensions of stochastic resonance include stochastic resonance phenomena in coupled systems, reviewed in Sec. VII.B, and stochastic resonance in deterministic systems exhibiting chaos (see Sec. VI.C).

Stochastic resonance is by now a well-established phenomenon. In the following sections, the authors have attempted to present a comprehensive review of the present status of stochastic resonance theory, applications, and experimental evidences. After having introduced the reader into different quantitative measures of stochastic resonance, we outline the theoretical tools. A series of topical applications that are rooted in the physical and biomedical sciences are reviewed in some detail.

The authors trust that with the given selection of topics and theoretical techniques a reader will enjoy the tour through the multifaceted scope that underpins the physics of stochastic resonance. Moreover, this comprehensive review will put the reader at the very forefront of present and future stochastic resonance studies. The reader may also profit by consulting other, generally

more confined reviews and historical surveys, which in several aspects complement our work and/or provide additional insights into topics covered herein. In this context we refer the reader to the accounts given by Moss (1991, 1994), Jung (1993), Moss, Pierson, and O'Gorman (1994), Moss and Wiesenfeld (1995a, 1995b), Wiesenfeld and Moss (1995), Dykman, Luchinsky, *et al.* (1995), Bulsara and Gammaitoni (1996), as well as to the comprehensive proceedings of two recent conferences (Moss, Bulsara, and Shlesinger, 1993; Bulsara *et al.*, 1995).

II. CHARACTERIZATION OF STOCHASTIC RESONANCE

Having elucidated the main physical ideas of stochastic resonance in the preceding section, we next define the observables that actually quantify the effect. These observables should be physically motivated, easily measurable, and/or be of technical relevance. In the seminal paper by Benzi *et al.* (1981), stochastic resonance was quantified by the intensity of a peak in the power spectrum. Observables based on the power spectrum are indeed very convenient in theory and experiment, since they have immediate intuitive meaning and are readily measurable. In the neurophysiological applications of stochastic resonance another measure has become fashionable, namely the interval distributions between activated events such as those given by successive neuronal firing spikes or consecutive barrier crossings.

We follow here the historical development of stochastic resonance and first discuss important quantifiers of stochastic resonance based on the power spectrum. Along with the introduction of the quantifiers, we demonstrate their properties for two generic models of stochastic resonance; the periodically driven bistable two-state system and the double-well system. The detailed mathematical analysis of these models is the subject of Secs. III, IV, and the Appendix. Important results therein are used within this section to support a more intuitive approach. In a second part, we discuss quantifiers that are based on the interval distribution; these latter measures emphasize the synchronization aspect of stochastic resonance. We finish the section with a list of other, alternative methods and tools that have been used to study stochastic resonance. In addition, we present a list of experimental demonstrations.

A. A generic model

We consider the overdamped motion of a Brownian particle in a bistable potential in the presence of noise and periodic forcing

$$\dot{x}(t) = -V'(x) + A_0 \cos(\Omega t + \varphi) + \xi(t), \tag{2.1}$$

where $V(x)$ denotes the reflection-symmetric quartic potential

$$V(x) = -\frac{a}{2}x^2 + \frac{b}{4}x^4. \tag{2.2a}$$

By means of an appropriate scale transformation, cf. Sec. IV.A, the potential parameters a and b can be eliminated such that Eq. (2.2a) assumes the dimensionless form

$$V(x) = -\frac{1}{2}x^2 + \frac{1}{4}x^4. \tag{2.2b}$$

In Eq. (2.1) $\xi(t)$ denotes a zero-mean, Gaussian white noise with autocorrelation function

$$\langle \xi(t)\xi(0)\rangle = 2D\,\delta(t) \tag{2.3}$$

and intensity D. The potential $V(x)$ is bistable with minima located at $\pm x_m$, with $x_m = 1$. The height of the potential barrier between the minima is given by $\Delta V = \frac{1}{4}$ [see Fig. 1(a)].

In the absence of periodic forcing, $x(t)$ fluctuates around its local stable states with a statistical variance proportional to the noise intensity D. Noise-induced hopping between the local equilibrium states with the Kramers rate

$$r_K = \frac{1}{\sqrt{2}\pi}\exp\left(-\frac{\Delta V}{D}\right) \tag{2.4}$$

enforces the mean value $\langle x(t)\rangle$ to vanish.

In the presence of periodic forcing, the reflection symmetry of the system is broken and the mean value $\langle x(t)\rangle$ does not vanish. This can be intuitively understood as the consequence of the periodic biasing towards one or the other potential well.

Filtering all the information about $x(t)$, except for identifying in which potential well the particle resides at time t (known as two-state filtering), one can achieve a binary reduction of the two-state model (McNamara and Wiesenfeld, 1989). The starting point of the two-state model is the master equation for the probabilities $n_\pm$ of being in one of the two potential wells denoted by their equilibrium positions $\pm x_m$, i.e.,

$$\dot{n}_\pm(t) = -W_\mp(t)n_\pm + W_\pm(t)n_\mp, \tag{2.5}$$

with corresponding transition rates $W_\mp(t)$. The periodic bias toward one or the other state is reflected in a periodic dependence of the transition rates; see Eq. (3.3) below.

1. The periodic response

For convenience, we choose the phase of the periodic driving $\varphi = 0$, i.e., the input signal reads explicitly $A(t) = A_0 \cos(\Omega t)$. The mean value $\langle x(t)|x_0,t_0\rangle$ is obtained by averaging the inhomogeneous process $x(t)$ with initial conditions $x_0 = x(t_0)$ over the ensemble of the noise realizations. Asymptotically ($t_0 \to -\infty$), the memory of the initial conditions gets lost and $\langle x(t)|x_0,t_0\rangle$ becomes a periodic function of time, i.e., $\langle x(t)\rangle_{as} = \langle x(t+T_\Omega)\rangle_{as}$ with $T_\Omega = 2\pi/\Omega$. For small amplitudes, the response of the system to the periodic input signal can be written as

$$\langle x(t)\rangle_{as} = \bar{x}\cos(\Omega t - \bar{\phi}), \tag{2.6}$$

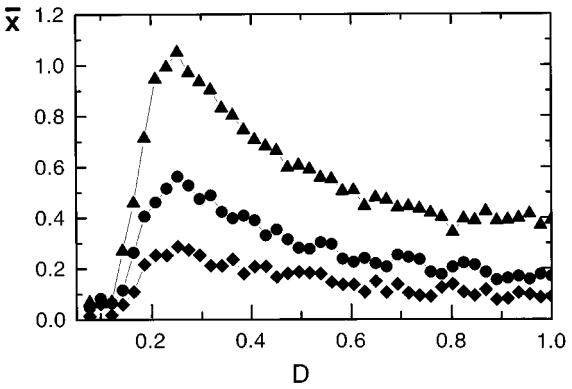

FIG. 2. Amplitude $\bar{x}(D)$ of the periodic component of the system response (2.6) vs the noise intensity D (in units of ΔV) for the following values of the input amplitude: $A_0 x_m/\Delta V=0.4$ (triangles), $A_0 x_m/\Delta V=0.2$ (circles), and $A_0 x_m/\Delta V=0.1$ (diamonds) in the quartic double-well potential (2.2a) with $a=10^4$ s^{-1}, $x_m=10$ (in units $[x]$ used in the experiment), and Ω=100 s^{-1}.

with amplitude $\bar{x}$ and a phase lag $\bar{\phi}$. Approximate expressions for the amplitude and phase shift read

$$\bar{x}(D)=\frac{A_0\langle x^2\rangle_0}{D}\frac{2r_K}{\sqrt{4r_K^2+\Omega^2}} \tag{2.7a}$$

and

$$\bar{\phi}(D)=\arctan\left(\frac{\Omega}{2r_K}\right), \tag{2.7b}$$

where $\langle x^2\rangle_0$ is the D-dependent variance of the stationary unperturbed system ($A_0=0$). Equation (2.7) has been shown to hold in leading order of the modulation amplitude $A_0 x_m/D$ for both discrete and continuous one-dimensional systems (Nicolis, 1982; McNamara and Wiesenfeld, 1989; Presilla, Marchesoni, and Gammaitoni, 1989; Hu, Nicolis, and Nicolis, 1990). While postponing a more accurate discussion of the validity of the above equations for $\bar{x}$ and $\bar{\phi}$ to Sec. IV.B, we notice here that Eq. (2.7a) allows within the two-state approximation, i.e., $\langle x^2\rangle_0=x_m^2$, a direct estimate for the noise intensity D_{SR} that maximizes the output $\bar{x}$ versus D for fixed driving strength and driving frequency.

The first and most important feature of the amplitude $\bar{x}$ is that it *depends* on the noise strength D, i.e., the *periodic* response of the system can be manipulated by changing the noise level. At a closer inspection of Eq. (2.7), we note that the amplitude $\bar{x}$ first increases with increasing noise level, reaches a maximum, and then decreases again. This is the celebrated *stochastic resonance* effect. In Fig. 2, we show the result of a simulation of the double-well system [Eqs. (2.1)–(2.3)] for several weak amplitudes of the periodic forcing A_0. Upon decreasing the driving frequency Ω, the position of the peak moves to smaller noise strength (see Fig. 6, below).

Next we attempt to assign a physical meaning to the value of D_{SR}. The answer was given originally by Benzi and co-workers (Benzi *et al.* 1981, 1982, 1983): an unperturbed bistable system with $A_0=0$ switches spontaneously between its stable states with rate r_K. The input signal modulates the symmetric bistable system, making successively one stable state less stable than the other over half a period of the forcing. Tuning the noise intensity so that the random-switching frequency r_K is made to agree closely with the forcing angular frequency Ω, the system attains the maximum probability for an escape out of the less stable state into the more stable one, before a random back switching event takes place. When the noise intensity D is too small ($D\ll D_{SR}$), the switching events become very rare; thus the periodic component(s) of the interwell dynamics are hardly visible. Under such circumstances, the periodic component of the output signal $x(t)$ is determined primarily by motion around the potential minima—the intrawell motion. A similar loss of synchronization happens in the opposite case when $D\gg D_{SR}$: The system driven by the random source flips too many times between its stable states within each half forcing period for the forced components of the interwell dynamics to be statistically relevant.

In this spirit, the time-scale matching condition in Eq. (1.2), which with $T_K=1/r_K$ is recast as $\Omega=\pi r_K$, provides a reasonable condition for the maximum of the response amplitude $\bar{x}$. Although the time-scale matching argument yields a value for D_{SR} that is reasonably close to the exact value it is important to note that it is *not exact* (Fox and Lu, 1993). Within the two-state model, the value D_{SR} obeys the transcendental equation

$$4r_K^2(D_{SR})=\Omega^2(\Delta V/D_{SR}-1), \tag{2.8}$$

obtained from Eq. (2.7a). The time-scale matching condition obviously does not fulfill Eq. (2.8); thus underpinning its approximate nature.

The phase lag $\bar{\phi}$ exhibits a transition from $\bar{\phi}=\pi/2$ at $D=0^+$ to $\bar{\phi}\propto\Omega$ in the vicinity of D_{SR}. By taking the second derivative of the function $\bar{\phi}$ in Eq. (2.7b) and comparing with Eq. (2.8) one easily checks that D_{SR} lies on the right-hand side of the point of inflection of $\bar{\phi}$, being $\bar{\phi}''(D_{SR})>0$.

It is important to note that the variation of the angular frequency Ω at a fixed value of the noise intensity D does not yield a resonance-like behavior of the response amplitude. This behavior is immediately evident from Eq. (2.7a) and also from numerical studies (for those who don't trust the theory). A more refined analysis (Thorwart and Jung, 1997) shows that the decomposition of the susceptibility into its real and imaginary parts restores a nonmonotonic frequency dependence—see also the work on dynamical hysteresis and stochastic resonance by Phillips and Schulten (1995), and Mahato and Shenoy (1994).

Finally, we introduce an alternative interpretation of the quantity $\bar{x}(D)$ due to Jung and Hänggi (1989, 1991a): the integrated power p_1 stored in the delta-like spikes of $S(\omega)$ at $\pm\Omega$ is $p_1=\pi\bar{x}^2(D)$. Analogously, the modulation signal carries a total power $p_A=\pi A_0^2$. Hence the spectral amplification reads

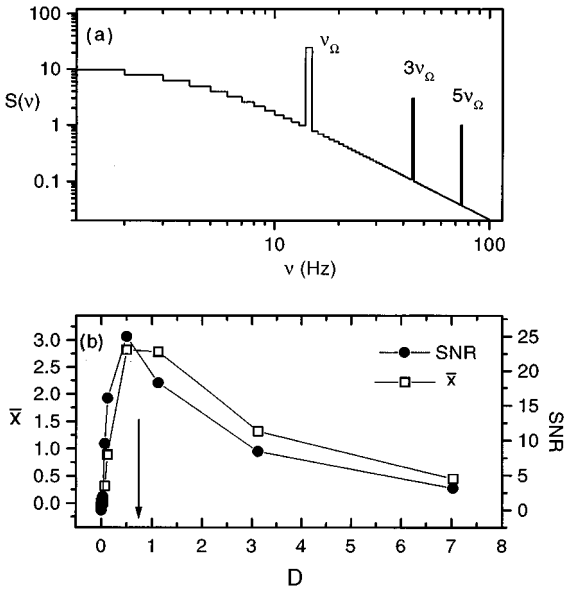

FIG. 3. Characterization of stochastic resonance. (a) A typical power spectral density $S(\nu)$ vs frequency ν for the case of the quartic double-well potential in Eq. (2.2a). The delta-like spikes at $(2n+1)\nu_\Omega$, $\Omega=2\pi\nu_\Omega$, with $n=0$, 1, and 2, are displayed as finite-size histogram bins. (b) Strength of the first delta spike, Eq. (2.12), and the signal-to-noise ratio SNR, Eq. (2.13), vs D (in units of ΔV). The arrow denotes the D value corresponding to the power spectral density plotted in (a). The other parameters are $Ax_m/\Delta V=0.1$, $a=10^4$ s^{-1}, and $x_m=10$ (in units $[x]$ used in the experiment).

$$\eta\equiv p_1/p_A=[\bar{x}(D)/A_0]^2. \tag{2.9}$$

In the linear-response regime of Eq. (2.7), η is independent of the input amplitude. This spectral amplification η will frequently be invoked in Sec. IV, instead of $\bar{x}(D)$.

2. Signal-to-noise ratio

Instead of taking the ensemble average of the system response, it sometimes can be more convenient to extract the relevant *phase-averaged* power spectral density $S(\omega)$, defined here as (see Secs. III and IV.A)

$$S(\omega)=\int_{-\infty}^{+\infty} e^{-i\omega\tau}\langle\langle x(t+\tau)x(t)\rangle\rangle d\tau, \tag{2.10}$$

where the inner brackets denote the ensemble average over the realizations of the noise and outer brackets indicate the average over the input initial phase φ. In Fig. 3(a) we display a typical example of $S(\nu)$ ($\omega=2\pi\nu$) for the bistable system. Qualitatively, $S(\omega)$ may be described as the superposition of a background power spectral density $S_N(\omega)$ and a structure of delta spikes centered at $\omega=(2n+1)\Omega$ with $n=0,\pm1,\pm2\ldots$. The generation of only *odd* higher harmonics of the input frequency are typical fingerprints of periodically driven symmetric nonlinear systems (Jung and Hänggi, 1989). Since the strength (i.e., the integrated power) of such spectral spikes decays with n according to a power law such as A_0^{2n}, we can restrict ourselves to the first spectral spike, being consistent with the linear-response assumption implicit in Eq. (2.6). For small forcing amplitudes, $S_N(\omega)$ does not deviate much from the power spectral density $S_N^0(\omega)$ of the unperturbed system. For a bistable system with relaxation rate $2r_K$, the hopping contribution to $S_N^0(\omega)$ reads

$$S_N^0(\omega)=4r_K\langle x^2\rangle_0/(4r_K^2+\omega^2). \tag{2.11}$$

The spectral spike at Ω was verified experimentally (Debnath, Zhou, and Moss, 1989; Gammaitoni, Marchesoni, *et al.*, 1989; Gammaitoni, Menichella-Saetta, Santucci, Marchesoni, and Presilla, 1989; Zhou and Moss, 1990) to be a delta function, thus signaling the presence of a periodic component with angular frequency Ω in the system response [Eq. (2.6)]. In fact, for $A_0x_m\ll\Delta V$ we are led to separate $x(t)$ into a noisy background (which coincides, apart from a normalization constant, with the unperturbed output signal) and a periodic component with $\langle x(t)\rangle_{as}$ given by Eq. (2.6) (Jung and Hänggi, 1989). On adding the power spectral density of either component, we easily obtain

$$S(\omega)=(\pi/2)\bar{x}(D)^2[\delta(\omega-\Omega)+\delta(\omega+\Omega)]+S_N(\omega), \tag{2.12}$$

with $S_N(\omega)=S_N^0(\omega)+\mathcal{O}(A_0^2)$ and $\bar{x}(D)$ given in Eq. (2.7a). In Fig. 3(b) the strength of the delta-like spike of $S(\omega)$ (more precisely $\bar{x}$) is plotted as a function of D.

Stochastic resonance can be envisioned as a particular problem of signal extraction from background noise. It is quite natural that a number of authors tried to characterize stochastic resonance within the formalism of data analysis, most notably by introducing the notion of signal-to-noise ratio (SNR) (McNamara *et al.*, 1988; Debnath *et al.*, 1989; Gammaitoni, Marchesoni, *et al.*, 1989; Vemuri and Roy, 1989; Zhou and Moss, 1990; Gong *et al.*, 1991, 1992). We adopt here the following definition of the signal-to-noise ratio

$$SNR=2\left[\lim_{\Delta\omega\to0}\int_{\Omega-\Delta\omega}^{\Omega+\Delta\omega}S(\omega)d\omega\right]\Big/S_N(\Omega). \tag{2.13}$$

Hence on combining Eqs. (2.11) and (2.12), the SN ratio for a symmetric bistable system reads in leading order

$$SNR=\pi(A_0x_m/D)^2r_K. \tag{2.14}$$

Note that the factor of 2 in the definition (2.13) was introduced for convenience, in view of the power spectral density symmetry $S(\omega)=S(-\omega)$. The SN ratio SNR for the power spectral density plotted in Fig. 3(a) versus frequency ν ($\omega=2\pi\nu$) is displayed in Fig. 3(b). The noise intensity $\bar{D}_{SR}$ at which SNR assumes its maximum *does not coincide* with the value D_{SR} that maximizes the response amplitude $\bar{x}$, or equivalently the strength of the delta spike in the power spectrum given by Eq. (2.12). As a matter of fact, if the prefactor of the Kramers rate is independent of D, we find that the SN ratio of Eq. (2.14) has a maximum at

$$\bar{D}_{SR}=\Delta V/2. \tag{2.15}$$

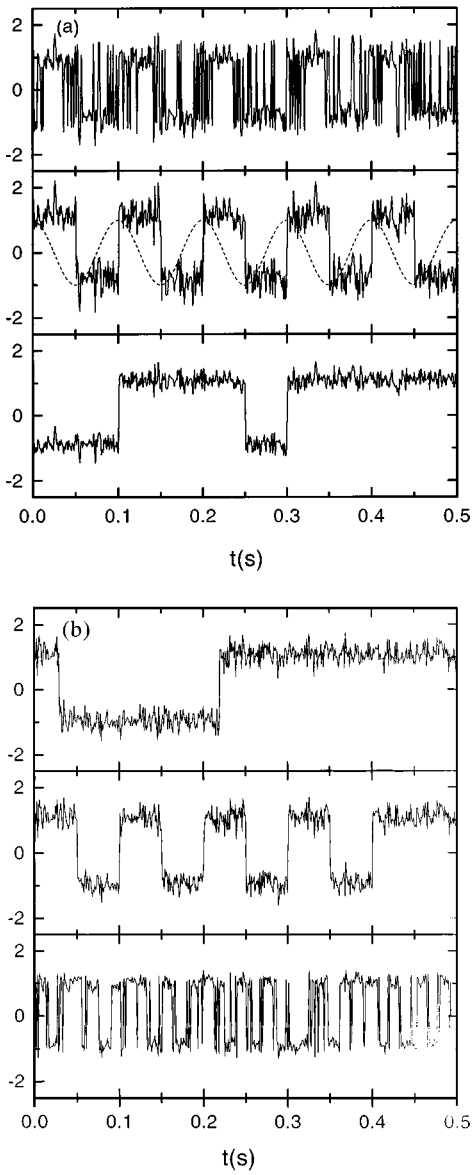

FIG. 4. Example of input/output synchronization in the symmetric bistable system of Eqs. (2.1)–(2.2a). (a) Varying the noise intensity D with Ω held constant. The sampled signal shown with dashes is the input $A(t)$ (arbitrary units). The remaining trajectories are the corresponding system output (in units of x_m) for increasing D values (from bottom to top). (b) Effect of varying Ω with D held constant. The three output samples $x(t)$ (in units of x_m) are displayed for increasing Ω values (from top to bottom). The parameters for (a) and (b) are $Ax_m/\Delta V=0.1$, $a=10^4$ s^{-1}, and $x_m=(a/b)^{1/2}=10$, cf. in Fig. 2.

B. Residence-time distribution

In Sec. II.A we interpreted the resonant-like dependence of the amplitude $\bar{x}(D)$ of the periodic response on the noise intensity D by means of a synchronization argument, originally formulated by Benzi and coworkers (Benzi *et al.*, 1981). Moreover, we pointed out that the response amplitude does not show this synchronization if the driving frequency Ω is tuned against the escape rate r_K. However, any experimentalist who ever tried to reproduce stochastic resonance in a real system (including here the analog circuits) knows by experience that a synchronization phenomenon takes place any time the condition $r_K \sim \Omega$ is established by varying either D or Ω. In Figs. 4(a) and 4(b) we depict the typical input-output synchronization effect in the bistable system Eqs. (2.1)–(2.3). In Fig. 4(a) the noise intensity is increased from low (rare random switching events) up to very large values, crossing the resonance values D_{SR} of Eqs. (2.8). In the latter case the output signal $x(t)$ becomes tightly locked to the periodic input. In Fig. 4(b), the noise intensity D is kept fixed and the forcing frequency Ω is increased. At low values of Ω, we notice an alternate asymmetry of the output signal towards either positive or negative values, depending on the sign of the input signal. However, many switches occur in both directions within any half forcing period. At large values of Ω, the effect of the time modulation is averaged out and the symmetry of the output signal seems to be fully restored. Finally, at $\Omega \sim r_K$ the synchronization mechanism is established with clear resemblance to Fig. 4(a). In the following subsection we characterize stochastic resonance as a "resonant" synchronization phenomenon, resulting from the combined action of noise and periodic forcing in a bistable system. The tool employed to this purpose is the residence-time distribution. Introduced as a tool (Gammaitoni, Marchesoni, *et al.*, 1989; Zhou and Moss, 1990; Zhou, *et al.*, 1990; Löfstedt and Coppersmith, 1994b; Gammaitoni, Marchesoni, and Santucci, 1995), such a notion proved useful for applications in diverse areas of natural sciences (Bulsara *et al.*, 1991; Longtin *et al.*, 1991; Simon and Libchaber, 1992; Carroll and Pecora, 1993b; Gammaitoni, Marchesoni, *et al.* 1993; Mahato and Shenoy, 1994; Mannella *et al.*, 1995; Shulgin *et al.*, 1995).

1. Level crossings

A deeper understanding of the mechanism of stochastic resonance in a bistable system can be gained by mapping the continuous stochastic process $x(t)$ (the system output signal) into a *stochastic point process* $\{t_i\}$. The symmetric signal $x(t)$ is converted into a point process by setting two crossing levels, for instance at $x_\pm=\pm c$ with $0 \leqslant c \leqslant x_m$. On sampling the signal $x(t)$ with an appropriate time base, the times t_i are determined as follows: data acquisition is triggered at time $t_0=0$ when $x(t)$ crosses, say, x_- with negative time derivative $[x(0)=-c,\ \dot{x}(0)<0]$; t_1 is the subsequent time when $x(t)$ first crosses x_+ with positive derivative $[x(t_1)=c,\ \dot{x}(t_1)>0]$; t_2 is the time when $x(t)$ switches back to negative values by recrossing x_- with negative derivative, and so on. The quantities $T(i)=t_i-t_{i-1}$ represent the residence times between two subsequent switching events. For simplicity and to make contact with the theory of Sec. IV.C, we set $c=x_m$. The statistical properties of the stochastic point process $\{t_i\}$ are the subject of intricate theorems of probability theory (Rice, 1944; Papoulis, 1965; Blake and Lindsey, 1973). In particular, no systematic way is known to find the distribution of

threshold crossing times. An exception is the symmetric bistable system: here, the *long* intervals T of consecutive crossings obey Poissonian statistics with an exponential distribution (Papoulis, 1965)

$$N(T)=(1/T_K)\exp(-T/T_K). \tag{2.16}$$

The distribution (2.16) is important for the forthcoming discussion, because it describes to a good approximation the first-passage time distribution between the potential minima in unmodulated bistable systems [see also Hänggi, Talkner, and Borkovec (1990), and references therein].

2. Input-output synchronization

In the absence of periodic forcing, the residence time distribution has the exponential form of Eq. (2.16). In the presence of the periodic forcing (Fig. 5), one observes a series of peaks, centered at odd multiples of the half driving period $T_\Omega=2\pi/\Omega$, i.e., at $T_n=(n-\frac{1}{2})T_\Omega$, with $n=1,2,\ldots$. The heights of these peaks decrease exponentially with their order n. These peaks are simply explained: the best time for the system to switch between the potential wells is when the relevant potential barrier assumes a minimum. This is the case when the potential $V(x,t)=V(x)-A_0x\cos(\Omega t+\varphi)$ is tilted most extremely to the right or the left (in whichever well the system is residing). If the system switches at this time into the other well it then takes *half a period* waiting time in the other well until the new relevant barrier assumes a minimum. Thus $T_\Omega/2$ is a preferred residence interval. If the system "misses" a "good opportunity" to jump, it has to wait another full period until the relevant potential barrier for a switch again assumes the minimum. The second peak in the residence-time distribution is therefore located at $3/2T_\Omega$. The location of the other peaks is evident. The peak heights decay exponentially because the probabilities of the system to jump over a minimal barrier are statistically independent. We now argue that the strength P_1 of the first peak at $T_\Omega/2$ (the area under the peak) is a measure of the synchronization between the periodic forcing and the switching between the wells: If the mean residence time of the system in one potential well is much larger than the period of the driving, the system is not likely to jump the first time the relevant potential barrier assumes its minimum. The escape-time distribution exhibits in such a case a large number of peaks where P_1 is small. If the mean residence-time of the system in one well is much shorter than the period of the driving, the system will not "wait" with switching until the relevant potential barrier assumes its maximum and the residence-time distribution has already decayed practically to zero before the time $T_\Omega/2$ is reached and the weight P_1 is again small. Optimal synchronization, i.e., a maximum of P_1, is reached when the mean residence time matches half the period of the driving frequency, i.e., our old time-scale matching condition Eq. (1.2). This resonance condition can be achieved by varying either Ω or D. This is demonstrated in Figs. 5(a) and 5(b). In the insets we have plotted the strength of the peak at $T_\Omega/2$ as a function of the noise strength D [Fig. 5(a)] and as a function of the driving frequency Ω [Fig. 5(b)]. In passing, we

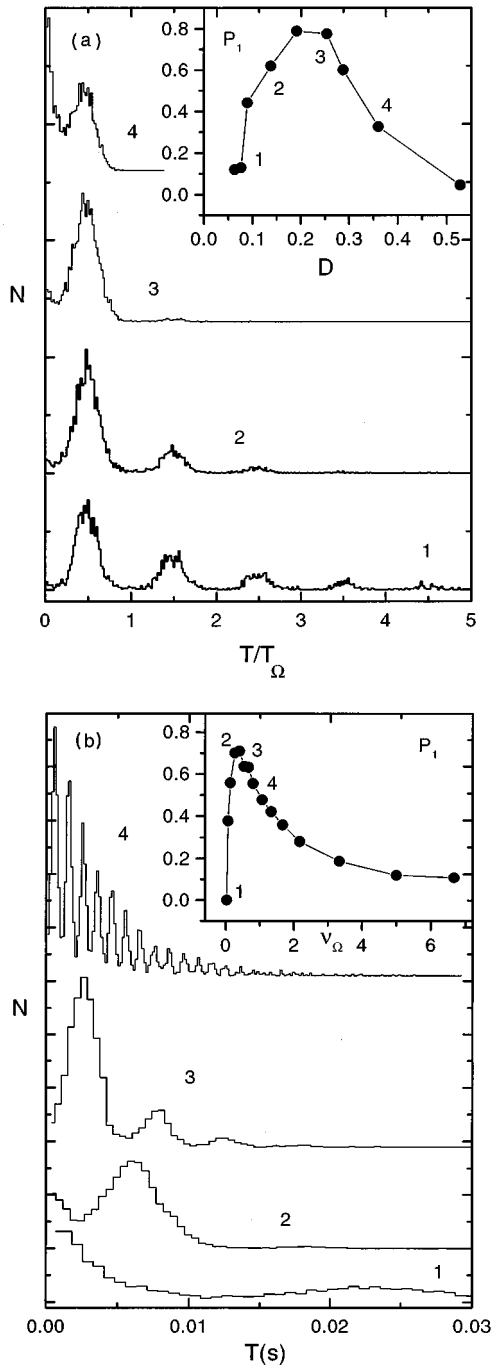

FIG. 5. Residence time distributions $N(T)$ for the symmetric bistable system of Eqs. (2.1)–(2.2a). (a) Increasing D (from below) with Ω held constant; inset: the strength P_1 of the first peak of $N(T)$ vs D (in units of ΔV). The definition of P_1 is as in Eq. (4.67) with $\alpha=1/4$. (b) Increasing Ω (from below) with D held constant; inset: P_1 versus ν_Ω. Here, Ω is in units of r_K. The numbers 1–4 in the insets correspond to the D values (a) and the Ω values (b) of the distributions on display. The parameters for (a) and (b) are $Ax_m/\Delta V=0.1$, $a=10^4$ s^{-1}, and $x_m=(a/b)^{1/2}=10$, cf. Fig. 2.

anticipate that also the remaining peaks of $N(T)$ at T_n with $n>1$ exhibit stochastic resonance [see Sec. IV.C].

We conclude with a comment on the multipeaked residence-time distributions: the existence of peaks in the residence-time distribution $N(T)$ at T_n with $n>1$ should not mislead the reader to think that the power spectral density $S(\omega)$ exhibits subharmonics of the fundamental frequency Ω (i.e., delta spikes at frequencies smaller than Ω). Although it may happen that the system waits for an odd number of half forcing periods (i.e., an integer number of extra "wait loops") before switching states, such occurrences are randomly spaced in time and, therefore, do not correspond to any definite spectral component (Papoulis, 1965).

C. Tools

The seminal paper by Benzi *et al.* (1981) provoked no immediate reaction in the literature. Apart from a few early theoretical studies by Nicolis (1982), Eckmann and Thomas (1982), and Benzi *et al.* (1982, 1983, 1985), only one experimental paper (Fauve and Heslot, 1983) addressed the phenomenon of stochastic resonance. One reason may be the technical difficulty of treating nonstationary Fokker-Planck equations with time-dependent coefficients (Jung, 1993). Moreover, extensive numerical computations were not yet everyday practice. The experimental article by McNamara, Wiesenfeld, and Roy (1988) marked a *renaissance* of stochastic resonance, which has flourished and developed ever since in different directions. Our present knowledge of this topic has been reached through a variety of investigation tools. In the following paragraphs, we outline the most popular ones, with particular attention given to their advantages and limitations.

1. Digital simulations

The first evidence of stochastic resonance was produced by simulating the Budyko-Sellers model of climate change (Benzi *et al.*, 1982) on a Digital Instruments mainframe computer (model PDP 1000), an advanced computer at the time! Nowadays accurate digital simulations of either continuous or discrete stochastic processes can be carried out at home on unsophisticated personal desktop computers. Regardless of the particular algorithm adopted in the diverse cases, digital simulations proved particularly useful in the study of stochastic resonance in numerous cases (Nicolis *et al.*, 1990; Dayan *et al.*, 1992; Mahato and Shenoy, 1994; Masoliver *et al.*, 1995) and in chaotic (Carroll and Pecora, 1993a, 1993b; Hu, Haken, and Ning, 1993; Ippen *et al.*, 1993; Anishchenko *et al.*, 1994) or spatially extended systems (Neiman and Schimansky-Geier, 1994, 1995; Jung and Mayer-Kress, 1995; Lindner *et al.*, 1995). A decisive contribution to the understanding of the stochastic resonance phenomenon was produced in Augsburg (Germany) by Jung and Hänggi (1989, 1990, 1991a, 1991b, 1993), who encoded the matrix-continued fraction algorithm (Risken, 1984; Risken and Vollmer, 1989). Convergence problems at low noise intensities and small driving frequencies, due to the truncation procedure, are the main limitations of this algorithm.

2. Analog simulations

This type of simulation allows more flexibility than digital simulation and for this reason has been preferred by a number of researchers. Rather than quoting all of them individually, we mention here the prominent groups, including those active in Perugia (Italy) (Gammaitoni, Marchesoni, *et al.*, 1989, 1993, 1994, 1995; Gammaitoni, Menichella-Saetta, *et al.*, 1989), in St. Louis (USA) (Debnath *et al.*, 1989; Zhou and Moss, 1990; Moss, 1991, 1994), in Lancaster (England) (Dykman, Mannella, *et al.*, 1990b, 1992) and in Beijing (China) (Hu *et al.*, 1991; Gong *et al.*, 1991, 1992). Analog simulators of stochastic processes are easy to design and assemble. Their results are not as accurate as digital simulations, but offer some advantages: (a) a large range of parameter space can be explored rather quickly; (b) high-dimensional systems may be simulated more readily than by computer, though systematic inaccuracies must be estimated and treated carefully. The block diagram of the Perugia simulator is illustrated in Sec. V.B.1 for the case of a damped quartic double-well oscillator subjected to both noisy and periodic driving. In passing, we mention here that Figs. 1–5 were actually obtained by means of that simulation circuit. In order to give the reader an idea of the reliability of analog simulation, we point out that all directly measured quantities are given with a maximum error of about 5%.

3. Experiments

By now, stochastic resonance has been repeatedly observed in a large variety of experiments. The first experiment was on an electronic circuit. Fauve and Heslot (1983) used a Schmitt trigger to demonstrate the effect. A first *in situ* physical experiment by McNamara, Wiesenfeld, and Roy (1988) used a bistable ring laser to demonstrate stochastic resonance in the noise-induced switching between the two counter-propagating laser modes. Stochastic resonance has also been demonstrated optically in a semiconductor feedback laser (Iannelli *et al.*, 1994), in a unidirectional photoreactive ring resonator (Jost and Sahleh, 1996), and in optical heterodyning (Dykman, Golubev, *et al.*, 1995). Relevance of stochastic resonance in electronic paramagnetic resonance has been identified by Gammaitoni, Martinelli, Pardi, and Santucci (1991, 1993). Simon and Libchaber (1992) observed SR in a beautifully designed optical trap, where a dielectric particle moves in the field of two overlapping Gaussian laser-beams that try to pull the particle into their center. Spano and collaborators (1992) have observed stochastic resonance in a paramagnetically driven bistable buckling ribbon. Magnetostochastic resonance in ferrite-garnet films has been measured by Grigorenko *et al.* (1994) and in yttrium-iron spheres by Reibold *et al.* (1997). I and Liu (1995) observed stochastic resonance in weakly ionized magnetoplasmas, and Claes and van den Broeck (1991) for dis-

persion of particles suspended in time-periodic flows. A first demonstration of stochastic resonance in a semiconductor device, more precisely in the low-temperature ionization breakdown in p-type germanium, has been reported by Kittel *et al.* (1993). Stochastic resonance has been observed in superconducting quantum interference devices (SQUID) by Hibbs *et al.* (1995) and Rouse *et al.* (1995). Furthermore, Rouse *et al.* provided the first experimental evidence of noise-induced resonances (see Sec. VII.D.1) in their SQUID system. In recent experiments by Mantegna and Spagnolo (1994, 1995, 1996), stochastic resonance was demonstrated in yet another semiconductor device, a tunnel diode. Stochastic resonance has also been observed in modulated bistable chemical reaction dynamics (Minimal-Bromate and Belousov-Zhabotinsky reactions) by Hohmann, Müller, and Schneider (1996).

Undoubtedly, the neurophysiological experiments on stochastic resonance constitute a cornerstone in the field. They have triggered the interest of scientists from biology and biomedical engineering to medicine. Longtin, Bulsara, and Moss (1991) have demonstrated the surprising similarity between interspike interval histograms of periodically stimulated sensory neurons and residence-time distributions of periodically driven bistable systems (see Secs. II.B and IV.C). Stochastic resonance in a living system was first demonstrated by Douglass *et al.* (1993) (see also in Moss *et al.*, 1994) in the mechanoreceptor cells located in the tail fan of crayfish. A similar experiment using the sensory hair cells of a cricket was performed by Levin and Miller (1996). A cricket can detect an approaching predator by the coherent motion of the air although the coherence is buried under a huge random background. Fairly convincing arguments had been given by Levin and Miller that stochastic resonance is actually responsible for this capability of the cricket. Since the functionality of neurons is based on gating ion channels in the cell membrane, Bezrukov and Vodyanoy (1995) have studied the impact of stochastic resonance on ion-channel gating. Stochastic resonance has been studied in visual perceptions [Riani and Simonotto, 1994, 1995; Simonotto *et al.* (1997); Chialvo and Apkarian (1993)] and in the synchronized response of neuronal assemblies to a global low-frequency field (Gluckman *et al.*, 1996).

III. TWO-STATE MODEL

In this section we discuss the simplest model that epitomizes the class of symmetric bistable systems introduced in Sec. II.A. Such a *discrete* model was proposed originally as a stochastic resonance study case by McNamara and Wiesenfeld (1989), who also pointed out that under certain restrictions it renders an accurate representation of most *continuous* bistable systems. For this reason, we discuss the two-state model in some detail. Most of the results reported below are of general validity and provide the reader with a preliminary analytical scheme on which to rely.

Let us consider a symmetric unperturbed system that switches between two discrete states $\pm x_m$ with rate W_0 out of either state. We define $n_\pm(t)$ to be the probabilities that the system occupies either state $\pm$ at time t, that is $x(t)=\pm x_m$. In the presence of a periodic input signal $A(t)=A_0\cos(\Omega t)$, which biases the state $\pm$ alternatively, the transition probability densities $W_\mp(t)$ out of the states $\pm x_m$ depend periodically on time. Hence the relevant master equation for $n_\pm(t)$ reads

$$\dot{n}_\pm(t)=-W_\mp(t)n_\pm+W_\pm(t)n_\mp \tag{3.1a}$$

or, making use of the normalization condition $n_++n_-=1$,

$$\dot{n}_\pm(t)=-[W_\pm(t)+W_\mp(t)]n_\pm+W_\pm(t). \tag{3.1b}$$

The solution of the rate equation (3.1) is given by

$$n_\pm(t)=g(t)\left[n_\pm(t_0)+\int_{t_0}^{t}W_\pm(\tau)g^{-1}(\tau)d\tau\right],$$

$$g(t)=\exp\left(-\int_{t_0}^{t}[W_+(\tau)+W_-(\tau)]d\tau\right), \tag{3.2}$$

with unspecified initial condition $n_\pm(t_0)$. For the transition probability densities $W_\mp(t)$, McNamara and Wiesenfeld (1989) proposed to use periodically modulated escape rates of the Arrhenius type

$$W_\mp(t)=r_K\exp\left[\mp\frac{A_0x_m}{D}\cos(\Omega t)\right]. \tag{3.3}$$

On assuming, as in Sec. II.A, that the modulation amplitude is small, i.e., $A_0x_m\ll D$, we can use the following expansions in the small parameter A_0x_m/D,

$$W_\mp(t)=r_K\left[1\mp\frac{A_0x_m}{D}\cos(\Omega t)+\frac{1}{2}\left(\frac{A_0x_m}{D}\right)^2\cos^2(\Omega t)\mp\ldots\right],$$

$$W_+(t)+W_-(t)=2r_K\left[1+\frac{1}{2}\left(\frac{A_0x_m}{D}\right)^2\cos^2(\Omega t)+\ldots\right]. \tag{3.4}$$

In Sec. IV.C, we discuss in more detail the validity of the expression (3.3) for the rates. The most important condition is a small driving frequency (adiabatic assumption). The integrals in Eq. (3.2) can be performed analytically to first order in A_0x_m/D,

$$n_+(t|x_0,t_0)=1-n_-(t|x_0,t_0)=\tfrac{1}{2}\{\exp[-2r_K(t-t_0)]\times[2\delta_{x_0,x_m}-1-\kappa(t_0)]+1+\kappa(t)\}, \tag{3.5}$$

where $\kappa(t)=2r_K(A_0x_m/D)\cos(\Omega t-\bar{\phi})/\sqrt{4r_K^2+\Omega^2}$, and $\bar{\phi}=\arctan[\Omega/(2r_K)]$. The quantity $n_+(t|x_0,t_0)$ in Eq. (3.5) should be read as the conditional probability that $x(t)$ is in the state + at time t, given that its initial state is $x_0\equiv x(t_0)$. Here the Kronecker delta δ_{x_0,x_m} is 1 when the system is initially in the state +.

From Eq. (3.5), any statistical quantity of the discrete process $x(t)$ can be computed to first order in A_0x_m/D, namely:

(a) The time-dependent response $\langle x(t)|x_0,t_0\rangle$ to the periodic forcing. From the definition $\langle x(t)|x_0,t_0\rangle=\int xP(x,t|x_0,t_0)dx$ with $P(x,t|x_0,t_0)\equiv n_+(t)\,\delta(x-x_m)+n_-(t)\,\delta(x+x_m)$, it follows immediately that in the asymptotic limit $t_0\to-\infty$,

$$\lim_{t_0\to-\infty}\langle x(t)|x_0,t_0\rangle\equiv\langle x(t)\rangle_{as}=\bar{x}(D)\cos[\Omega t-\bar{\phi}(D)], \tag{3.6}$$

with

$$\bar{x}(D)=\frac{A_0x_m^2}{D}\frac{2r_K}{\sqrt{4r_K^2+\Omega^2}} \tag{3.7a}$$

and

$$\bar{\phi}(D)=\arctan\left(\frac{\Omega}{2r_K}\right). \tag{3.7b}$$

Equation (3.7) coincides with Eq. (2.7) for $\langle x^2\rangle_0=x_m^2$.

(b) The autocorrelation function $\langle x(t+\tau)x(t)|x_0,t_0\rangle$. The general definition

$$\langle x(t+\tau)x(t)|x_0,t_0\rangle=\int\int xyP(x,t+\tau|y,t)\times P(y,t|x_0,t_0)dxdy \tag{3.8}$$

greatly simplifies in the stationary limit $t_0\to-\infty$,

$$\lim_{t_0\to-\infty}\langle x(t+\tau)x(t)|x_0,t_0\rangle\equiv\langle x(t+\tau)x(t)\rangle_{as}=x_m^2\exp(-2r_K|\tau|)[1-\kappa(t)^2]+x_m^2\kappa(t+\tau)\kappa(t). \tag{3.9}$$

In Eq. (3.9) we can easily separate an exponentially decaying branch due to randomness and a periodically oscillating tail driven by the periodic input signal. Note that even in the stationary limit $t_0\to-\infty$, the output-signal autocorrelation function depends on both times $t+\tau$ and t. However, in real experiments t represents the time set for the trigger in the data acquisition procedure. Typically, the averages implied by the definition of the autocorrelation function are taken over many sampling records of the signal $x(t)$, triggered at a large number of times t within one period of the forcing T_Ω. Hence, the corresponding phases of the input signal, $\theta=\Omega t+\varphi$, are uniformly distributed between 0 and 2π. This corresponds to averaging $\langle x(t+\tau)x(t)\rangle_{as}$ with respect to t uniformly over an entire forcing period, whence

$$\langle\langle x(t+\tau)x(t)\rangle\rangle=x_m^2\exp(-2r_K|\tau|)\left[1-\frac{1}{2}\left(\frac{A_0x_m}{D}\right)^2\frac{4r_K^2}{4r_K^2+\Omega^2}\right]+\frac{x_m^2}{2}\left(\frac{A_0x_m}{D}\right)^2\frac{4r_K^2}{4r_K^2+\Omega^2}\cos(\Omega\tau), \tag{3.10}$$

where the outer brackets $\langle\ldots\rangle$ stay for $(1/T_\Omega)\int_0^{T_\Omega}[\ldots]dt$.

(c) The power spectral density $S(\omega)$. The power spectral density commonly reported in the literature is the Fourier transform of Eq. (3.10) [see Eq. (2.10)]

$$S(\omega)=\left[1-\frac{1}{2}\left(\frac{A_0x_m}{D}\right)^2\frac{4r_K^2}{4r_K^2+\Omega^2}\right]\frac{4r_Kx_m^2}{4r_K^2+\omega^2}+\frac{\pi}{2}\left(\frac{A_0x_m}{D}\right)^2\frac{4r_K^2x_m^2}{4r_K^2+\Omega^2}[\delta(\omega-\Omega)+\delta(\omega+\Omega)], \tag{3.11}$$

which has the same form as the expression for $S(\omega)$ derived in Eq. (2.12). As a matter of fact, $S_N(\omega)$ is the product of the Lorentzian curve obtained with no input signal $A_0=0$ and a factor that depends on the forcing amplitude A_0, but is smaller than unity. The total output power, signal plus noise, for the two-state model discussed here, is $2\pi x_m^2$, independent of the input-signal amplitude A_0 and frequency Ω. Hence the effect of the input signal is to transfer power from the broadband noise background into the delta spike(s) of the power spectral density. Finally, the SN ratio follows as

$$SNR=\pi\left(\frac{A_0x_m}{D}\right)^2r_K+\mathcal{O}(A_0^4). \tag{3.12}$$

To leading order in A_0x_m/D, Eq. (3.12) coincides with Eq. (2.14).

The residence-time distribution $N(T)$ for the two-state model was calculated by Zhou, Moss, and Jung (1990), and by Löfstedt and Coppersmith (1994a, 1994b) within a two-state model, yielding in leading order of A_0x_m/D [cf. Sec. IV.D],

$$N(T)=\mathcal{N}_0[1-(1/2)(A_0x_m/D)^2\cos(\Omega T)]r_K\times\exp(-r_KT), \tag{3.13}$$

with $\mathcal{N}_0^{-1}=1-(1/2)(A_0x_m/D)^2/[1+(\Omega/r_K)^2]$. Note that $N(T)$ exhibits the peak structure of Fig. 5, with $T_n=(n-1/2)T_\Omega$. Furthermore, the strength P_1 of the first peak can be easily calculated by integrating $N(T)$ over an interval $[(\frac{1}{2}-\alpha),(\frac{1}{2}+\alpha)]T_\Omega$, with $0<\alpha\leqslant1/4$. Skipping the details of the integration, one realizes that P_1 is a function of the ratio Ω/r_K and attains its maximum for $r_K\simeq2\nu_\Omega$ as illustrated in the inset of Fig. 5(b).

In this section we detailed the symmetric two-state model as an archetypal system that features stochastic resonance. We profited greatly from the analytical study of McNamara and Wiesenfeld (1989). The two-state model can be regarded as an *adiabatic approximation* to any continuous bistable system, like the overdamped quartic double-well oscillator of Eqs. (2.1)–(2.3), provided that the input-signal frequency is low enough for the notion of transition rates [Eq. (3.4)] to apply.

In general, the difficulty lies in the derivation of time-dependent transition rates in a continuous model. A systematic method consists of finding the unstable periodic orbits in the absence of noise, since they act as basin boundaries in an extended phase-space description (Jung and Hänggi, 1991b). Rates in periodically driven systems can be defined as the transition rates across

those basin boundaries and correspond to the lowest-lying Floquet eigenvalue of the time-periodic Fokker-Planck operator (Jung, 1989, 1993)—see also the Sec. VII.D.3. Depending on the degree of approximation needed, the intrawell dynamics may become significant and more sophisticated formalisms may be required.

IV. CONTINUOUS BISTABLE SYSTEMS

A two-state description of stochastic resonance is of limited use for a number of reasons. First, the dynamics is reduced to the switching mechanism between two metastable states only. Thus it neglects the short-time dynamics that takes place within the immediate neighborhood of the metastable states themselves. Moreover, our goal is to describe both the linear as well as the nonlinear stochastic resonance response in the whole regime of modulation frequencies, extending from exponentially small Kramers rates up to intrawell frequencies, and higher. Put differently, a more elaborate approach has to model the nonadiabatic regime of driving in the whole accessible state space of the dynamical process $x(t)$. This goal will be presented within the class of continuous-state random systems (Stratonovitch, 1963; Hänggi and Thomas, 1982; Risken, 1984; van Kampen, 1992), which can be modeled in terms of a Fokker-Planck equation.

A. Fokker-Planck description

As a generic system modeling stochastic resonance we shall consider a Brownian particle of mass m that moves in a bistable potential $V(x)$ and is subjected to thermal noise $\xi(t)$ of the Nyquist type at temperature T. Moreover, we perturb the particle with a periodically varying force, i.e., we start from the Langevin equation

$$m\ddot{x} = -m\gamma\dot{x} - V'(x) + mA_0\cos(\Omega t+\varphi) + \sqrt{2m\gamma kT}\,\xi(t). \tag{4.1}$$

Here $\xi(t)$ denotes a Gaussian white noise with zero average and autocorrelation function $\langle \xi(t)\xi(s)\rangle = \delta(t-s)$. The external forcing term is characterized by an amplitude A_0, an angular frequency Ω, and an arbitrary but fixed initial phase φ. The statistically equivalent description for the corresponding probability density $p(x,v=\dot{x},t;\varphi)$ is governed by the two-dimensional Fokker-Planck equation

$$\frac{\partial}{\partial t}p(x,v,t;\varphi) = \left\{ -\frac{\partial}{\partial x}v + \frac{\partial}{\partial v} \times[\gamma v + f(x) - A_0\cos(\Omega t+\varphi)] + \gamma D\frac{\partial^2}{\partial v^2}\right\} p(x,v,t;\varphi), \tag{4.2}$$

where we introduced $f(x) = -V'(x)/m$ and the diffusion strength $D = kT/m$. For large values of the friction coefficient γ we can simplify the above inertial dynamics through adiabatic elimination of the velocity variable $\dot{x} = v$ (Marchesoni and Grigolini, 1983; Risken, 1984; Grigolini and Marchesoni, 1985) to arrive at the periodically modulated Langevin equation

$$\gamma\dot{x} = f(x) + A_0\cos(\Omega t+\varphi) + \sqrt{2\gamma D}\,\xi(t). \tag{4.3}$$

With the choice $f(x) = (ax - bx^3)/m$, where $a>0$, $b>0$, we recover the bistable quartic double-well potential $V(x) = -(1/2)ax^2 + (1/4)bx^4$ of Fig. 1. On making use of the rescaled variables:

$$\bar{x} = x/x_m, \quad \bar{t} = at/\gamma, \quad \bar{A}_0 = A_0/ax_m,$$
$$\bar{D} = D/ax_m^2, \quad \bar{\Omega} = \gamma\Omega/a, \tag{4.4}$$

where $\pm x_m = \sqrt{a/b}$ locate the minima of $V(x)$, the relevant Fokker-Planck equation takes on a dimensionless form. Dropping, for the sake of convenience, all overbars one recovers the Smoluchowski limit of Eq. (4.2); i.e., in terms of an operator notation we obtain

$$\frac{\partial}{\partial t}p(x,t;\varphi) = \mathcal{L}(t)p(x,t;\varphi) \equiv [\mathcal{L}_0 + \mathcal{L}_{ext}(t)]p(x,t;\varphi). \tag{4.5}$$

Here, the Fokker Planck operator

$$\mathcal{L}_0 = -\frac{\partial}{\partial x}(x-x^3) + D\frac{\partial^2}{\partial x^2} \tag{4.6}$$

describes the unperturbed dynamics in the rescaled bistable potential

$$V(x) = -\frac{1}{2}x^2 + \frac{1}{4}x^4, \tag{4.7}$$

with barrier height $\Delta V = \frac{1}{4}$. The operator $\mathcal{L}_{ext}(t)$ denotes the gradient-type perturbation

$$\mathcal{L}_{ext}(t) = -A_0\cos(\Omega t+\varphi)\frac{\partial}{\partial x}. \tag{4.8}$$

1. Floquet approach

The inertial, as well as the overdamped Brownian dynamics in Eqs. (4.2) and (4.5) describe a nonstationary Markovian process where the symmetry under time translation is retained in a discrete manner only. Since the Fokker-Planck operators in Eqs. (4.2) and (4.5) are invariant under the discrete time translations $t \to t + T_\Omega$, where $T_\Omega = 2\pi/\Omega$ denotes the modulation period, the Floquet theorem (Floquet, 1883; Magnus and Winkler, 1979) applies to the corresponding partial differential equation. For a general periodic Fokker-Planck operator such as $\mathcal{L}(t) = \mathcal{L}(t+T_\Omega)$, defined on the multidimensional space of state vectors $X(t) = (x(t); v(t) = \dot{x}(t); \ldots)$, one finds that the relevant Floquet solutions are functions of the type

$$p(X,t;\varphi) = \exp(-\mu t)p_\mu(X,t;\varphi) \tag{4.9}$$

with Floquet eigenvalue μ and periodic Floquet modes p_μ,

$$p_\mu(X,t;\varphi) = p_\mu(X,t+T_\Omega;\varphi). \tag{4.10}$$

The periodic Floquet modes $\{p_\mu\}$ are the (right) eigenfunctions of the Floquet operator

$$\left[\mathcal{L}(t)-\frac{\partial}{\partial t}\right]p_\mu(X,t;\varphi)=-\mu p_\mu(X,t;\varphi). \tag{4.11}$$

Here the Floquet modes $\{p_\mu\}$ are elements of the product space $L_1(X)\oplus\mathcal{T}_\Omega$, where $\mathcal{T}_\Omega$ is the space of functions that are periodic in time with period T_Ω, and $L_1(X)$ is the linear space of the functions that are integrable over the state space. In view of the identity

$$\begin{aligned}\exp(-\mu t)p_\mu(X,t;\varphi)&=\exp[-(\mu+ik\Omega)t]p_\mu(X,t;\varphi)\\&\quad\times\exp(ik\Omega t)\\&\equiv\exp(-\hat{\mu}t)\hat{p}_\mu(X,t;\varphi),\end{aligned} \tag{4.12}$$

where $\hat{\mu}=\mu+ik\Omega$, $k=0,\pm1,\pm2,\ldots$, and $\hat{p}_\mu(X,t;\varphi)=p_\mu(X,t;\varphi)\exp(ik\Omega t)=\hat{p}_\mu(X,t+T_\Omega;\varphi)$, we observe that the Floquet eigenvalues $\{\mu_n\}$ can be defined only mod$(i\Omega)$. Likewise, we introduce the set of Floquet modes of the adjoint operator $\mathcal{L}^\dagger(t)$, that is

$$\left[\mathcal{L}^\dagger(t)+\frac{\partial}{\partial t}\right]p^\dagger_\mu(X,t;\varphi)=-\mu p^\dagger_\mu(X,t;\varphi). \tag{4.13}$$

Here the sets $\{p_\mu\}$ and $\{p^\dagger_\mu\}$ are bi-orthogonal, obeying the equal-time normalization condition

$$\frac{1}{T_\Omega}\int_0^{T_\Omega}dt\int dX p_{\mu_n}(X,t;\varphi)p^\dagger_{\mu_m}(X,t;\varphi)=\delta_{n,m}. \tag{4.14}$$

Eqs. (4.11) and (4.13) allow for a spectral representation of the time inhomogeneous conditional probability $P(X,t|Y,s)$: With $t>s$ we find

$$\begin{aligned}P(X,t|Y,s)&=\sum_{n=0}^{\infty}p_{\mu_n}(X,t;\varphi)p^\dagger_{\mu_n}(Y,s;\varphi)\\&\quad\times\exp[-\mu_n(t-s)]\\&=P(X,t+T_\Omega|Y,s+T_\Omega).\end{aligned} \tag{4.15}$$

With all real parts Re$[\mu_n]>0$ for $n>0$, the limit $s\to-\infty$ of Eq. (4.15) yields the ergodic, time-periodic probability

$$p_{as}(X,t;\varphi)=p_{\mu=0}(X,t;\varphi). \tag{4.16}$$

The asymptotic probability $p_{as}(X,t;\varphi)$ can be expanded into a Fourier series, i.e.,

$$p_{as}(X,t;\varphi)=\sum_{m=-\infty}^{\infty}a_m(X)\exp[im(\Omega t+\varphi)]. \tag{4.17}$$

With the arbitrary initial phase being distributed *uniformly*, i.e., with the probability density for φ given by $w(\varphi)=(2\pi)^{-1}$, the time average of Eq. (4.17) equals the phase average (Jung and Hänggi, 1989, 1990; Jung, 1993). Hence

$$\begin{aligned}\bar{p}_{as}(X)&=\frac{1}{2\pi}\int_0^{2\pi}p_{as}(X,t;\varphi)d\varphi\\&=\frac{1}{T_\Omega}\int_0^{T_\Omega}p_{\mu=0}(X,t;\varphi)dt=a_0(X).\end{aligned} \tag{4.18}$$

At this stage it is worth pointing out a peculiarity of all periodically driven stochastic systems: With $\theta=\Omega t+\varphi$ we could as well embed a periodic N-dimensional Fokker-Planck equation into a Markovian $(N+1)$-dimensional, time-homogeneous Fokker-Planck equation by noting that $\dot{\theta}=\Omega$. With the corresponding stationary probability $p_{as}(x,\theta)$ not explicitly time dependent, an integration over θ does *not* yield the ergodic probability $p_{as}(x,t;\varphi)$ in Eq. (4.16) but rather the time-averaged result $\bar{p}_{as}$ of Eq. (4.18), not withstanding a claim to the contrary (Hu *et al.*, 1990).

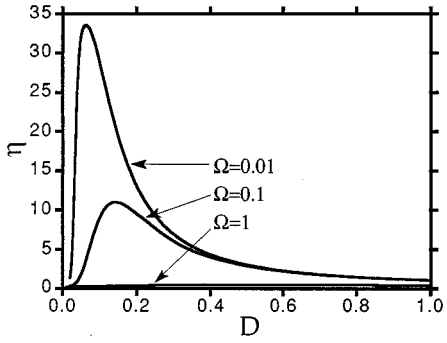

FIG. 6. The spectral amplification η for stochastic resonance in the symmetric bistable quartic double well is depicted vs the dimensionless noise strength D at a fixed modulation amplitude $A_0=0.2$ for three different values of the frequency Ω. The results were evaluated with the nonadiabatic Floquet theory for the corresponding time-periodic Fokker-Planck equation in Eq. (4.5). After Jung and Hänggi (1991a).

Given the spectral representation (4.15) for the conditional probability, we can evaluate mean values and correlation functions. Of particular importance for stochastic resonance is the asymptotic expectation value

$$\langle X(t)\rangle_{as}=\langle X(t)|Y_0,t_0\to-\infty\rangle, \tag{4.19}$$

where $\langle X(t)|Y_0,t_0\rangle$ is the conditional average $\langle X(t)|Y_0,t_0\rangle=\int dXXP(X,t|Y_0,t_0)$. With $P(X,t|Y_0,t_0\to-\infty)$ approaching the asymptotic time-periodic probability, the relevant asymptotic average $\langle X(t)\rangle_{as}$ is also periodic in time and thus admits the Fourier series representation

$$\langle X(t)\rangle_{as}=\sum_{n=-\infty}^{\infty}M_n\exp[in(\Omega t+\varphi)]. \tag{4.20}$$

The complex-valued amplitudes $M_n\equiv M_n(\Omega,A_0)$ depend nonlinearly on both the forcing frequency Ω and the modulation amplitude A_0. Within a linear-response approximation (see Sec. IV.B), only the contributions with $|n|=0,1$ contribute to Eq. (4.20). Nonlinear contributions to the stochastic resonance observables, both for M_1 and higher-order harmonics with $|n|>1$ have been evaluated numerically by Jung and Hänggi (1989, 1991a) by implementing the Floquet approach for the Fokker-Planck equation of the overdamped driven quartic double-well potential. The spectral amplification η of Eq. (2.9), i.e., the integrated power in the time-averaged power spectral density at $\pm\Omega$ (Jung and Hänggi, 1989, 1991a) [note also Eq. (4.24) below], is expressed in terms of $|M_1|$, i.e.,

$$\eta=\left(\frac{2|M_1|}{A_0}\right)^2. \tag{4.21}$$

Its behavior versus the noise strength D is depicted for different angular driving frequencies in Fig. 6. We observe that for a fixed modulation amplitude A_0 the stochastic resonance behavior of the spectral power amplification η *decreases* upon *increasing* the forcing frequency Ω. The behavior of η versus increasing Ω at *fixed* noise strength D is generally that of a monotonically decreasing function. An exception occurs in a symmetric bistable potential composed of two square wells and a square barrier with one well depth modulated periodically. For this case the *SNR* versus Ω has been shown to be nonmonotonic (Berdichevsky and Gitterman, 1996). The dependence on the modulation amplitude A_0 at fixed forcing frequency Ω is depicted in Fig. 7. We note that the maximum of the spectral amplification *decreases* with *increasing* amplitude A_0. Hence nonlinear response effects tend to diminish the stochastic resonance phenomenon. For a small, *fixed* noise strength D (so that the driving frequency Ω exceeds the Kramers rate r_K), the spectral amplification η exhibits, however, a maximum as a function of the forcing amplitude A_0—note the behavior in Fig. 7 below $D\sim 0.15$, and Fig. 36 in Sec. V.C.5.

The analog of the correlation function of a stationary process is the asymptotic time-inhomogeneous correlation

$$\langle X(t)X(t')\rangle_{as}=K(t,t';\varphi)=\int\int XYP(X,t|Y,t') \times p_{as}(Y,t';\varphi)dXdY, \tag{4.22}$$

where $t=t'+\tau$, with $\tau\geqslant 0$ and $t'\to\infty$. An additional averaging procedure (indicated by the double brackets) over a uniformly distributed initial phase φ for $K(t,t';\varphi)$ (or equivalently, a time average over one modulation cycle) yields a time-homogeneous, stationary correlation function

$$K(\tau)=\langle\langle X(t)X(t')\rangle\rangle_{as}\equiv\frac{1}{2\pi}\int K(t,t';\varphi)d\varphi. \tag{4.23}$$

In terms of the Fourier amplitudes $\{M_n\}$ of Eq. (4.20), the long-time limit of $K(\tau)$ assumes the oscillatory expression

$$\begin{aligned}K(\tau)\xrightarrow{\tau\to\infty}&\equiv K_{as}(\tau)=\langle\langle X(t+\tau)\rangle_{as}\langle X(t)\rangle_{as}\rangle\\&=\sum_{n=-\infty}^{\infty}|M_n|^2\exp(in\Omega\tau)\\&=2\sum_{n=1}^{\infty}|M_n|^2\cos(n\Omega\tau).\end{aligned} \tag{4.24}$$

In the last equality we used the fact that $M_0=0$ for a reflection-symmetric potential. Note that this asymptotic result is independent of the initial phase φ (no phase lag here!). This is in contrast with $\langle X(t)\rangle_{as}$, where the complex-valued amplitudes $\{M_n\}$ bring in an additional phase lag $\bar{\phi}_n$ for each Fourier component (see Sec. IV.B below).

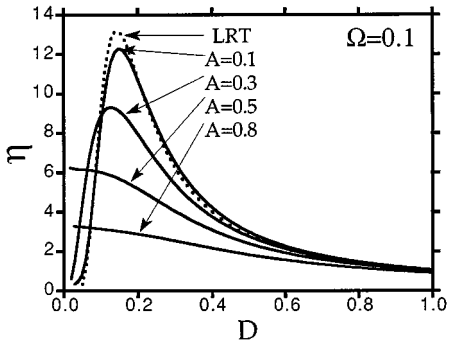

FIG. 7. The spectral amplification η versus the noise intensity D at a fixed modulation frequency $\Omega=0.1$ is depicted for four values of the driving amplitude $A\equiv A_0$. The result of the linear response approximation in Eq. (4.51) is depicted by the dotted line. From Jung and Hänggi (1991a).

This oscillatory, asymptotic long-time behavior yields in turn sharp δ spikes at multiples of the driving angular frequency Ω for the power spectral density of $\bar{K}(\tau)$. Depending on the symmetry properties of the Floquet operator, one finds that some of the amplitudes M_n assume vanishing weights (Jung and Hänggi, 1989; Hänggi *et al.*, 1993). In particular, for a symmetric double well, all even-numbered amplitudes M_{2n} assume zero weight; likewise a multiplicative driving $xA_0\cos(\Omega t)$ in Eq. (4.2) in a symmetric double well yields identically vanishing weights for all $n=0,\pm 1,\pm 2,\ldots$.

Before we proceed by introducing the linear-response theory (LRT), we also point out that the result for the corresponding conditional probability (4.15) for zero forcing $A_0=0$ boils down to the time-homogeneous conditional probability density, i.e., with $\tau=(t-s)>0$

$$P_0(X,\tau|Y,0)=\sum_{n=0}^{\infty}\psi_n(X)\varphi_n(Y)\exp(-\lambda_n\tau). \tag{4.25}$$

Here, for $A_0\to 0$ the set $\{\mu_n\}$ (with $k=0$) reduces to the set of eigenvalues $\{\lambda_n\}$ of $\mathcal{L}_0$, the set $\{p_{\mu_n}(X,t)\}$ reduces to the right eigenfunction $\{\psi_n\}$ of $\mathcal{L}_0$, and $\{p^{\dagger}_{\mu_n}(Y,s)\}$ to the right eigenfunctions $\{\varphi_n(Y)\}$ of $\mathcal{L}_0^{\dagger}$, respectively.

B. Linear-response theory

As detailed in the Introduction, the prominent role of the stochastic resonance phenomenon is that it can be used to boost *weak* signals embedded in a noisy environment. Thus the linear-response concept, or more general, the concept of perturbation theory (see Appendix) for spectral quantities like the Floquet modes and the Floquet eigenvalues as discussed in the previous section are adequate methods for studying the basic physics that characterizes stochastic resonance. Both concepts have been repeatedly invoked and investigated in stochastic resonance studies by several research groups (Fox, 1989;

McNamara and Wiesenfeld, 1989; Presilla *et al.*, 1989; Dykman *et al.*, 1990a, 1990b; Hu *et al.*, 1990; Jung and Hänggi, 1991a, 1993; Dykman, Mannella, *et al.*, 1992; Hu, Haken, and Ning, 1992; Dykman, Luchinsky, *et al.*, 1995). Here we shall focus on the linear-response concept, which also emerges as a specific application of perturbation theory. In doing so, we shall rely on the linear-response theory pioneered by Kubo (1957, 1966) for equilibrium systems—and extended by Hänggi and Thomas (1982) to the wider class of stochastic processes that admit also nonthermal, stationary nonequilibrium states. This extension is of particular relevance because many prominent applications of stochastic resonance in optical, chemical, and biological systems operate *far* from thermal equilibrium. Without lack of generality, we confine the further analysis to a one-dimensional Markovian observable $x(t)$ subjected to an external weak periodic perturbation. Following Hänggi (1978) and Hänggi and Thomas (1982), the long-time limit of the response $\langle x(t)\rangle_{as}$ due to the perturbation $A(t)=A_0\cos(\Omega t)$, i.e., we set $\varphi=0$, assumes up to first order the form

$$\langle x(t)\rangle_{as}=\langle x(t)\rangle_0+\int_{-\infty}^{t} ds\chi(t-s)A_0\cos(\Omega s), \tag{4.26}$$

where $\langle x(t)\rangle_0$ denotes the stationary average of the unperturbed process. The memory kernel $\chi(t)$ of Eq. (4.26) is termed, hereafter, the *response function*. For an external perturbation operator of the general form

$$\mathcal{L}_{ext}(t)\equiv A_0\cos(\Omega t)\Gamma_{ext}, \tag{4.27}$$

$\chi(t)$ is expressed by

$$\chi(t)=H(t)\int\int\int dxdydzP_0(x,t|y,0)x\Gamma_{ext}(y,z)p_0(z). \tag{4.28}$$

$H(t)$ denotes the (Heaviside) step function expressing causality of the response, $p_0(z)$ is the stationary probability density of the corresponding unperturbed, generally nonthermal equilibrium process, $P_0(x,t|y,0)$ denotes the conditional probability density, and $\Gamma_{ext}(x,y)$ denotes the kernel of the operator Γ_{ext} that describes the perturbation in the master operator (either an integral operator or a differential operator such as in the Fokker-Planck case of Sec. IV.A, e.g., $\Gamma_{\rm ext}(y,z)=\delta'(z-y)$ for Eq. (4.8)). An appealing form of the response function can be obtained by introducing the fluctuation $\zeta(x(t))$ defined by

$$\int dy\Gamma_{ext}(x,y)p_0(y)=-\int dz\mathcal{L}_0(x,z)\zeta(z)p_0(z), \tag{4.29}$$

where $\mathcal{L}_0(x,z)$ is the kernel of the unperturbed Fokker-Planck operator. We note that $\zeta(x(t))$ is indeed a fluctuation, i.e., it satisfies $\langle\zeta(x(t))\rangle_0=0$. The response function (4.28) can then be expressed through the *fluctuation theorem*

$$\chi(t)=-H(t)\frac{d}{dt}\langle x(t)\zeta(x(0))\rangle_0. \tag{4.30}$$

For $\delta x(t)=x(t)-\langle x(t)\rangle_0$ this can be recast as

$$\chi(t)=-H(t)\frac{d}{dt}\langle\delta x(t)\zeta(x(0))\rangle_0. \tag{4.31}$$

This result is intriguing: the linear-response function can be obtained as the time derivative of a stationary, generally nonthermal correlation function between the two unperturbed fluctuations $\delta x(t)$ and $\zeta(x(t))$. From the spectral representation of the time-homogeneous conditional probability (4.25), it follows immediately that (on assuming that the eigenvalue $\lambda_0=0$ is not degenerate)

$$\chi(t)=H(t)\sum_{n=1}^{\infty} g_n\lambda_n\exp(-\lambda_n t). \tag{4.32}$$

The coefficients $\{g_n\}$ are given by

$$g_n=\langle\delta x\psi_n(x)\rangle_0\langle\zeta(y)\varphi_n(y)\rangle_0. \tag{4.33}$$

The corresponding Fourier transform $\int_0^\infty\exp(-i\omega\tau)\chi(\tau)d\tau$ will be denoted by $\chi(\omega)$, with $\chi(\omega)=\chi'(\omega)-i\chi''(\omega)$. Generally, the eigenvalues of the real-valued operator $\mathcal{L}_0$ are complex valued and occur by the pair, e.g., λ_n and λ_n^* with the corresponding eigenfunctions $\psi_n(x)$ and $\phi_n(x)$ introduced above. Hence the contribution of each pair of complex conjugate eigenvalues is a real-valued quantity, thus yielding an overall real expression for $\chi(t)$ in Eq. (4.32). Upon substituting Eq. (4.32) into Eq. (4.26) we find the linear-response approximation

$$\langle\delta x(t)\rangle=\langle x(t)\rangle_{as}-\langle x(t)\rangle_0=\frac{A_0}{2}\sum_{n=1}^{\infty}\lambda_n g_n \times\left[\frac{e^{i\Omega t}}{\lambda_n+i\Omega}+\frac{e^{-i\Omega t}}{\lambda_n-i\Omega}\right]. \tag{4.34}$$

Moreover, on Fourier transforming Eq. (4.32) we derive the spectral representation of $\chi(t)$, i.e.,

$$\chi(\omega)=\chi'(\omega)-i\chi''(\omega)=\sum_{n=1}^{\infty}\frac{\lambda_n g_n}{\lambda_n+i\omega}. \tag{4.35}$$

Therefore, the result of Eq. (4.34) can be cast into the form

$$\langle\delta x(t)\rangle=2|M_1|\cos(\Omega t-\bar{\phi}), \tag{4.36}$$

where the spectral amplitude $|M_1|$ is given by

$$|M_1|=\frac{A_0}{2}|\chi(\Omega)|, \tag{4.37}$$

and the retarded positive phase shift $\bar{\phi}$ reads

$$\bar{\phi}=\arctan\left\{\frac{\chi''(\Omega)}{\chi'(\Omega)}\right\}. \tag{4.38}$$

The above results are valid for a general nonthermal stationary system. The fluctuation $\zeta(x(t))$ can be evaluated in a straightforward manner for all one-dimensional systems modeled by a Fokker-Planck equation. Examples include the stochastic resonance for absorptive optical bistability, Sec. V.A.3, or that for colored noise-driven bistable systems in Sec. VI.D.

For the case of the quartic double-well potential [Eqs. (2.1)–(2.3)], where the unmodulated system admits thermal equilibrium, the perturbation operator $\mathcal{L}_{ext}(t)$ is of the gradient type: from Eq. (4.8), $\mathcal{L}_{ext}(t) = A_0 \cos(\Omega t)[-\partial/\partial x]$. This, in turn, implies that the response function obeys the well-known fluctuation-dissipation theorem known from classical equilibrium statistical mechanics (Kubo, 1957, 1966), i.e.,

$$\chi(t) = -[H(t)/D] \frac{d}{dt} \langle \delta x(t) \delta x(0) \rangle_0, \tag{4.39}$$

where the corresponding fluctuation ζ reads $\zeta(x(0)) = \delta x(0)/D$. Note that this result holds true irrespective of the detailed form of the equilibrium dynamics.

1. Intrawell versus interwell motion

Given the spectral representation (4.35) of the response function $\chi(t)$, we can express the two stochastic resonance quantifiers, namely the spectral amplification η of Eqs. (2.9), Eq. (4.21), and the signal-to-noise ratio of Eq. (2.13) in terms of the spectral amplitude $|M_1|$. From Eq. (4.36) we find for the spectral amplification within linear response

$$\eta = (2|M_1|/A_0)^2 = |\chi(\Omega)|^2. \tag{4.40}$$

In view of the unperturbed power spectral density $S_N^0(\Omega)$ of the fluctuations $\delta x(t)$, i.e.,

$$S_N^0(\omega) = \int_{-\infty}^{\infty} e^{-i\omega\tau} \langle \delta x(\tau) \delta x(0) \rangle_0 d\tau, \tag{4.41}$$

the linear response result for the *SNR* reads

$$SNR = 4\pi |M_1|^2 / S_N^0(\Omega) = \pi A_0^2 |\chi(\Omega)|^2 / S_N^0(\Omega). \tag{4.42}$$

Both stochastic resonance observables possess a spectral representation via the spectral representations of $|\chi(\omega)|$ and $S_N^0(\omega)$.

In the following we shall explicitly assume that the noise strength D is weak. This implies that for a general bistable dynamics there exists a clear-cut separation of time scales. These are the escape time scale to leave the corresponding wells, i.e., the exponentially large time scale for interwell hopping, and the time scale that characterizes local relaxation within a metastable state. The eigenvalue λ_1 that characterizes the intrawell dynamics is always real valued and of the Kramers type (Hänggi *et al.*, 1990), i.e.,

$$\lambda_1 = 2r_K = r_+ + r_- \equiv \lambda, \tag{4.43}$$

where $r_\pm$ are the forward and backward transition rates, respectively. The rates $r_\pm$ depend through the Arrhenius factor on the activation energies $\Delta\Phi_0^\pm$, where $\Phi_0(x)$ is the generalized (non-thermal-equilibrium) potential associated with the unperturbed stationary probability density

$$p_0(x) = Z^{-1}(x) \exp(-\Phi_0(x)/D). \tag{4.44}$$

The relevant intrawell relaxation rates in the two wells located at $x = x_{1,2}^0$ are estimated as the real part of the two smallest eigenvalues that describe the equilibration of the probability density in the vicinity of the two stable states x_m, $m = 1,2$, respectively. For small noise intensities, these eigenvalues can be approximated as

$$\lambda_2 = \Phi_0''(x = x_1) \tag{4.45}$$

and

$$\lambda_3 = \Phi_0''(x = x_2). \tag{4.46}$$

Note that, here, the indices of λ_2 and λ_3 have been chosen for later convenience and do not necessarily coincide with the index ordering of the Fokker-Planck spectrum $\{\lambda_n\}$. Given these three dominant time scales, the response at weak noise is cast as the sum of three terms, i.e., for a driving phase $\varphi = 0$ we have the weak-noise approximation

$$\langle \delta x(t) \rangle = \frac{A_0}{2} \sum_{m=1,2,3} \lambda_m g_m \left[\frac{e^{i\Omega t}}{\lambda_m + i\Omega} + \frac{e^{-i\Omega t}}{\lambda_m - i\Omega} \right], \tag{4.47}$$

yielding corresponding estimates for $\chi(\Omega)$ and the stochastic resonance quantifiers η and the *SNR*. The weights g_m can be evaluated from the corresponding approximate eigenfunctions (Hänggi and Thomas, 1982; Dykman, Haken, *et al.*, 1993), or from a three-term exponential ansatz for the response function (Jung, 1993).

For the overdamped, symmetric quartic double-well dynamics [Eq. (4.7)], the spectral amplification given by Eq. (4.40) has been evaluated in the literature by means of Eq. (4.37) to give (Jung and Hänggi, 1991a, 1993)

$$\eta = D^{-2} \left[\frac{4g_1^2 r_K^2}{4r_K^2 + \Omega^2} + \frac{g^2 \alpha^2}{\alpha^2 + \Omega^2} + \frac{4g_1 g \alpha r_K (2\alpha r_K + \Omega^2)}{(4r_K^2 + \Omega^2)(\alpha^2 + \Omega^2)} \right]. \tag{4.48}$$

where $\lambda_2 = \lambda_3 \equiv \alpha$, with $\alpha = 2$, and $g_2 = g_3 \equiv g/2$. The relevant weights g_n for $D \to 0$ read

$$g_1 \simeq 1 - (1 + \alpha^{-1}) D + O(D^2),$$
$$g = D/\alpha + O(D^2), \tag{4.49}$$

and r_K is the steepest-descent approximation for the Kramers rate

$$r_K = (\sqrt{2}\pi)^{-1} \exp[-1/(4D)]. \tag{4.50}$$

Upon neglecting the intrawell motion, the leading-order contribution in Eq. (4.48) reproduces Eq. (2.7a), i.e.,

$$\eta \simeq \frac{1}{D^2} \left[1 + \frac{\pi^2}{2} \Omega^2 \exp\left(\frac{1}{2D} \right) \right]^{-1}. \tag{4.51}$$

This approximation exhibits the typical bell-shaped sto-

chastic resonance behavior as a function of increasing noise intensity D—see again Fig. 7, and also Figs. 18 and 19 below. Likewise, we can evaluate the *SNR* for the potential under study. In the weak-noise limit we have

$$S_N^0(\Omega)\simeq\frac{4r_K}{4r_K^2+\Omega^2}+\frac{2g\lambda_2}{\lambda_2^2+\Omega^2}, \tag{4.52}$$

whence yielding the linear-response result for the SNR (Hu *et al.*, 1992; Jung, 1993), i.e.,

$$SNR=\frac{\pi A_0^2}{2D^2}\,\frac{4g_1^2r_K^2(\alpha^2+\Omega^2)+(g\alpha)^2(4r_K^2+\Omega^2)+4\alpha g_1 r_K(2\alpha r_K+\Omega^2)}{2g_1r_K(\alpha^2+\Omega^2)+g\alpha(4r_K^2+\Omega^2)}. \tag{4.53}$$

This result, when plotted vs D displays a bell-shaped behavior for Ω not too large (see Fig. 8). Moreover, note that the result for the *SNR diverges* as $D\to 0$, proportional to D^{-1}. This is due to the intrawell contributions in Eq. (4.53). This feature is in agreement with simulations (McNamara and Wiesenfeld, 1989). On neglecting intrawell contributions, i.e., by setting $g_2=g_3=0$, one finds in leading order the result of Eq. (2.14) (Gammaitoni, Marchesoni, *et al.*, 1989; McNamara and Wiesenfeld, 1989; Presilla *et al.*, 1989; Dykman *et al.*, 1990b), i.e.,

$$SNR=(\pi A_0^2/D^2)r_K=[A_0^2/(\sqrt{2}D^2)]\exp[-1/(4D)]. \tag{4.54}$$

We remark that within this interwell approximation the *SNR*—contrary to the spectral amplification η in Eq. (4.51)—is no longer dependent on the angular modulation frequency Ω! This effective two-state approximation also exhibits a bell-shaped behavior, typical for stochastic resonance. In contrast to Eq. (4.53) the SN ratio vanishes for $D\to 0$. It is also worthwhile to point out the difference in how r_K enters the two stochastic resonance observables. The leading order contribution to *SNR* in Eq. (4.54) is proportional to r_K, while η in Eq. (4.51) is proportional to r_K^2.

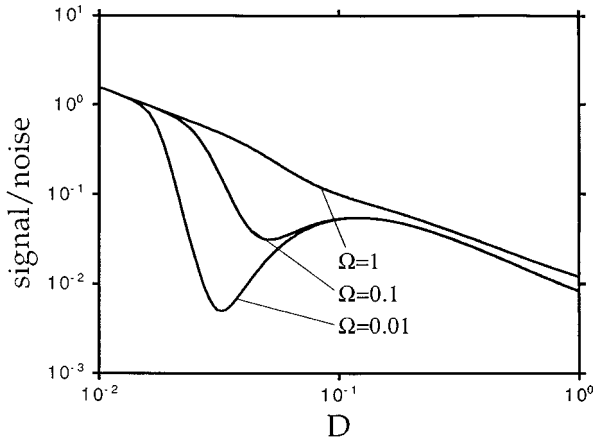

FIG. 8. The signal-to-noise ratio as function of the noise strength D for $A_0=0.1$ and different driving frequencies Ω. In contrast to the spectral amplification η—see Fig. 7—we note that the signal-to-noise ratio *diverges* as the noise strength $D\to 0$.

2. Role of asymmetry

In this subsection we study the effect of a potential asymmetry on stochastic resonance detectability. Here, the asymmetry of $\Phi_0(x)$ is characterized by the difference $\epsilon=\Delta\Phi_0^- -\Delta\Phi_0^+$ between the Arrhenius energies for backward and forward transitions. We shall assume that $\epsilon>0$; thus the backward rate r_- is exponentially suppressed over the forward escape rate. Such an asymmetry implies also an exponential suppression of the corresponding weight $g_1\sim 1\to\exp(-\epsilon/D)$ [see Eq. (6.3.46) of Hänggi and Thomas, 1982]. As a consequence, the spectral amplification suffers an exponential suppression proportional to $[\exp(-\epsilon/D)]^2=\exp(-2\epsilon/D)$, while the suppression of the SN ratio is weaker, being proportional to $\exp(-\epsilon/D)$.

On inspecting the leading order results in Eq. (4.51) for η and Eq. (4.54) for SNR, we note that the stochastic resonance maximum is located in the neighborhood where the monotonic decreasing function $y_1=D^{-2}$ crosses the monotonic, exponentially increasing Arrhenius factor $y_2=\exp(-\Delta\Phi_0/D)$ for the symmetric barrier with $\Delta\Phi_0^+=\Delta\Phi_0^-=\Delta\Phi_0$. The suppression caused by asymmetry now modifies y_2 into $\exp(-\epsilon/D)y_2$. Hence the intersection point of y_1 and y_2 as functions of D is moved to *larger* noise intensities. Both the exponential decrease (induced by the asymmetry in activation barriers in the unperturbed potential) of the peak for η (and likewise for the *SNR*), as well as the shift to larger noise intensities of the peak position have been confirmed numerically for a nonequilibrium optical bistable system (Bartussek, Jung, and Hänggi, 1993; Bartussek, Hänggi, and Jung, 1994) (see also Sec. V.A.3) and again numerically in an asymmetric rf SQUID loop by Bulsara, Inchiosa, and Gammaitoni (1996). The detailed analysis for an asymmetric quartic bistable well with asymmetry energy ϵ, but identical curvatures, gives for the spectral amplification (Jung and Bartussek, 1996; Grifoni *et al.*, 1996)

$$\eta=\frac{1}{D^2}\left[\cosh^4\left(\frac{\epsilon}{2D}\right)\left(1+\frac{\Omega^2}{4r_K^2(\epsilon)}\right)\right]^{-1}, \tag{4.55}$$

with $r_K(\epsilon)=r_K\cosh(\epsilon/2D)$, while the corresponding result for the *SNR* in the in presence of an asymmetry ϵ reads

$$SNR(\epsilon)=\frac{\pi A_0^2}{D^2}\,\frac{1}{\cosh^2(\epsilon/2D)}\,r_K(\epsilon). \tag{4.56}$$

An important feature of Eq. (4.55) is its universal shape for vanishing driving frequencies: In contrast to the symmetric case $\epsilon=0$, where the maximum of the spectral amplification increases with decreasing driving frequencies Ω (see Fig. 6 and Fig. 18 below for the optical bistability) the spectral amplification in asymmetric systems (see Fig. 19 below) approaches for $\Omega\to 0$ a limiting curve, with the stochastic resonance maximum assumed at a finite noise level. As a result, there exists no obvious time-scale matching condition in asymmetric systems.

3. Phase lag

The asymptotic probability $p_{as}(x,t;\varphi)$ [see Eq. (4.17)] depends periodically on the modulation phase $\theta=\Omega t+\varphi$. Moreover, due to the complex-valued amplitudes $a_m(x)$, the contribution to $p_{as}(x,t;\varphi)$ stemming from the pair of $\pm m$ introduces each its own additional phase lag $\bar{\phi}_m$. For periodically driven (linear) Gauss-Markov processes, only the terms with $m=\pm 1$ and $m=0$ contribute to Eq. (4.17). The corresponding phase lag $\bar{\phi}_1$ for the asymptotic probability of a Brownian harmonic oscillator has been evaluated explicitly as a function of the friction coefficient γ by Jung and Hänggi (1990). Analogously, in Eq. (4.20) each nonlinear contribution to $\langle x(t)\rangle_{as}$ with power amplitude M_n introduces its own phase lag $\bar{\phi}_m$.

From the linear-response function $\chi(\Omega)$ we obtain the phase lag $\bar{\phi}\equiv\bar{\phi}_1$ of Eq. (4.38). Correspondingly, the linear-response approximation for $p_{as}(x,t;\varphi)$ in Eq. (4.17) yields such a phase lag in terms of the amplitude M_1 of Eqs. (4.20) and (4.37). Neglecting all the intrawell terms g_n with $n\geqslant 2$ in Eq. (4.32) gives the single-exponential approximation (2.7b) for the phase lag $\bar{\phi}$ (Nicolis, 1982; McNamara and Wiesenfeld, 1989; Gammaitoni, Marchesoni, *et al.*, 1991), i.e.,

$$\bar{\phi}=\arctan\left(\frac{\Omega}{2r_K}\right). \tag{4.57}$$

$\bar{\phi}$ decreases *monotonically* from $\pi/2$ at $D=0^+$ to zero (for $\Omega\to 0$) as D is made to grow to infinity. Note that this is the equivalent of the two-state approximation of Sec. III. The inclusion of intrawell terms (Dykman, Mannella, *et al.*, 1992; Gammaitoni and Marchesoni, 1993; Dykman, Mannella, McClintock, and Stocks, 1993) changes this monotonic behavior into a bell-shaped behavior, as long as the modulation amplitude A_0 remains small. This feature is consistent with the linear-response result [Eq. (4.47)], which accounts for the hopping term with rate r_K and the two intrawell terms with rates λ_2 and λ_3. In particular, in a symmetric bistable potential with $D\to 0$, $\bar{\phi}$ approaches $\arctan(\Omega/\alpha)$—see the definition of α below Eq. (4.48). The presence of the intrawell dynamics suppresses at low noise the influence of the interwell dynamics on the phase lag. Hence within the regime of validity of the linear-response approximation, the peak of the phase shift marks the turnover between the regimes dominated by hopping and intrawell motion. Note that this maximum is not physically related to the maximum that characterizes stochastic resonance. Put differently, the noise value for the maximum of η, or SNR, is in no immediate relationship with the noise value that characterizes the maximum of $\bar{\phi}$: The stochastic resonance phenomenon is rooted in a physical *synchronization* effect between the interwell time scale and the period of the modulation signal, which acts here as an external "clock" (Jung and Hänggi, 1991a, 1993; Fox and Lu, 1993; Gammaitoni, Marchesoni, and Santucci, 1995). In contrast, a peak in $\bar{\phi}$ vs noise intensity D at small amplitude A_0 and small angular frequency Ω is due to the *competition* between hopping and intrawell dynamics—and should not be mistaken for a signature of stochastic resonance. The peak behavior of $\bar{\phi}$ vanishes with increasing modulation amplitude A_0 (Jung and Hänggi, 1993), where no clear-cut time-scale separation for hopping versus intrawell motion occurs. Such a dependence on the modulation amplitude is depicted in Fig. 9 as a function of the angular driving frequency Ω. The characteristic dependence of $\bar{\phi}$ on the driving strength A_0 (Ω held constant) clearly lies beyond the regime of validity of linear-response theory (Jung and Hänggi, 1993; Gómez-Ordóñez and Morillo, 1994).

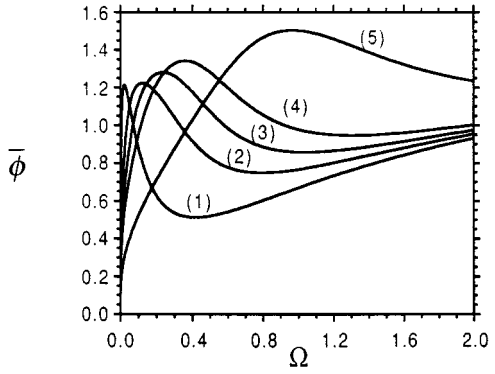

FIG. 9. Phase shift $\bar{\phi}$ of stochastic resonance in a periodically driven, overdamped quartic double well for a dimensionless noise strength $D=0.05$ vs driving frequency Ω for increasing driving amplitudes (1) $A_0=0.1$, (2) $A_0=0.3$, (3) $A_0=0.4$, (4) $A_0=0.5$, and (5) $A_0=1$. The lines are evaluated within a full nonadiabatic Floquet approach for the overdamped, time-periodic Fokker-Planck equation; see Jung and Hänggi (1993).

C. Residence-time distributions

The residence-time distribution offers another possibility to characterize stochastic resonance. Historically, residence-time distributions were first employed in the stochastic resonance literature by Gammaitoni, Marchesoni, Menichella-Saetta, and Santucci (1989) and Zhou and Moss (1990) and then interpreted theoretically by Zhou, Moss, and Jung (1990).

Residence-time distributions were mentioned briefly in Sec. II. In this section, we discuss in more detail how these residence-time distributions can be obtained approximately and how stochastic resonance is manifested in their properties.

In the absence of periodic forcing, an escape-time distribution is defined as the distribution of times it takes for the system to escape out of a potential well. For weak noise, such a distribution is independent of the initial point apart from a small boundary layer around the basin boundary. In periodically driven systems, escape-time distributions depend additionally on the initial phase of the periodic forcing—they represent therefore a conditional escape-time distribution.

Residence-time distributions are defined as the distribution of time intervals Δ_n between two consecutive escape events, regardless of the phases of the periodic forcing $\phi=\Omega t$ at which these switching events occur. Each time interval Δ_n corresponds to a different switching phase ϕ_n which in turn depends on the prehistory of the process. The approximation strategy of Zhou, Moss, and Jung (1990) to obtain the residence-time distributions is to first compute the conditional escape-time distribution and then to average over the distribution function of the switching phases ϕ: i.e., the temporal modulation of the potential must be slow.

Although we refer to the quartic double-well potential [Eq. (2.2)] throughout, the conclusions we arrive at are of general validity since only hopping between the stable states is taken into account—relaxational motion within the potential wells is neglected. We therefore essentially resort to a two-state description, discussed in Sec. II. Furthermore, the subsequent analysis holds true only for low forcing frequencies according to the adiabatic approximation; this means that the temporal change of the adiabatic potential [Eq. (4.59) below] has to be slow in comparison to the intrawell relaxation. Such a restriction is needed here for the definition of the interwell transition rates $r_{\pm}(t)$ to make sense. On the other hand, it is clear (see below) that under such a circumstance, the two-state model is a good approximation to the continuous dynamics of a bistable process.

A detailed calculation of both the escape- and residence-time distributions has been reported in a recent paper by Choi, Fox, and Jung (1998). To help the reader interpret the results in Figs. 4 and 5, without bogging down in complicated algebraic manipulations, we outline here the simplified approach developed earlier by Zhou, Moss, and Jung (1990), with the caution that its validity is restricted to relatively large values of Ω. The starting point for the calculation of the conditional escape-time distribution $\rho_e(t)$ out of the left potential well is the instantaneous rate equation for the population in the left well $n_-(t,\phi)$, i.e.,

$$\dot{n}_-(t;\phi)=-r_+(\Omega t+\phi)n_-(t;\phi). \tag{4.58}$$

The quasistationary forward rate $r_+(\Omega t+\phi)$ denotes the adiabatic transition rate, obtained for a frozen potential

$$V_{ad}(x,t)=x^4/4-x^2/2-A_0x\ \cos(\Omega t+\phi). \tag{4.59}$$

Initially, the system is in the left well, yielding the initial condition $n_-(0,\phi)=1$. The quasistationary rate $r_+(\Omega t+\phi)$ can be obtained from the weakly driven double-well potential upon combining the Kramers approach with the adiabatic assumption of a slow potential $V_{\rm ad}(x,t)$ (Jung, 1989), i.e.,

$$r_+(\Omega t+\phi)=\frac{1}{2\pi}\sqrt{|V''_{ad}(x_b)|V''_{ad}(x_m)}\times\exp\left[-\frac{\Delta V_-(\Omega t+\phi)}{D}\right], \tag{4.60}$$

where the barrier height $\Delta V_-(\Omega t+\phi)$ and the curvatures of the adiabatic potential at the barrier top $V''(x_b)$ and in the left potential minimum $V''(x_m)$ can be obtained for small A_0 to give

$$r_+(\Omega t+\phi)\approx r_K\left[1-\frac{3}{4}A_0\ \cos(\Omega t+\phi)\right]\times\exp\left[\frac{A_0}{D}\cos(\Omega t+\phi)\right]. \tag{4.61}$$

The escape rate of the undriven system r_K is given in Eq. (2.4). As mentioned above, the applicability of Eq. (4.61) is restricted to the adiabatic regime, i.e., the frequency Ω has to be small compared to the local relaxation rate. In our scaled units this means $\Omega\ll 2$, as well as weak forcing, i.e., $A_0\ll\sqrt{4/27}$. The two-state model rates $W_{\pm}(t)$ of Eq. (3.3) can thus be recovered from this adiabatic theory when prefactor corrections due to the forcing are neglected.

On coming back to Eq. (4.58), we note that the conditional escape-time distribution $\rho_e(t;\phi)$ can be written as

$$\rho_e(t;\phi)=-\dot{n}_-(t;\phi)=r_+(\Omega t+\phi)\times\exp\left[-\frac{1}{\Omega}\int_0^{\Omega t}r_+(\theta+\phi)d\theta\right]. \tag{4.62}$$

In order to obtain the residence-time distribution we have to find an expression for the distribution of the jump phase out of the left well $Y_-(\phi)$. It should be noted that this problem has not yet been solved systematically. For driving frequencies much smaller than the Kramers rate, there is no preferred phase and thus $Y(\phi)=1/(2\pi)$. For larger frequencies, the following self-consistent approximation has been proposed:

$$Y_{\pm}(\phi)=\frac{1}{2\pi I_0(A_0/D)}\exp\left(\pm\frac{A_0}{D}\cos(\phi)\right), \tag{4.63}$$

with $I_0(x)$ being a modified Bessel function (Abramowitz and Stegun, 1965). The residence-time distribution in the symmetric bistable potential of Eq. (2.2) thus reads

$$N(T)=\langle N(t;\phi)\rangle=\int_0^{2\pi}Y_-(\phi)r_+(\Omega T+\phi)\times\exp\left[-\frac{1}{\Omega}\int_0^{\Omega T}r_+(\theta+\phi)d\theta\right]d\phi. \tag{4.64}$$

Performing a series expansion for small A_0/D in Eq. (4.64) we find after some algebra that

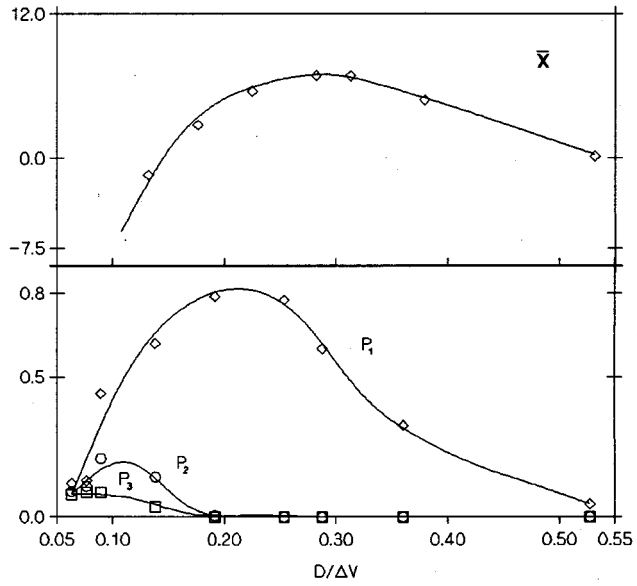

FIG. 10. Observable $\bar{x}$ (arbitrary logarithmic scale) and height of the nth peak P_n with $n=1,2,3$ vs D for $\nu_\Omega=40$ Hz and $\alpha=\frac{1}{4}$. Data obtained by means of analog simulation of system of Eqs. (4.3)–(4.7) with $A_0 x_m=0.5\Delta V$ and $a=3.2\times10^4$ s^{-1}. After Gammaitoni, Marchesoni, and Santucci (1995).

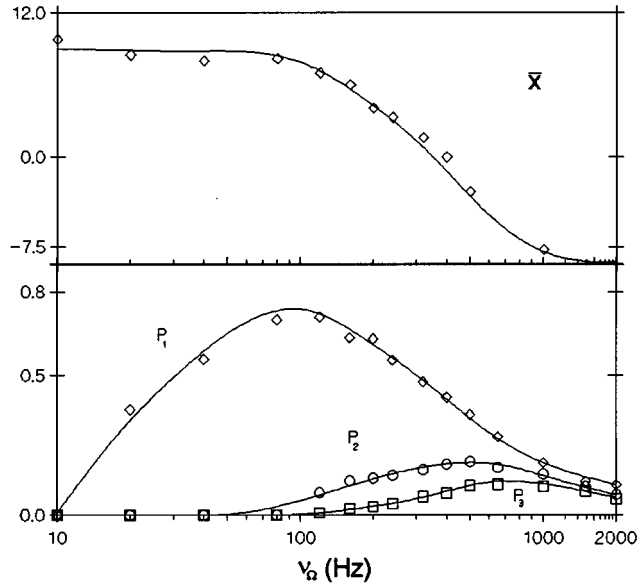

FIG. 11. Observable $\bar{x}$ (arbitrary logarithmic scale) and height of the nth peak P_n with $n=1,2,3$ vs ν_Ω for $D=0.3\Delta V$ and $\alpha=1/4$. Other simulation circuit parameters are as in Fig. 10. An independent measurement yielded $\mu_K=1.8\times10^{-2}a$. After Gammaitoni, Marchesoni, and Santucci (1995).

$$N(T)=\mathcal{N}_0\left[1-\frac{1}{2}\left(\frac{A_0}{D}\right)^2\cos(\Omega T)\right]r_K e^{-r_K T}, \quad (4.65)$$

with $\mathcal{N}_0^{-1}=1-\frac{1}{2}(A_0x_m/D)^2/[1+(\Omega/r_K)^2]$. To indicate the dimensional dependence we use $1=x_m$ throughout the remaining part of this section. The opposite limit, namely $\Delta V \gg A_0 x_m \gg D$, is reported here for completeness, though it will be used only in Sec. IV.D. The saddle-point approximation for the integral in Eq. (4.64) yields

$$\begin{aligned}N(T)\simeq&\exp[-(A_0/D)\cos(\Omega T)]\\&\times\exp\{-(r_{max}/2\Omega)(2\pi D/A_0)^{1/2}\\&\times[2n+1+\mathrm{erf}(\sqrt{A_0/2D}(\Omega T-\pi)]\},\end{aligned} \quad (4.66)$$

where $\mathrm{erf}(x)$ denotes the error function (Abramowitz and Stegun, 1965), $r_{\max}=r_K\exp(A_0/D)$ and $\Omega T=\mathrm{mod}(\Omega T,2\pi)$. Both limiting expressions (4.65) and (4.66) for $N(T)$ exhibit a series of peaks centered at $T_n=(2n-1)(T_\Omega/2)$ (see Fig. 5). The location of the first peak is due to the fact that the clock was triggered at $T=0$, immediately after the system had crossed the barrier at $x=0$ and half a forcing period before the relevant escape barrier attained a minimum for the first time. The nth peak corresponds to the event that the system switches first after $n-1$ entire periods. Such "wait loops" do not correspond to any subharmonic component in the process power spectral distribution as pointed out in Sec. II.B.

We are now in a position to discuss the synchronization mechanism that occurs in the bistable potential of Eq. (2.2) subjected to a periodic driving. In order to quantify the strength of the nth peak of $N(T)$, we introduce the areas under the peaks

$$P_n=\int_{T_n-\alpha T_\Omega}^{T_n+\alpha T_\Omega}N(T)dT, \quad (4.67)$$

with $n=1,2,\ldots$ and $0<\alpha\leqslant\frac{1}{4}$. The actual value of the parameter α is immaterial for the behavior of P_1. Let us focus now on the distribution of Eq. (4.65). In the regime of validity of Eq. (4.65), i.e., $r_K<\Omega\ll2$, the background of the distribution $N(T)$ is negligible. The strength P_n of the nth peak is thus a function of the ratio r_K/Ω alone. As a consequence, P_n attains its maximum by setting either the forcing frequency ν_Ω to

$$\nu_n\simeq(2n-1)r_K/2, \quad (4.68)$$

or tuning the noise, with constant ν_Ω, according to Eq. (4.68). The picture of SR as a "resonant" synchronization mechanism is thus fully established (Gammaitoni, Marchesoni, and Santucci, 1995). However, the reader should keep in mind that although the weight P_1 exhibits a maximum as a function of the frequency, the underlying mechanism is not a resonance in the sense of dynamical systems. While a dynamical resonance is due to the interaction of two degrees of freedom when their time scales agree, the nature of the peak of P_1 as a function of Ω is merely due to the coincidence of two time scales. For the sake of comparison, in Figs. 10 and 11 we show the dependence of P_n on D and Ω, as produced by means of an analog simulation. The basic properties of the synchronization mechanism are clearly visible: (i) For D tending to zero at fixed Ω (Fig. 10), all P_n approach a constant value independent on n, as expected in the nonadiabatic weak-noise limit of Sec. IV.D. (ii) Each curve $P_n=P_n(D)$ passes through a

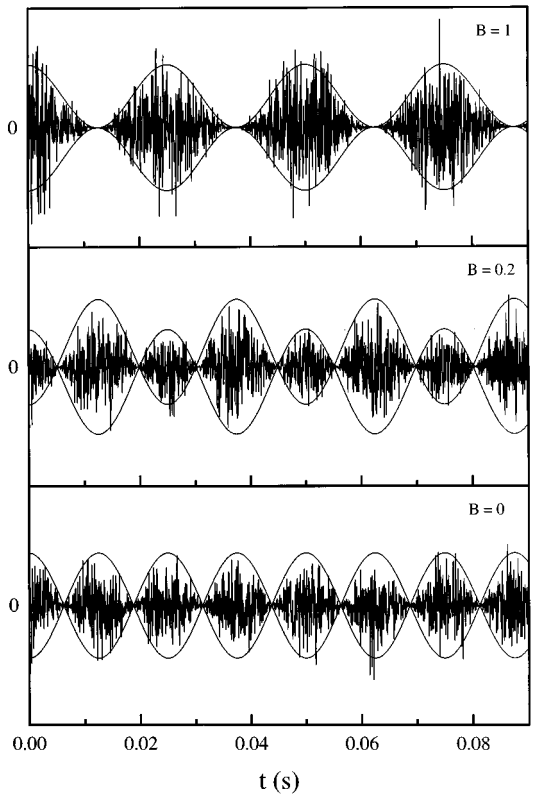

FIG. 12. Digitized time series for $f(t)$ with $\nu_\Omega=40$ Hz, $A_0=1$, and different values of B. The envelope function $\pm|A_0\cos(\Omega t)+B|$ is drawn for convenience. Ordinate units are arbitrary (Gammaitoni, Marchesoni, and Santucci, 1994).

maximum, the position D_n of which shifts progressively towards smaller values with the index n. (iii) The observables $\bar{x}(D)$ and P_1 peak at different D values, in agreement with the predictions for D_{SR}, Eq. (2.8), and D_1, Eq. (4.68). (iv) Contrary to $\bar{x}$, which decreases monotonically with the forcing frequency, the curves $P_n=P_n(\nu_\Omega)$ of Fig. 11 exhibit a clear-cut resonant-like profile. The positions ν_n of the maxima of P_n are apparently odd multiples of the fundamental frequency $r_K/2$; (v) Moreover, we notice that the inequality $P_n(\nu_\Omega)>P_m(\nu_\Omega)$ holds for $n<m$ in the whole range of simulated forcing frequencies. Finally, we stress that for $\Omega\sim r_K$ or smaller, condition in Eq. (4.68) may be fulfilled by the exponential background of the distribution $N(T)$ alone, even in the absence of peaks at T_n. Of course, in this limit the quantities P_n provide no characterization of the synchronization mechanism.

As an application of the residence-time analysis, we now show how stochastic resonance may occur in the absence of symmetry breaking. Following Dykman, Luchinsky, *et al.* (1992), we consider the symmetric bistable process

$$\dot{x}=-V'(x)+f(t), \tag{4.69}$$

where the potential function $V(x)$ is as in Eq. (2.2) and

$$f(t)=[A_0\cos(\Omega t+\varphi)+B]\xi(t), \tag{4.70}$$

with A_0, $B\geq 0$. On setting $\varphi=0$ for convenience, the autocorrelation function of the noise reads

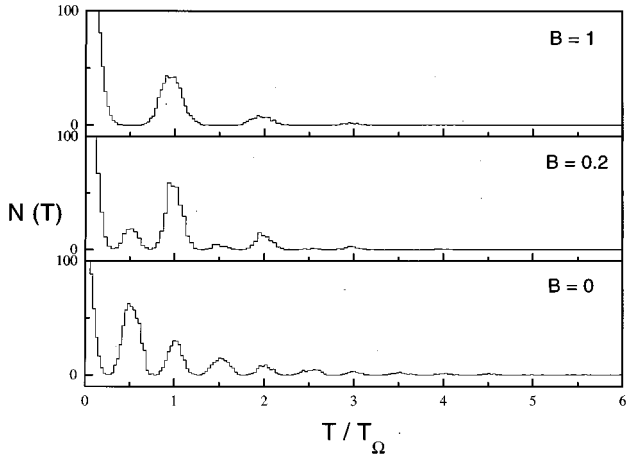

FIG. 13. Simulated residence-time distribution $N(T)$ for the system of Eqs. (4.69) and (4.70) with $\nu_\Omega=40$ Hz, $A_0=1$, and different values of B. Other circuital parameters are $a=2\times10^4$ s^{-1}, $x_m=1$, and $\bar{D}=0.16\Delta V$. After Gammaitoni, Marchesoni, and Santucci (1994).

$$\langle f(t)f(t')\rangle=2D\,\delta(t-t')[A_0\cos(\Omega t)+B]^2. \tag{4.71}$$

In Fig. 12 we show examples of digitized time series for $f(t)$ in the three typical cases discussed below, i.e., for $A_0=1$ and $B=0$, for $B=0.2$ and $B=1$, and for fixed effective noise intensity $\bar{D}=D(B^2+A_0^2/2)$.

Contrary to the process of Eqs. (2.1)–(2.3), the process under investigation here is symmetric under parity transformation $x\to -x$ at any time. As a consequence, $\langle x(t;\phi)\rangle_{as}=0$ vanishes identically and no peak is detectable in the power spectrum $S(\omega)$.

Evidence of stochastic resonance effects can be detected through a synchronization-based analysis (Gammaitoni, Marchesoni, Menichella-Saetta, and Santucci, 1994). In Fig. 13, residence-time distributions are displayed for the same A_0 and B values as in Fig. 12. The series of exponentially decaying peaks is apparent. Moreover, the dependence of $N(T)$ on the offset parameter B [see Eq. (4.71)] is also noteworthy. As illustrated in Fig. 12 for $B\geq A_0$ the modulation period of $f(t)$ is T_Ω, whence the peaks of $N(T)$ are centered at $T_n=nT_\Omega$. For $B=0$, instead, the $f(t)$ modulation period is half the forcing period and, accordingly, the peaks of $N(T)$ are located at $T_n=nT_\Omega/2$. In the intermediate case $0<B<A_0$, two series of higher and lower peaks show up with maxima at the even and odd multiples of $T_\Omega/2$, respectively.

When the strength of the first peak is plotted against the noise intensity D, the curves $P_1(D)$ pass through a maximum for $D_1=D_1(B)$. The B dependence of D_1 can be interpreted quantitatively as follows. For $A_0\ll B$ the rate performs small oscillations about the unperturbed rate $r_K(B^2D)$, where B^2D is the effective intensity $\bar{D}$ for $A_0=0$. Therefore, according to the stochastic resonance condition (4.68), the synchronization of switching events and periodic noise amplitude modulation is maximum for $\nu_\Omega=r_K(B^2D_1)/2$. For $A_0\gg B$, the characteristic switching rate to compare with is the

Kramers rate r_K with effective noise intensity $D=A_0^2D_1/2$. On remembering that the period of the $f(t)$ amplitude modulation is now $T_\Omega/2$, we conclude that the relevant stochastic resonance condition is $2\nu_\Omega=r_K(A_0^2D_1/2)/2$. Of course, such estimates for $D_1(B)$, which fit very closely the simulation results of Gammaitoni, Marchesoni, Menichella-Saetta, and Santucci (1994), could have been obtained by explicitly calculating the relevant distributions $N(T)$.

D. Weak-noise limit of stochastic resonance—power spectra

The most common approach in investigating stochastic resonance (apart from numerical solutions or analog simulations) is linear-response theory or the perturbation theory outlined in the Appendix. The condition for linear-response theory and perturbation theory to work well is that the effect of the periodic forcing can be treated as a small perturbation, i.e., $A_0x_m \ll D$. The response of the periodic driving can then be described in terms of quantities of the unperturbed Fokker-Planck equation, such as its eigenfunctions and eigenvalues and/or some corresponding unperturbed correlation function.

In this section, we consider the complementary limit where $A_0x_m \gg D$, i.e., linear-response theory is no longer valid. This weak noise limit, sometimes also termed nonlinear stochastic resonance limit, reveals some peculiar properties of the power spectrum that we shall discuss (Shneidman *et al.*, 1994a, 1994b; Stocks, 1995). The starting point for these investigations is, as in Sec. III, the two-state master equation Eq. (3.1) for the population dynamics. Assuming adiabatic conditions, i.e., the change of the adiabatic potential $V(x,t)=V_0(x)-A_0x\cos(\Omega t)$ is slower than the thermal relaxation within a potential well (in our units $\Omega \ll 2$), the two stable states in the master equation are given by the local (time-dependent) minima $x_\pm(t)$ of the adiabatic potential $V(x,t)$. Fluctuations of the system within the potential wells will be neglected, or treated as a small perturbation.

We consider a situation in which the noise strength D is the smallest parameter. The driving frequency is large enough (though adiabatically slow) so that almost all escape events take place when the potential barriers assume their smallest values. Under these conditions, the transition probability densities $W_\pm(t)$ are sharply peaked at those instants when the escape times are minimal. For the continuous bistable systems under study, two adiabatic transition rates $r_\pm(t)$ were introduced in Eq. (4.61). As a starting point, on taking the limit $D/A_0x_m \to 0$ of Eq. (4.61) for $A_0x_m \ll \Delta V$, we set

$$W_\mp(t)=\alpha\delta[t-(2m+\delta_{\pm 1,1})(\pi/\Omega)]. \tag{4.72}$$

The constant α, not related to the quantity in Sec. IV.B.1, is the escape probability $(r_{\max}/\Omega)(2\pi D/A_0x_m)^{1/2}$, with $r_{\max}=r_K\exp(A_0x_m/D)$, and $m=0,\pm 1,\pm 2,\ldots$ (phase locking approximation).

Heading towards the power spectrum of this two-state process, we subtract the periodic oscillations of the asymptotic correlation (see Sec. IV.A) by introducing the newly defined correlation function, i.e., with φ set 0 we write

$$K(t+\tau,t)=\langle[x(t+\tau)-\langle x(t+\tau)\rangle][x(t)-\langle x(t)\rangle]\rangle. \tag{4.73}$$

The phase-averaged correlation function $K(\tau)$, defined by averaging $K(t+\tau,t)$ over one period of t, has been obtained by solving the two-state master equation to yield

$$K(\tau)=4\frac{x_m^2\mu^{\tau/\Delta+1}}{(1+\mu)^2}\mu^{[\tau/\Delta]}(1-(1-\mu)[\tau/\Delta]), \tag{4.74}$$

where $\Delta=T_\Omega/2$, $\mu\equiv\exp(-\alpha)$, and $[\tau/\Delta]$ denotes the integer part of τ in units of Δ (Shneidman *et al.*, 1994a, 1994b). The autocorrelation function $K(\tau)$ exhibits cusps at each multiple of $T_\Omega/2$. While such cusps of $K(\tau)$ look to be a minor artifact of the phase-locking approximation for $D/A_0x_m \to 0$, the periodicity of their recurrence will affect the corresponding power spectral density in a rather peculiar way. The Fourier transform of $K(\tau)$ reads

$$S(\omega)=\frac{4x_m^2}{\Delta}\frac{\mu(1-\mu)}{(1+\mu)\omega^2}\times\frac{1-\cos(\Delta\omega)}{[1-\mu\cos(\Delta\omega)]^2+\mu^2\sin^2(\Delta\omega)}. \tag{4.75}$$

We next discuss this result and its regime of validity.

(i) $S(\omega)$ corresponds to the noise background component of the power spectral density of the periodically driven dynamics analyzed in Sec. IV.A. It depends on the forcing frequency Ω through a modulation factor and decays according to the same "universal" ω^{-2} power law as the unperturbed system does. Equation (4.75) was derived by assuming the deltalike transition rates of Eq. (4.72). On increasing the noise intensity or, equivalently, upon decreasing the forcing frequency, such an assumption becomes progressively invalid: The switching phase may no longer be locked to the phase of the input signal.

(ii) $S(\omega)$ exhibits sharp dips at even multiples of the driving frequency. In the asymptotic approximation [Eq. (4.75)] the power spectral density vanishes at $2n\Omega$, that is $S(2n\Omega)=0$. These zeros in the profile of $S(\omega)$ are the fingerprints of the periodic structure of nonanalytical cusps in the correlation function $K(\tau)$.

(iii) The experimental observability of the $S(\omega)$ dips is a delicate matter. For finite noise intensities these dips broaden and undergo a "wash out" effect to an extent that we estimate only at the end of this subsection. Here, we limit ourselves to noticing that the width of the sharp peaks in the transition rates $r_\pm(t)$ is, in fact, of order $(D/A_0x_m)^{1/2}\Omega^{-1}$. It follows that for spectral frequencies ω smaller than $\Omega(A_0x_m/D)^{1/2}$ the deltalike approximation (4.72) is sound, and the predictions of the present analysis are physically correct. For larger frequencies,

i.e., a finer temporal resolution, the cusps of $K(\tau)$ become increasingly unphysical. The condition of observability for the mth dip is thus

$$(2m)^2 \ll A_0 x_m / D. \tag{4.76}$$

Note that detecting even the fundamental dip requires a sufficiently large value of the ratio $A_0 x_m / D$. This explains why dips have not been predicted within the linear-response treatment where $A_0 x_m / D \ll 1$ (see Secs. IV.B and Appendix). The fact that sometimes (at weak noise) the dips were seen experimentally (termed "unexplained" or "strange"—see Zhou and Moss, 1990; Bulsara *et al.*, 1991; Kiss *et al.*, 1993), and sometimes (at strong noise) not, has continued to baffle experimentalists and theorists at the heyday of early stochastic resonance simulations.

(iv) In the derivation of $S(\omega)$, the modulation of the quasiequilibrium states $x_\pm(t)$ has been neglected. This effect is significant at large frequencies, when the system, far from being synchronized, may sojourn many forcing cycles in one well. The approximation $x_+(t) - x_-(t) = 2x_m$ employed to derive Eq. (4.74) ought to be improved. Without specializing our analysis to any potential, we observe that the next-to-leading order correction to the difference $x_+(t) - x_-(t)$ is proportional to $(A_0 x_m / \Delta V)^2 \cos^2(\Omega t + \varphi)$. It follows that only corrections to fourth order in $A_0 x_m / \Delta V$, i.e., proportional to $(A_0 x_m / \Delta V)^4 \cos(2\Omega t)\cos[2\Omega(t+\tau)]$, may become important in the computation of the phase-averaged correlation function $K(\tau)$ and its Fourier transform $S(\omega)$. Shneidman, Jung, and Hänggi (1994a, 1994b) concluded that for

$$\Omega \gg r_{\max}(2\pi D / A_0 x_m)^{1/2}(\Delta V / A_0 x_m)^2, \tag{4.77}$$

a *finite-width* intrawell peak may become detectable at 2Ω, and may even dominate over the relevant $S(\omega)$ dip. Furthermore, on accounting for higher-order terms of the time modulation $x_\pm(t)$, we can generate a harmonic structure of intrawell peaks at all even multiples of the forcing frequency.

In the weak-noise limit, the residence-time distribution can be calculated analytically without much effort. We can either proceed as for the two-state model, or adopt the approach of the foregoing Sec. IV.C. In both cases, consistently with the assumptions used above, we can assume a phase-switch distribution given by $Y_\pm(\phi) = \delta(\phi - \pi\delta_{\pm 1,1})$. Not surprisingly, the final result coincides with Eq. (4.66), the low-noise expression for $N(T)$ in the adiabatic approximation. It follows immediately that the ratio of any two consecutive $N(T)$ peaks is given by

$$N(T_{n+1}) / N(T_n) = \exp(-\alpha/2), \tag{4.78}$$

with $T_n = (n - 1/2)T_\Omega$, and α defined below Eq. (4.72). Thus, as anticipated in Sec. IV.C, the strengths P_n of the $N(T)$ peaks approach one another in the asymptotic limit $\alpha \to 0$. Moreover, the width of such peaks is of the order of $(D/A_0 x_m)^{1/2}\Omega^{-1}$, namely the same as that of the sharp peaks of the actual transition densities $r_\pm(t)$ at low noise, cf. Eq. (4.61).

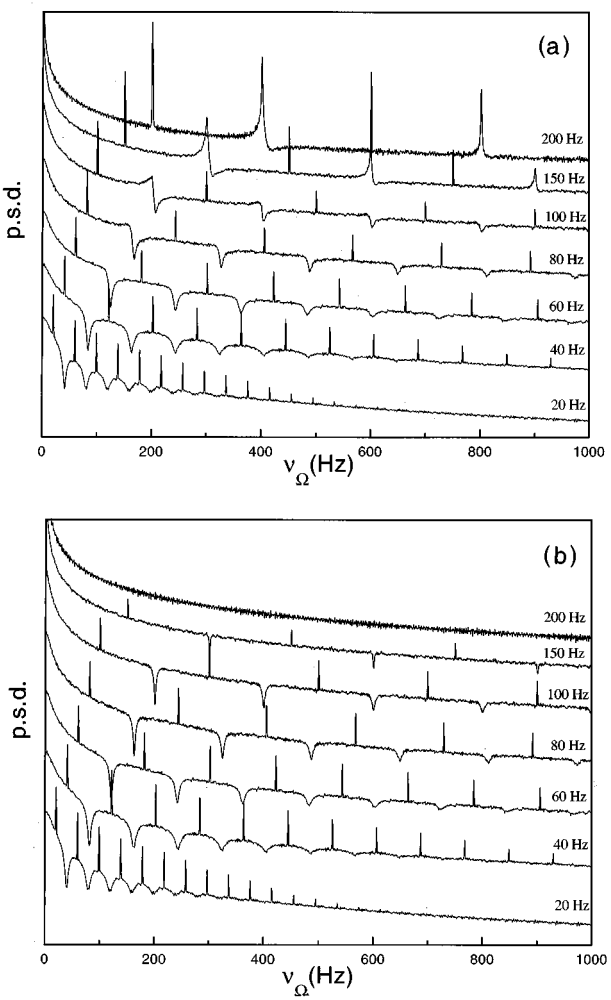

FIG. 14. Unsubtracted power spectral density (p.s.d.) (arbitrary units) of: (a) the full signal; (b) the filtered signal, for different values of the forcing frequency $\nu_\Omega = \Omega/2\pi$. The circuital parameters are $\Delta V/D = 1.6\times 10^3$, $A_0 x_m / D = 2.3\times 10^3$, and $a = 3.2\times 10^4\ \mathrm{s}^{-1}$. After Gammaitoni, Marchesoni, Menichella-Saetta, and Santucci (1995).

In a recent paper, Gammaitoni, Marchesoni, Menichella-Saetta, and Santucci (1995) used analog simulations for the periodically driven weak-noise limit of the quartic double-well dynamics to verify the theoretical predictions of Eqs. (4.75)–(4.78). In order to build up significant statistics, these authors increased the amplitude A_0 of the input signal close to, but smaller than, the critical value A_c above which bistability is lost when the maximal tilt is assumed. In this way, the ratios of $A_0 x_m / D$ became of the order 10^3, and could easily be simulated (strong-forcing regime). As a matter of fact, the condition $A_0 x_m \ll \Delta V$ does not enter explicitly in the discrete-switching approximation. It was originally introduced to simplify $r_\pm(\theta)$ to $r_K \exp[\mp(A_0 x_m / D)\cos\theta]$ in Eq. (4.61) and to determine the probability α in Eq. (4.72). Therefore, we expect that in the strong-forcing regime $r_{\max}$ does differ substantially from $r_K \exp(A_0 x_m / D)$ in Eq. (4.72), but its physical role remains unchanged. Gammaitoni, Marchesoni, Menichella-Saetta, and Santucci (1995) verified that in

the limit of weak noise and strong forcing the shape of the nth $N(T)$ peak is approximated well by a Gaussian function with standard deviation $\sigma_T=(D/A_0x_m)^{1/2}\Omega^{-1}$ independent of n. Furthermore, the peak height $N(T_n)$ turned out to decay according to the exponential law (4.78), whence the estimate of the parameter α. Mantegna and Spagnolo (1996) reached the same conclusion in their experimental investigation of the switching-time distributions in a periodically driven tunnel diode.

Gammaitoni, Marchesoni, Menichella-Saetta, and Santucci (1995) experimentally confirmed the predictions of Shneidman, Jung, and Hänggi (1994a, 1994b) in great detail. In particular, the following.

(a) The interwell and intrawell dynamics were separated by filtering the output signal $x(t)$ through a two-state filter ($x=\pm x_m$) and contrasting the statistics of the filtered signal with that of the full signal. The *nonsubtracted* power spectral densities for both output signals are displayed in Fig. 14. In both cases the number of resolved dips m is bounded from above by the inequality in Eq. (4.76).

(b) The dip structure of the power spectral densities becomes more apparent by filtering $x(t)$. Most notably, the spectral dips tend to disappear with increasing Ω, and their shape is not as sharp as that predicted by Eq. (4.75).

(c) No peak structure due to the intrawell modulation is observable in the power spectral density of the filtered signal. In contrast, for the full signal, broad peaks located in the vicinity around $2n\Omega$ can be resolved at relatively high values of Ω, namely for $\alpha\ll 1$, in agreement with Eq. (4.77) for $A_0x_m\simeq\Delta V$. Moreover, such peaks get sharper on further increasing Ω, and their height decreases with increasing peak index.

(d) Dips and peaks of the power spectral density may coexist for the full signal, as suggested by items (a) and (b). In such a case, their position deviates slightly from the predicted value $2n\Omega$, by shifting to the right and, possibly, to the left. At very low Ω values, no intrawell modulation peak is detectable, whereas at high Ω values, peaks dominate over dips which, in turn, tend to vanish. We additionally remark that these intrawell modulation peaks should not be mistaken for the delta-like spikes at $(2n+1)\Omega$.

Finally, we mention that in addition to the detailed experimental analog simulations (Gammaitoni, Marchesoni, Menichella-Saetta, and Santucci, 1995), the structure of the characteristic dips in the time-averaged power spectrum $S(\omega)$ at even-numbered harmonics have also been observed in computer simulations of a neural network using a model describing the perceptual interpretation of ambiguous figures (Riani and Simonotto, 1994, 1995) and even in *in situ* experiments with human observers (Riani and Simonotto, 1995). These latter experiments yielded results that are in good qualitative agreement with the neural model predictions for the stochastic resonance power spectra that characterize the perceptual bistability in the presence of noise and weak periodic perturbations.

V. APPLICATIONS

A. Optical systems

1. Bistable ring laser

A ring laser (Sargent *et al.*, 1974) consists of a ring interferometer formed by three or more mirrors and a laser medium inside the cavity. In two-mode ring lasers, the light can travel in a clockwise or counterclockwise direction. Bistability with respect to the direction has been discussed in large detail—see, for example, Mandel, Roy, and Singh (1981). Random switching of the beam intensities, initiated by spontaneous emission in the laser medium and fluctuations in the pump mechanism, indicates bistable operation of the ring laser. To demonstrate stochastic resonance, the symmetry between the two modes has to be broken by applying a periodic modulation that favors one of the modes. In the pioneering experiment by McNamara, Wiesenfeld, and Roy (1988), an acousto-optic modulator (Roy *et al.*, 1987) has been used to convert an acoustic frequency to a modulation of the pump parameter. Gage and Mandel (1988) have alternatively used Faraday and quartz rotators to control the asymmetry of the modes. Before we discuss the experiment by McNamara, Wiesenfeld, and Roy (1988), we briefly review the theoretical description of bistable ring lasers.

The semiclassical equations for a two-mode ring laser (Sargent *et al.*, 1974) augmented by noise sources $\Gamma_{1,2}(t)$ to account for the effect of spontaneous emission and pump noise $p(t)$ assume in dimensionless units the form

$$\dot{I}_1=2I_1(a_1+p(t)-I_1-\xi I_2)+\sqrt{2I_1}\Gamma_1(t),$$
$$\dot{I}_2=2I_2(a_2+p(t)-I_2-\xi I_1)+\sqrt{2I_2}\Gamma_2(t), \tag{5.1}$$

where I_1 and I_2 are the scaled dimensionless intensities of the modes. The terms linear in $I_{1,2}$ describe the net gain of the laser modes, those with $I_{1,2}^2$ describe saturation and the mixed terms ξI_1I_2 represent coupling between the laser modes. The fluctuations of the pumping mechanism are described by the exponentially correlated Gaussian noise $p(t)$, i.e.,

$$\langle p(t)p(t')\rangle=\frac{P}{\tau_c}\exp\left(-\frac{1}{\tau_c}|t-t'|\right),$$
$$\langle p(t)\rangle=0 \tag{5.2}$$

with correlation time τ_c and intensity P, while the spontaneous-emission noise terms are assumed to be uncorrelated:

$$\langle\Gamma_i(t)\Gamma_j(t')\rangle=\delta_{ij}\delta(t-t'),$$
$$\langle\Gamma_{i,j}(t)\rangle=0. \tag{5.3}$$

The pump parameters a_1 and a_2 are modulated antisymmetrically by noise and a periodic signal (Vemuri and Roy, 1989)

$$a_1(t)=\bar{a}+\Delta a(t)+r(t),$$
$$a_2(t)=\bar{a}-\Delta a(t)-r(t), \tag{5.4}$$

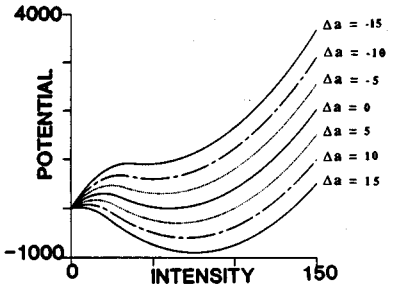

FIG. 15. The effective potential of Eq. (5.8) for the intensity of a single laser mode in a bistable ring laser is plotted as a function of the intensity at the pump strength $\bar{a}=60$ and the coupling $\xi=2$ for different amplitudes $\Delta a=A_0\cos(\Omega t)$ of the external field (i.e., during one period of the external field). It is seen that the effective barrier height for a transition between the "ON" state and the "OFF" state becomes periodically modulated. After Vemuri and Roy (1989).

with $r(t)$ being white Gaussian (injected) noise

$$\langle r(t)r(t')\rangle=2R\delta(t-t'),$$

$$\langle r(t)\rangle=0, \tag{5.5}$$

and

$$\Delta a(t)=A_0\cos(\Omega t). \tag{5.6}$$

In the absence of the periodic modulation (Δa=const.), pump noise, and injected noise, the stationary probability $P_{st}(I_1,I_2)$ can be obtained analytically (Sargent *et al.*, 1974). Integration over the intensity I_2 yields the stationary probability density of I_1, which can be written as

$$P_{st}(I_1)=\int_0^\infty P_{st}(I_1,I_2)dI_2=\frac{1}{Z}\exp[-V(I_1)], \tag{5.7}$$

with the effective potential

$$V(I_1)=-\frac{1}{4}(\xi^2-1)I_1^2+\left[\frac{1}{2}\,\bar{a}(\xi-1)-\frac{1}{4}\Delta a(\xi+1)\right]I_1$$
$$-\ln\left\{\operatorname{erfc}\left[\frac{1}{2}\xi I_1-\frac{1}{2}\,\bar{a}+\frac{1}{4}\Delta a\right]\right\}, \tag{5.8}$$

and erfc being the complementary error function (Abramowitz and Stegun, 1965). For slow and weak periodic driving, the potential $V(I_1)$ undergoes a periodic change obtained by substituting Δa by $A_0\cos(\Omega t)$, but it remains bistable. The minimum corresponding to the ON state (high intensity) rocks up and down—see Fig. 15. This situation looks similar to the quartic double-well potential, discussed in Sec. IV. There are, however, some differences:

(1) The potential $V(I_1)$ is only an effective potential. For its construction, the pump noise and injected noise had been neglected. The intuitive picture of a particle (here the intensity) moving in the effective potential can be used only as a heuristic guideline.
(2) The original Langevin equations (5.1) exhibit no inversion symmetry.

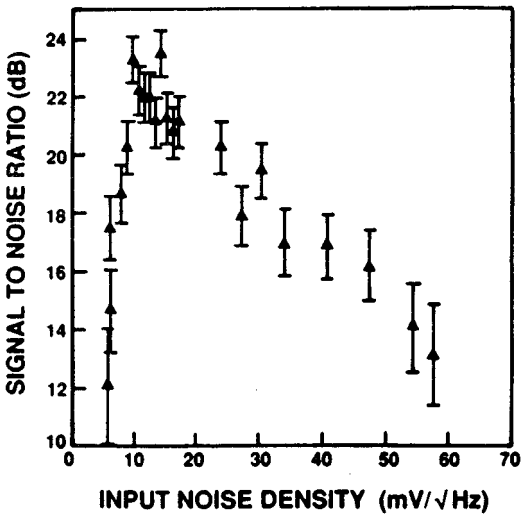

FIG. 16. The signal-to-noise ratio, obtained from the time dependence of the intensity of one laser mode, shown as a function of the injected noise strength. After McNamaura, Wiesenfeld, and Roy (1988).

In the experiment by McNamara, Wiesenfeld, and Roy (1988), the intensity of one of the two modes has been extracted from the ring laser. The time series for the intensity has subsequently been compressed into a binary pulse train that contains only information on whether the mode was "ON" or "OFF." This procedure has been repeated for a large number of samples to obtain the sample-averaged power spectrum. The power spectrum consists of a smooth background, a sharp peak at the frequency of the modulating field Ω, and smaller peaks at multiples of Ω. Most significantly, the intensity of the peaks at the driving frequency first increases with increasing injected noise strength, passes through a maximum and then decreases again. The signal-to-noise ratio, shown in Fig. 16, reflects this characteristic bell-shaped behavior.

For the archetypal quartic bistable potential in Sec. IV, the power spectrum contains peaks only at odd multiples of the driving frequency. In the power spectrum

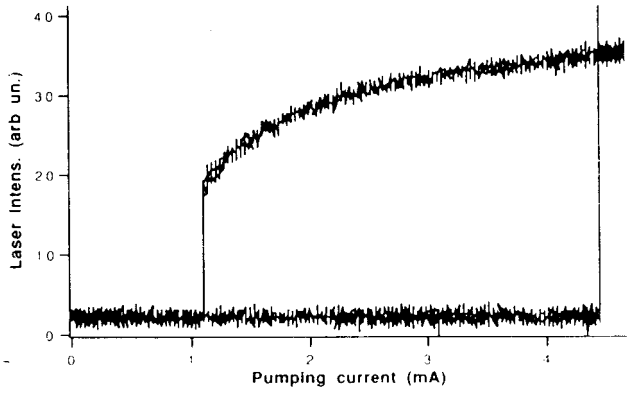

FIG. 17. The light intensity of a single-mode laser with a saturable absorber shown as a function of the pump current. The hysteresis loop indicates optical bistability.

here, however, a peak at twice the driving frequency can be observed, reflecting the lack of inversion symmetry of the two-mode laser Langevin equations (5.1), or the effective potential (5.8).

Digital simulations of Eq. (5.1) in Vemuri and Roy (1989) are in qualitative agreement with the experimental results.

2. Lasers with saturable absorbers

A laser with a saturable absorber is a quantum device consisting of a laser cavity where an amplifying as well as an absorbing medium are placed. Bistability has been observed in these devices by Arimondo and Dinelli (1983) and Arimondo *et al.* (1987). Within a certain range of the pump intensity, the output of the laser can be in two different modes, depending on its previous history.

In Fig. 17, the laser intensity (Fioretti *et al.*, 1993) is shown as a function of the pump current, which was slowly increased until the output switched to the high intensity level, and then decreased again. The observed hysteresis loop is an indication of bistability.

In the experiment by Fioretti *et al.* (1993), the dc pump current is chosen in order that the laser operates in the bistable regime. The pump current is modulated around this dc value by a small periodic signal plus an external Gaussian noise source whose intensity can be controlled.

The periodic signal is too small to cause switching by itself. In the presence of pump noise, however, switching takes place. The intensity of the laser light has been recorded as a function of time and subsequently filtered by a two-bit filter, which only detects "ON" and "OFF" information. The extracted signal-to-noise ratios exhibit maxima as a function of noise strength Q (see below).

The laser with a saturated absorber is described on a semiclassical level by a system of three ordinary differential equations (Zambon *et al.*, 1989)

$$\dot{E}=-\frac{1}{2}\left(D+\frac{\bar{A}}{1+a|E|^2}+1\right)E+\xi(t),$$

$$\dot{D}=-\gamma(D+A+D|E|^2)-c_1(S-D),$$

$$\dot{S}=-\gamma_1(S-D), \tag{5.9}$$

where E is the complex field amplitude and D is the difference between the population of the upper and lower energy level of the amplifier medium relevant for lasing. The quantity S describes the influence of other energy levels coupled to the populations of the lasing levels; A and $\bar{A}$ describe the strength of the amplifying and absorbing medium, respectively. Quantum fluctuations are modeled by zero-mean white Gaussian noise $\xi(t)$ with $\langle\xi^*(t)\xi(t')\rangle = 4q\,\delta(t-t')$. In order to simplify the laser equations, S and D are adiabatically eliminated by assuming the field strength E to be small and much slower varying in time than S and D. Periodic modulation and (Gaussian) fluctuations $\zeta(t)$ of the pump current are taken into account by modulating the amplifier strength A, i.e., $A\rightarrow A(t)=A+F\cos(\Omega t)+\zeta(t)$, with

$$\langle\zeta(t)\zeta(t')\rangle=2q\,\delta(t-t'),$$

$$\langle\zeta(t)\rangle=0. \tag{5.10}$$

One finally arrives at the equation of motion for the field intensity $I\equiv E^*E$

$$\dot{I}=-I\left(1+\frac{\bar{A}}{1+aI}-\frac{A}{1+I}-\frac{\zeta(t)+F\cos(\Omega t)}{1+I}\right)+\sqrt{I}\Gamma(t), \tag{5.11}$$

with the real-valued zero-mean Gaussian noise $\Gamma(t)$, characterized by the correlation function

$$\langle\Gamma(t)\Gamma(t')\rangle=2Q\,\delta(t-t'). \tag{5.12}$$

Again, in contrast to the quartic double-well system in Sec. IV.A, the equation of motion (5.11) does not have inversion symmetry. The stationary intensities in the absence of fluctuations and modulation, are determined by the zeros of $F(I)=I(1+\bar{A}/(1+aI)-A/(1+I))$. For $a>A/(A-1)$, the dynamical system exhibits a subcritical pitchfork bifurcation at $A=\bar{A}+1$, which explains the hysteretic behavior (see Fig. 17), bistability, and stochastic resonance observed in the experiment when the pump current A is ramped slowly up and down.

3. Model for absorptive optical bistability

Consider a ring interferometer with a passive medium placed in it. Light is coupled into the interferometer through a semipermeable mirror and, likewise, light is transmitted at another mirror. Measuring the intensity of the transmitted wave against the intensity of the incident wave, one finds an S-shaped curve; e.g., for some values of the intensity of the incident beam the intensity of the transmitted wave can have a small and a large intensity. There are different mechanisms that can be responsible for this behavior. One of them is due to nonlinear absorption in the passive medium.

A model for purely absorptive optical bistability in a cavity was introduced by Bonifacio and Lugiato (1978). For the scaled dimensionless amplitude y of the input light and the scaled dimensionless amplitude of the transmitted light x, they have derived the equation of motion

$$\dot{x}=y-x-\frac{2cx}{1+x^2}+\frac{x}{1+x^2}\Gamma(t), \tag{5.13}$$

with $\Gamma(t)$ denoting Gaussian fluctuations of the inversion

$$\langle\Gamma(t)\Gamma(t')\rangle=2D\,\delta(t-t'),$$

$$\langle\Gamma(t)\rangle=0. \tag{5.14}$$

The dimensionless parameter c is proportional to the population difference in the two relevant atomic levels.

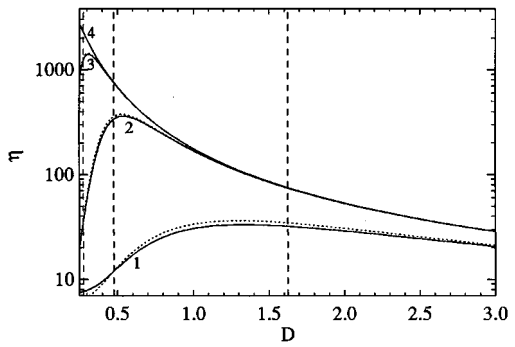

FIG. 18. The numerical results for the spectral amplification η are shown by the solid lines for the "symmetric case" $y_0=6.72584$ at $c=6$ and $A_0=10^{-4}$. Different lines labeled according to "n" correspond to the external angular frequency $\Omega=10^{-n}$. The dotted lines correspond to results within the linear-response approximation. They can be distinguished from the numerical results only for frequencies larger than about 10^{-2}. The vertical dashed lines indicate the position D_{SR} of the maxima determined by the argument of matching time scales discussed in Sec. II, and also in Bartussek, Hänggi, and Jung (1994).

For a large enough population difference c, the stationary transmitted light amplitude is an S-shaped function of the amplitude of the injected light, thus indicating bistability.

In the presence of a small, periodic perturbation of the incident light, the parameter y in Eq. (5.13) has to be modified by $y\rightarrow y(t)=y+A_0\cos(\Omega t)$. The Fokker-Planck equation corresponding to the Langevin equation (5.13) with the modulated parameter y has been solved numerically by Bartussek, Hänggi, and Jung (1994) by using the matrix-continued fraction technique, and alternatively with linear-response theory for weak modulation A_0. According to Sec. IV, the spectral amplification η [see Eq. (4.21)] of the periodic modulation has been constructed from the asymptotic long-time solution of the Fokker-Planck equation.

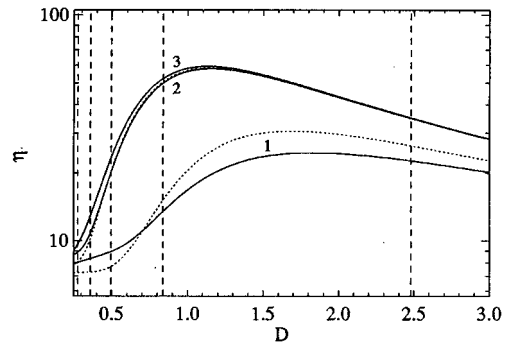

FIG. 19. The numerical results for the spectral amplification η are shown by the solid lines for the "asymmetric case" $y_0=6.8$ at $c=6$ and $A_0=10^{-4}$. Different lines labeled according to "n" correspond to the external frequency $\Omega=10^{-n}$. The curves for $\Omega<10^{-3}$ are not distinguishable from the curve for $\Omega=10^{-3}$. The dotted lines correspond to results within the linear-response approximation. They can be distinguished from the numerical results only for frequencies larger than about 10^{-2}. The rightmost dashed vertical line indicates the position D_{SR} of the maximum determined by the argument of matching time scales between the period of driving T_Ω and the sum of corresponding two escape times at $\Omega=10^{-1}$; see Bartussek, Hänggi, and Jung (1994). The angular driving frequencies corresponding to the vertical dashed lines from right to left are $\Omega=10^{-1}$, $\Omega=10^{-2}$, $\Omega=10^{-3}$, $\Omega=10^{-4}$, and $\Omega=10^{-7}$.

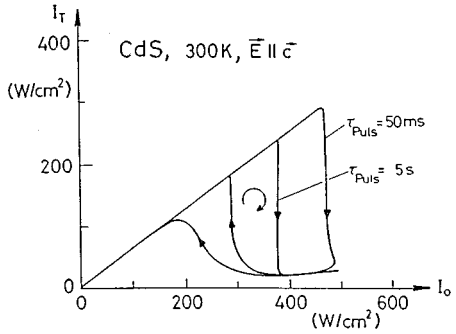

FIG. 20. Transmitted intensity I_t vs incident light intensity I_0 for a laser-illuminated sample of the optical bistable semiconductor CdS. The pulse length of the incident light intensity determines the rate at which the hysteresis loop is run through.

The following discussion is restricted to the bistable regime. Here, it is important to distinguish a symmetric case from an asymmetric case. In the symmetric case the stationary probability density in the absence of periodic driving has two peaks with the same heights in the zero-noise limit $D\rightarrow 0$. For all other cases (asymmetric cases), the peaks have different probabilistic weights at weak noise.

In the symmetric case, one observes stochastic resonance very much like in the quartic bistable double-well potential (see Fig. 18), i.e., a peak in the amplification of the modulation when the sum of the mean escape times out of both stable states equals the period of the driving (the values of the noise strength D where we have such a time-scale matching are indicated by dashed lines in Fig. 18).

In the asymmetric case (Fig. 19), the spectral amplification is suppressed at weak noise, because—in contrast to the symmetric case—the contribution of the hopping motion to the response of the system disappears exponentially for small noise; cf. Sec. IV.B.2. As a consequence, the maximum of the spectral amplification does not indicate a time-scale matching as in the symmetric case. For small driving frequencies, the maximum of the spectral amplification becomes independent of the driving frequency.

4. Thermally induced optical bistability in semiconductors

It has been shown that semiconductors exhibit a thermally induced optical bistability facilitated by the thermal shift of the fundamental band edge (Lambsdorff *et al.*, 1986; Grohs *et al.*, 1989). The semiconductor is almost transparent at low intensities of the incident light.

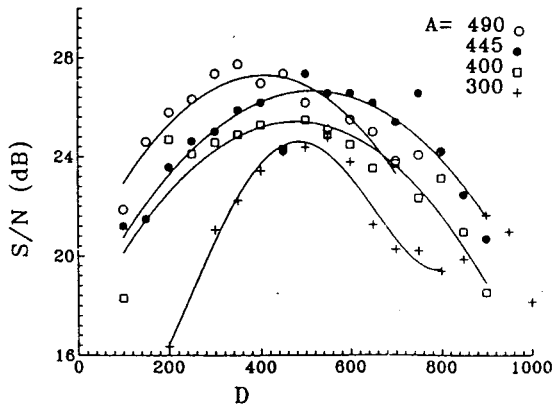

FIG. 21. The signal-to-noise ratio of the transmitted light intensity as a function of the noise strength (in arbitrary units) for different amplitudes A (in arbitrary units) of the modulation of the incident light intensity. The lines are to guide the eye.

Increasing the intensity, the absorbed fraction of light heats up the probe, which in turn induces a stronger light absorption—a nonlinear effect. For large intensities of the incoming light, the transmitted intensity is therefore small. Ramping down the intensity of the incoming light, the transmitted intensity becomes larger again, but describes a hysteresis loop (see Fig. 20) if the absorbed fraction of light is a steep function of the temperature. For increasing ramping speed, the hysteresis loop smears out, but its area increases (a quantitative study of the overshoot has been done by Grohs *et al.*, 1991, and Jung *et al.*, 1990). Thermally optically bistable semiconductors have been discussed for the design of optical parallel computers (Grohs *et al.*, 1989).

Experiments on stochastic resonance have been performed (Grohs *et al.*, 1994) with a semiconductor (CdS). The CdS crystal had a thickness of about 6 μm and shows thermally induced optical bistability (Lambsdorff *et al.*, 1986; Grohs *et al.*, 1989) under illumination with an Ar^+ laser ($\lambda = 514.5$ nm). A two-beam setup has been used for the experiments, with both beams incident on the same spot of the crystal and having an equal diameter of approximately 100 μm. The transmission state of the crystal is read by a constant beam with an intensity that is too small to induce nonlinear behavior by itself. The intensity of the second beam consists of a constant part to hold the system at the working point (i.e., in the bistable regime), and of a weak periodic signal. Moreover, the weak periodic signal is perturbed by additional injected noise ξ with a controllable amplitude. The transmitted intensity has been measured as a function of time and the power spectrum has been measured. In Fig. 21, the signal-to-noise ratio is shown as a function of the strength of the injected noise. It shows the bell-shaped curve, which is characteristic of stochastic resonance.

5. Optical trap

In the experiment by Simon and Libchaber (1992) a spatial bistable potential was generated by optical means. The experimental setup was based on the fact

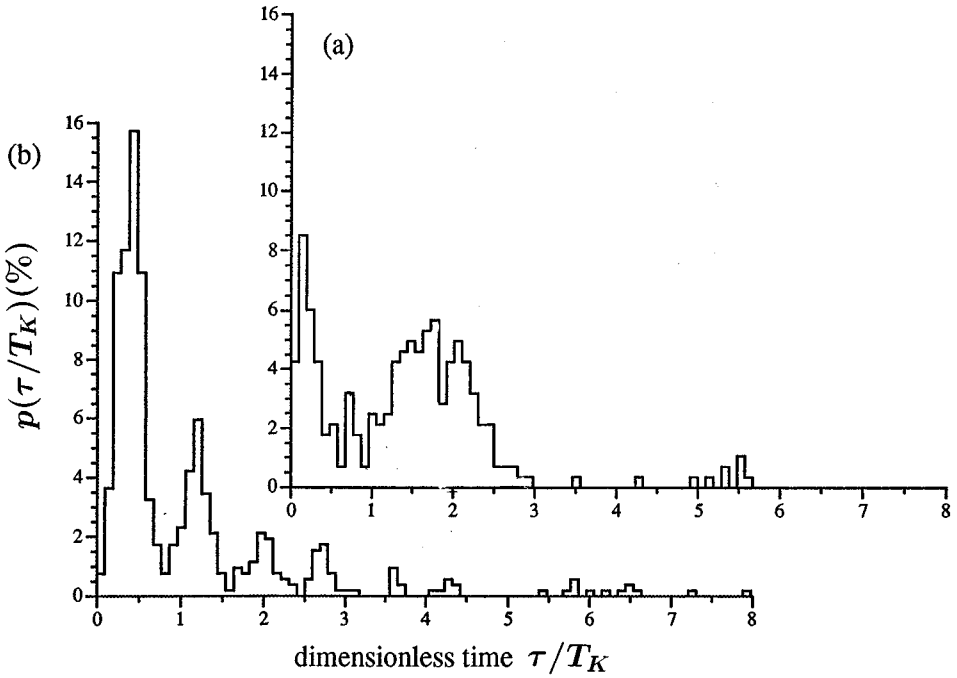

FIG. 22. Escape-time distributions of a particle in an optical trap. The time is measured in units of the mean escape time T_K (from one potential minimum to the other one). (a) The period of the forcing in units of the mean escape time was chosen as $T/T_K = 3.08 > 1$; (b) the period is given by $T/T_K = 0.76 < 1$. While in (b), the peaks are clearly located at odd multiples of half the forcing period, the second peak in (a) is shifted to the left (as far as the accuracy allows for such an interpretation).

that in the presence of an electrical field gradient, a dielectric object (here a 1 μm glass sphere) moves towards the region of highest field strength. The electric field of a laser beam has typically a transverse Gaussian intensity profile, so that dielectric objects are pulled into the beam axis. The two double wells are created by two Gaussian beams obtained from one beam of an Ar laser by utilizing beam splitters. In order to observe stochastic resonance, the depths of the potential wells have to be modulated periodically, which is achieved by modulating the intensity of the two partial beams. The experimental setup was positioned under a microscope so that the motion of the glass sphere in water was directly observable. The pictures were recorded on video and electronically analyzed.

Simon and Libchaber measured the distribution of times the dielectric sphere stayed in one well before it was kicked into the other one. In the absence of modulations, they obtained an exponentially decaying distribution. In the presence of the periodic forcing, they observed a sequence of peaks at odd multiples of the half driving period, with exponentially decaying peak height as shown in Fig. 22. The time is measured in units of the mean escape time T_K out of a potential well in the absence of periodic modulation, i.e., $\tilde{t}=t/T_K$. The period of the modulation in Fig. 22 is measured in the same units. They are given by $T/T_K=3.08$ (a) and $T/T_K=0.76$ (b). The first peaks are observed at $\tilde{t}\approx 1.54$ (a) and $\tilde{t}\approx 0.38$ (b), i.e., at the half period of the driving. The other peaks are located at odd multiples of the half period of the driving as predicted by the theory in Sec. IV.C.

In the case that the dwell time equals half the period T an optimal synchronization occurs, leading to the concentration of the escape within the first period; thus anticipating the notion of stochastic resonance in symmetric, bistable systems as a ''resonant'' synchronization phenomenon (see Sec. IV).

B. Electronic and magnetic systems

In this subsection we review some applications of stochastic resonance to electronic and magnetic systems. We recall that the very first experimental verification of stochastic resonance was realized in an electronic circuit, a simple Schmitt trigger (Fauve and Heslot, 1983). Since then, stochastic resonance has been observed in a variety of more or less complicated electronic devices, mostly constructed with the purpose of building flexible and inexpensive simulation tools. A rather peculiar electronic device that exhibits stochastic resonance is the tunnel diode, a semiconductor device with a bistable characteristic I-V curve, whose dynamics can be controlled by tuning the operating voltage. Due to the fast switching dynamics between stable states (a few tenths of a ns), stochastic resonance in a tunnel diode has been observed for forcing frequencies as high as 10 KHz (Mantegna and Spagnolo, 1994, 1995, 1996). More recently, stochastic resonance has been reported also in a non-bistable standard np semiconductor diode (Jung and Wiesenfeld, 1997). Further experimental evidence of stochastic resonance driven by externally time-modulated magnetic fields (magnetic stochastic resonance) was reported by Spano, Wun-Fogle, and Ditto (1992) in magnetoelastic ribbons, and by I and Liu (1995) in weakly ionized magnetoplasmas. Finally, magnetic stochastic resonance was predicted theoretically by Grigorenko, Konov, and Nikitin (1990) and Grigorenko and Nikitin (1995) for the interdomain magnetization tunneling in uniaxial ferromagnets, by Raikher and Stepanov (1994) for single-domain uniaxial superparamagnetic particles, and by Pérez-Madrid and Rubí (1995) in an assembly of single-domain ferromagnetic particles dispersed in a low-concentration solid phase. In recent experiments, stochastic resonance has been demonstrated in Bi-substituted ferrite-garnet films (Grigorenko *et al.*, 1994) and also in yttrium-iron garnet spheres, where the noise-free, chaotic spin-wave dynamics alone induces stochastic resonance in the presence of an external modulation (Reibold *et al.*, 1997).

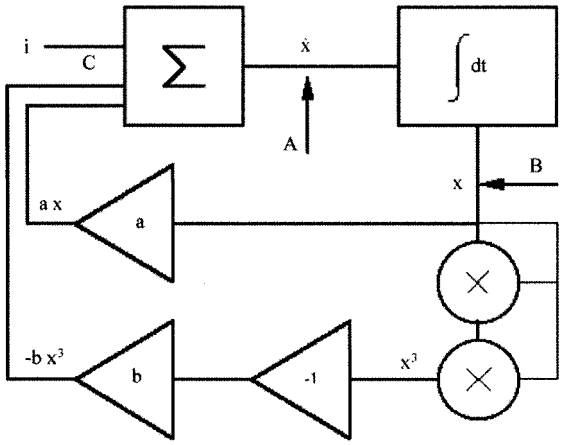

FIG. 23. Functional block scheme for simulating a heavily damped particle moving in a quartic double-well potential; see Eq. (2.1). The triangles denote operational amplifiers.

1. Analog electronic simulators

As mentioned in Sec. II.C, electronic circuits have been widely employed in the study of nonlinear stochastic equations (for reviews, see McClintock and Moss, 1989; Fronzoni *et al.*, 1989). Initially (Debnath *et al.*, 1989; Gammaitoni, Marchesoni, *et al.*, 1989; Gammaitoni, Menichella-Saetta, Santucci, Marchesoni, and Presilla, 1989; Zhou and Moss, 1990, Hu *et al.*, 1991), the stochastic resonance studies via analog simulations concentrated on the simulation of the standard quartic double-well system of Eq. (2.1). The temporal behavior of the stochastic process $x(t)$ can be reproduced by using a voltage source $v(t)$ that obeys Eq. (2.1): the coefficients for the dynamical flow are realized by means of a suitable combination of passive analog components, like resistors and capacitors. Active elements (transistors, signal generators, etc.) are employed to simulate more

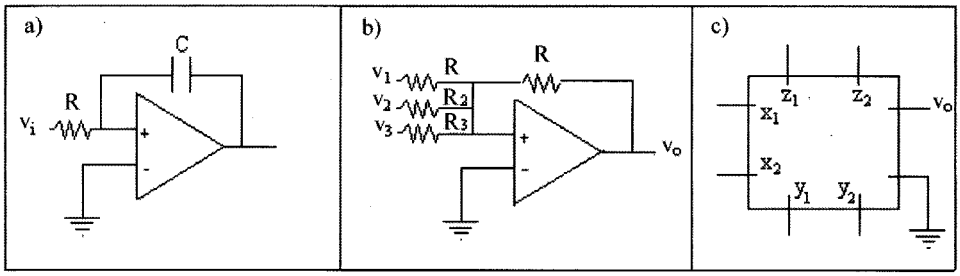

FIG. 24. Circuits for the functional blocks. (a) Miller integrator; (b) adder-amplifier; (c) multiplier.

complicated potential functions. The block scheme of the circuit corresponding to Eq. (2.1) is drawn in Fig. 23. The signal in **A** is assumed to represent the derivative $\dot{x}(t)$ of the variable of interest at time t. In **B**, after the integration block, the signal $x(t)$ is fed into three input terminals: the terminal of the amplifier block **a**, to obtain the signal ax, and the terminals of two multiplier blocks **X**, which yield x^2 after the first block, and x^3 after the second block. The latter signal is then inverted and amplified through two cascaded amplifying blocks. Finally, the three signals in **C** are added together through block Σ to give the starting signal $\dot{x}(t)$.

The realization of an electronic simulation circuit requires the design of specific electronic devices which operate as the single components of the block scheme depicted in Fig. 23. Nowadays, such a purpose is best served by the use of operational amplifiers (Millman, 1983): versatile electronic analog devices characterized by high input impedance, low output impedance, and wide frequency-response range. In Fig. 24 we show the main devices employed to simulate Eq. (2.1). The relevant output voltages v_0 are

$$v_0(t)=\frac{1}{RC}\int_0^t v_i(\tau)d\tau \tag{5.15}$$

for a Miller integrator,

$$v_0(t)=\frac{R}{R_1}v_1+\frac{R}{R_2}v_2+\frac{R}{R_3}v_3 \tag{5.16}$$

for an adder amplifier, and

$$v_0(t)=\frac{(x_1-x_2)(y_1-y_2)}{10}+(z_1-z_2) \tag{5.17}$$

for a multiplier. The block scheme of Fig. 23 can thus be translated into the electronic circuit scheme of Fig. 25. The underdamped dynamics of Eq. (4.1), with $V(x)$ defined in Eq. (4.7), can be simulated by a modified version of the previous circuit—see Fig. 26. Usually both the stochastic force $\xi(t)$ and the periodic modulation $A_0\cos(\Omega t)$ are fed into the simulation circuits by means of suitable voltage generators. The output voltage $v_0(t)$ is sampled at regularly spaced times t_m, with $t_{m+1}-t_m=\Delta t$, digitized as $v_{0,m}=v_0(t_m)$ and then stored into a digital memory unit. The sequence (t_m,v_m) is finally analyzed, mostly off line, by means of standard data-analysis algorithms.

The first, and probably the simplest circuit of this type employed to investigate stochastic resonance dates back to Fauve and Heslot (1983). It consists of a Schmitt trigger, a two-state hysteretic device, that can be easily realized by means of an operational amplifier with positive feedback (Fig. 27). If the input voltage v_i is lower than a threshold value V_+, the output voltage v_0 takes on the constant value $v_0=V$. On increasing v_i through V_+, the output voltage v_0 switches to $v_0=-V$ and stays negative as long as v_i is larger than a second threshold value V_- with $V_-<V_+$. Vice versa, the output transition from $-V$ to V occurs at $v_i=V_-$. The amplitude of the hysteresis cycle is given by V_+-V_-. The stochastic resonance phenomenon follows from the periodic modulation of the position of the center of the hysteresis cycle around the mean value $(V_++V_-)/2$. Such a modulation is reminiscent of the periodic tilting of the wells of a bistable potential model. As a matter of fact, Eqs. (2.6) and (2.7) apply to the output $x(t)\equiv v_0(t)$ of a symmetric Schmitt trigger (where, say, $V_+=-V_-=V_b$) with minor

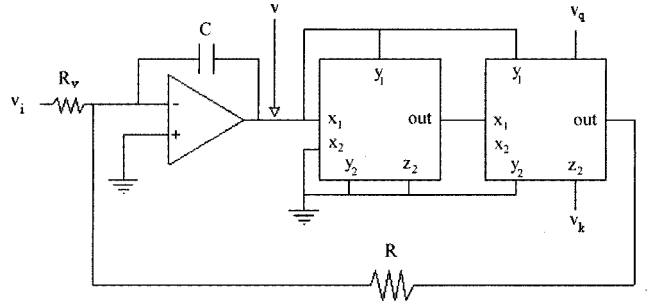

FIG. 25. Simulator circuit for the overdamped dynamics of Eq. (4.3).

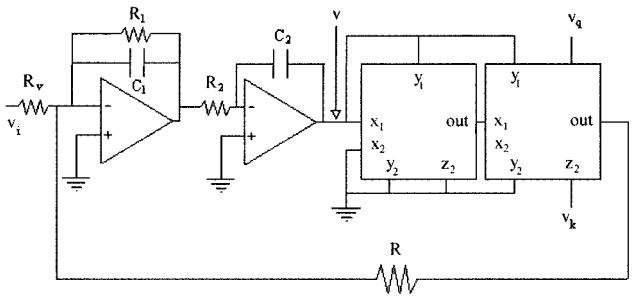

FIG. 26. Simulator circuit for the underdamped dynamics of Eq. (4.1).

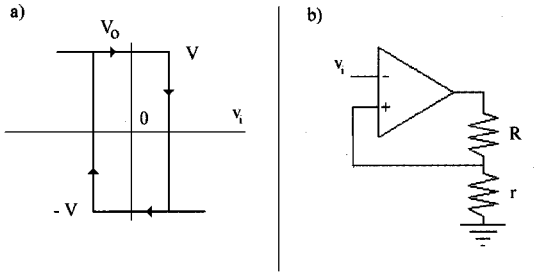

FIG. 27. Operational amplifier in the Schmitt trigger configuration: (a) transfer characteristic; (b) electronic scheme.

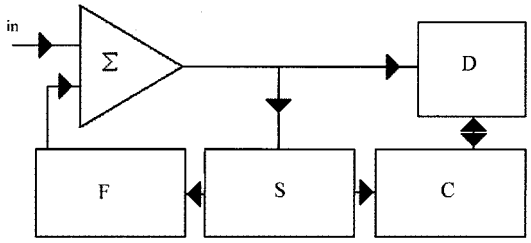

FIG. 28. Block scheme of an EPR system. Block **S**: EPR spectrometer; block **C**: measurement devices; block **D**: data-acquisition system; block **F**: feedback system; block Σ: adder.

changes. For a Gaussian, exponentially autocorrelated input signal $v_i(t)$ with zero mean, variance σ_i^2, and correlation time τ_i, the parameters in Eqs. (2.7) read $x_m=V$, $D=\sigma_i^2\tau_i$, and $r_K=[T_K]^{-1}$. The time $T_0(V_b)$ denotes the mean-first-passage time for $v_i(t)$ to diffuse from $-V_b$ up to V_b; in the subthreshold limit $\sigma_i \ll V_b$ it may be approximated to $\tau_i\sqrt{2\pi}(\sigma_i/V_b)\exp(V_b^2/2\sigma_i^2)$ (Melnikov, 1993; Shulgin *et al.*, 1995). Note that when the amplitude of the hysteresis cycle is forced to zero, the two thresholds overlap and we end up with a single threshold system (see Sec. VII.A.1).

By now, stochastic resonance has been studied in a variety of analog circuits: symmetric and asymmetric quartic double-well potentials (Debnath *et al.*, 1989; Dykman, Luchinsky, *et al.*, 1992; Gammaitoni, Marchesoni, and Santucci, 1994; Gammaitoni, Marchesoni, *et al.*, 1994); the Hopfield neuron potential (Bulsara, Jacobs, Zhou, Moss, and Kiss, 1991); the Fitzhugh-Nagumo neuron model (Wiesenfeld *et al.*, 1994), to mention only a few.

2. Electron paramagnetic resonance

An EPR system consists of a paramagnetic sample placed in a microwave cavity. A microwave generator irradiates the sample while a feedback electronic circuit locks the oscillator frequency to the resonant frequency ν_c of the cavity. A static magnetic field H_0 is applied to the cavity and slowly modulated in order to vary the Larmor frequency $\nu_0=\gamma H_0/2\pi$ of the sample. Here γ is the gyromagnetic factor. The cavity response, determined by measuring the reflected microwave power, usually exhibits a single minimum at $\nu=\nu_c$; however, in the presence of a strong coupling between the cavity and the spin system (a high number of paramagnetic centers), one observes a splitting of the resonance frequency into two frequencies and the cavity response exhibits two distinct minima separated by a local maximum. The block scheme of an EPR experiment is shown in Fig. 28: an electronic adder (block Σ); a standard microwave spectrometer (block **S**) made of a microwave generator, a resonant cavity, and the relevant circuitry; and the feedback system (block **F**) that locks the microwave source frequency to the maximum absorption of the cavity. Block **C** contains the measurement instrumentation, mainly a frequency counter, to monitor the working frequency, and a power meter to measure the power reflected from the cavity. Block **D** represents the data acquisition system.

In such a device, stochastic resonance was observed first by monitoring the working frequency ν (Gammaitoni, Marchesoni, *et al.*, 1991; Gammaitoni, Martinelli, *et al.*, 1991, 1992). A polypyrrole paramagnetic sample was placed in the resonant cavity. The reflection coefficient of the cavity, measured as the ratio between the reflected to the incoming power, was monitored by varying the working frequency. Under proper conditions (strong coupling) the reflection coefficient, as a function of the frequency, showed two separated minima, both stable working points for the spectrometer. The dynamical behavior of the frequency ν is driven by the feedback system. Under stationary conditions, ν fluctuates around the frequency of one of the two minima of the reflection coefficient due to the action of the internal noise of the system. When such noise intensity grows appreciable compared to the height of the barrier that separates the two minima, random switches are observed. Under such circumstances the EPR system shows a noise-driven operating frequency. Its dynamics can be described by the approximate stochastic differential equation:

$$\ddot{\nu}=-\gamma\dot{\nu}-V'(\nu)+\xi(t), \tag{5.18}$$

where $V(\nu)$ denotes the effective bistable potential related to the reflection coefficient. The same dynamics can be observed by measuring the error voltage signal generated by the feedback system. On inserting in the feedback loop an external signal made of a periodic and a random component and varying the intensity of the injected noise, behavior typical of stochastic resonance was detected and measured.

3. Superconducting quantum interference devices

The basic components of a SQUID are a superconducting loop and a Josephson junction. For practical purposes, a SQUID can be envisioned as an electromagnetic device that converts a magnetic flux variation into a voltage variation and, as such, it has been successfully employed in monitoring small magnetic field fluctuations. One of the major limitations to a wide use of these devices is their extreme sensitivity to environmental noise. Recently, two different groups (Hibbs *et al.*, 1995; Rouse *et al.*, 1995) succeeded in operating SQUIDs under stochastic resonance conditions with the aim of in-

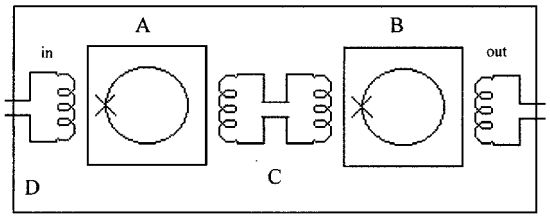

FIG. 29. Block scheme of the SQUID system. Block A: test SQUID, driven by the external signal; block B: measurement SQUID; block C: inductive coupling between the SQUIDs and with the outside circuitry; block D: low-temperature shield.

creasing low magnetic-field detection performance. The dynamics of the magnetic flux Φ trapped in a standard rf. SQUID can be generally described in terms of a second-order differential equation:

$$LC\ddot{\Phi} = -\tau_L\dot{\Phi} - V'(\Phi) + \Phi_e(t), \tag{5.19}$$

where

$$V(\Phi) = \Phi + (\beta/2\pi)\sin(2\pi\Phi) \tag{5.20}$$

plays the role of an effective potential and $\Phi_e(t)$ represents an externally induced flux variation. Here, the flux Φ is measured in units of the fundamental flux quantum $\Phi_0 = h/2e$; L is the inductance of the loop, while C is the junction capacitance and $\tau_L = L/R_j$, where R_j is the normal-state resistance of the junction. The quantity $\beta = 2\pi L i_c/\Phi_0$, with i_c being the loop critical current, is the adjustable parameter that allows us to set the shape of the effective potential. With a proper choice of β and for small Φ values, the system undergoes bistable dynamics. The SQUID loop can be shunted by a low resistance in order to reduce the capacitance and discard inertial effects in the flux [Eq. (5.19)].

The block scheme of a generic SQUID system is shown in Fig. 29. Blocks A and B represent two SQUIDs. The first one is driven with the external signal and the second one is used to pick up the signal output. The inductive coupling between the two loops and with the outside circuitry is also shown (block C). The system is shielded by a low-temperature cage (block D). Stochastic resonance was observed both in the external noise-injected configuration (Hibbs *et al.*, 1995) and in the thermally driven configuration (Rouse *et al.*, 1995), where the switching of the magnetic flux was driven by the internal noise inherent in the SQUID. In both cases a low-frequency periodic signal was injected externally.

C. Neuronal systems

The development of stochastic resonance took a large leap forward when its potential relevance for neurophysiological processes had been recognized. Longtin, Bulsara, and Moss (1991) observed that interspike interval histograms of periodically stimulated neurons exhibit a remarkable resemblance to residence-time distributions of periodically driven bistable systems (Gammaitoni, Marchesoni, Menichella-Saetta, and Santucci, 1989; Zhou *et al.*, 1990). In this section, we report on the relevant neurophysiological experiments and describe how stochastic resonance enters naturally into standard models for neuronal dynamics. By now, stochastic resonance is a well accepted paradigm in the biological and neurophysiological sciences, and several recent reviews on neurophysiological applications of stochastic resonance are available (Moss, 1994; Moss *et al.*, 1994; Moss and Wiesenfeld, 1995a, 1995b; Wiesenfeld and Moss, 1995). Thus we keep this subsection—though there is a prodigious potential for future applications—somewhat tight.

1. Neurophysiological background

There is a large variety of types of neurons in the nervous system of animals and humans with variations in structure, function, and size. Let us restrict ourselves here to a canonical neuron (Amit, 1989), which presents the underlying functional skeleton for all neurons. The canonical neuron is divided into three parts, an input part (the *dendritic arbor*), a processing part (the *soma*), and a signal transmission part (the *axon*).

A neuron communicates via *synapses*, which are the interfaces between its dendrites and axons of presynaptic neurons, i.e., neutrons that talk to the considered neuron. There are a number of dendritic trees entering the soma of the neuron. Usually, one axon leaves the soma and then, downstream, it branches repeatedly to communicate with many postsynaptic neurons, i.e., the neurons the specified neuron is talking to. The fundamental process of neural communication is based upon the following sequence:

(1) The neural axon is in one of two possible states. In the first state, it propagates an action potential based on the result of the processing in the soma. The shape and amplitude of the propagating action potential—the potential difference across the cell membrane—is very stable, and is replicated at the branching points in the axon. The amplitude is of the order of 10^{-1} mV. In the second state of the axon, i.e., the resting state, no action potential is propagated along the axons.
(2) When the propagating action potential reaches the endings of the axons it triggers the secretion of *neurotransmitters* into the synaptic cleft.
(3) The neurotransmitters travel across the synapse and reach the membrane of the postsynaptic neuron. The neurotransmitters bind to receptors that cause the opening of channels, allowing the penetration of ionic currents into the postsynaptic neuron. The amount of penetrating current per presynaptic spike is a parameter that specifies the efficiency of the synapse. There are different ion channels for different ions. To open, say, a potassium channel, a specific neurotransmitter substance is required.
(4) In the absence of a neurotransmitter the resting potential of the membrane of the postsynaptic neuron is determined by the balance of the resting fluxes of ions such as sodium and potassium. The resting

membrane voltage is typically slightly above the low-lying potassium voltage. The opening of say a sodium channel disturbs the equilibrium and triggers a postsynaptic potential close to the high sodium voltage. The membrane voltage is bound between the lower potassium voltage and the higher sodium voltage. The fact that the rest state is very close to the lower limit leads to a rectification of external stimulus in sensory neurons and is of particular importance for the study of stochastic resonance in neurons.

(5) The postsynaptic potential diffuses in a graded manner towards the soma. It loses thereby around 80% of its amplitude. Here, in the processing unit of the neuron, the inputs from all presynaptic neurons (of the order 10^4) are summed. The individual postsynaptic potentials are about 1 mV in amplitude. These inputs may be *excitatory*—depolarizing the membrane of the postsynaptic neuron, increasing the probability of a neuronal discharge event (spike), or they may be *inhibitory*—hyperpolarizing the postsynaptic membrane, thereby reducing the probability of a spike. The high connectivity allows for two kinds of summation processes, temporal and spatial summation. Both summation processes are used in nature. Having a serial input of a train of incoming pulses at **one** synapse, local summation can take place. The typical separation of the pulses is, however, of the same order as the typical decay time of a postsynaptical potential (leakage rate). Spatial summation of incoming events from **many** different synapses does not suffer from the leakage rate, but requires a spatial distribution of (even very little) information throughout a local neural network.

(6) If the sum of postsynaptic potentials arriving within a short period of time exceeds a certain threshold, the probability for the emission of a spike becomes very large. This threshold is of the order of tens of milliseconds and it therefore requires quite a number of inputs to produce a spike.

2. Stochastic resonance, interspike interval histograms, and neural response to periodic stimuli

Over the last 50 years a large body of research has been carried out to understand the encoding of acoustic information on the primary auditory nerve of mammalians (see, for example, Teich *et al.*, 1993, and references therein). Rose, Brugge, Anderson, and Hind (1967) measured the interspike interval histogram of sinusoidally stimulated auditory nerve fibers. A few typical examples from a squirrel monkey are shown in Fig. 30. On the vertical axes, the numbers of intervals of length τ (horizontal axes) between two subsequent spikes (taken from a long spike train) are shown. The first peak is located at the period T_Ω of the stimulus and the following peaks are located at multiples of T_Ω. In contrast to the conventional theory of auditory information encoding, the results above indicate that the information of the period of the stimulus is also encoded in the temporal sequence of the action potentials (spikes). In other words, there is a correlation between the temporal sequence of neuronal discharge and the time dependence of the stimulus. In the neurophysiological literature this correlation is termed *phase locking*. Earlier work reporting the limitation of the phase locking of the neural discharge to the stimulus to small frequencies (<6 kHz) (Rose *et al.*, 1967) has been suggested to be too pessimistic by Teich, Khanna, and Guiney (1993). These authors argue that the synchronization holds up to 18 kHz. They further argue that information about the period of the stimulus is encoded in the temporal sequence of the action potentials over virtually the complete band of acoustical perception.

The resemblance of interspike interval histograms and residence-time distributions of noisy driven bistable systems—see Sec. IV.D—has connected stochastic resonance research with neuronal processes. In Longtin, Bulsara, and Moss (1991), Longtin (1993), and Longtin *et al.* (1994), the interspike interval histograms of a sinusoidally stimulated auditory nerve from a cat have been compared with return-time distributions of the periodically driven quartic bistable potential, i.e.,

$$\dot{x} = x - x^3 + \xi(t) + A_0 \cos(\Omega t), \tag{5.21}$$

and a soft bistable potential

$$\dot{x} = -x + b \tanh(x) + \xi(t) + A_0 \cos(\Omega t), \tag{5.22}$$

with the Gaussian noise

$$\langle \xi(t)\xi(t') \rangle = \frac{D}{\tau_c} \exp\left(-\frac{|t-t'|}{\tau_c} \right),$$
$$\langle \xi(t) \rangle = 0. \tag{5.23}$$

The left potential well corresponds to a neuron that is quiescent; the right potential well corresponds to the firing state. The noise correlation time τ_c has been adjusted to a typical value of the decay of a membrane potential, i.e., $\tau_c = 10^{-4}$ in the same dimensionless units as in Eqs. (5.21) and (5.22). In Fig. 31, the return-time distributions, i.e., the density of time intervals T it takes for the system to be first kicked from one stable state to the other and back again (this second process simulates a reset mechanism), are compared with interspike interval histograms taken from the cat's primary auditory nerve. With only one fitting parameter, it was possible to achieve excellent agreement. In particular, the sequence of peaks in the return-time distributions as well as those in the interspike interval histograms decay exponentially for large return times.

The key question is whether neurons also exhibit stochastic resonance. To this end, Moss and collaborators set up an experiment to study the neural response of sinusoidally stimulated mechanoreceptor cells of crayfish (Douglass, Wilkens, Pantazelou, and Moss, 1993). This experiment has allowed detailed studies of interspike interval histograms to be carried out for a wide range of values of the amplitude and frequency of the stimulation. As in Longtin, Bulsara, and Moss (1991),

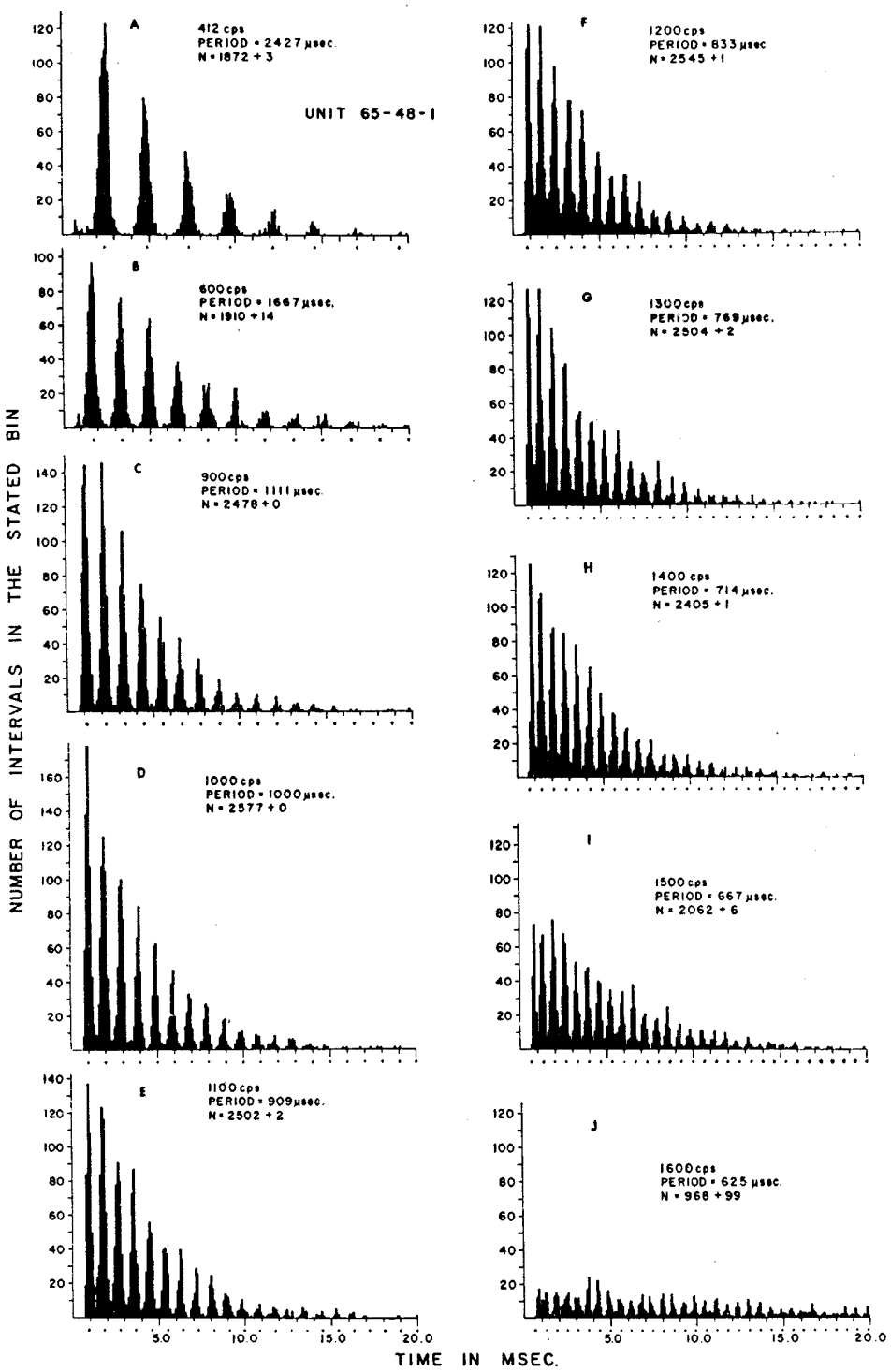

FIG. 30. Distributions of interspike intervals when pure tones of different frequencies activate the neuron. Stimulus frequency in cycles per second (cps) is indicated in each graph. Time on the abscissa is in milliseconds. The dots below the abscissa indicate multiples of the period for each frequency employed. On the ordinate, the number of intervals in one bin is plotted (1 bin=100 μs). N is the total number of interspike intervals in the sample. N is given as two numbers: the first indicates the number of intervals plotted; the second is the number of intervals whose values exceeded the maximal value of the abscissa. After Rose *et al.* (1967).

the interspike interval histograms have been reproduced by return-time distributions of periodically driven bistable systems. Without a stimulus, the interspike interval histograms decay exponentially for large return times. In the presence of periodic driving, Moss *et al.* (1993) found—as in the earlier experiments—a multipeaked structure with exponentially decaying peak heights. In order to identify stochastic resonance, the

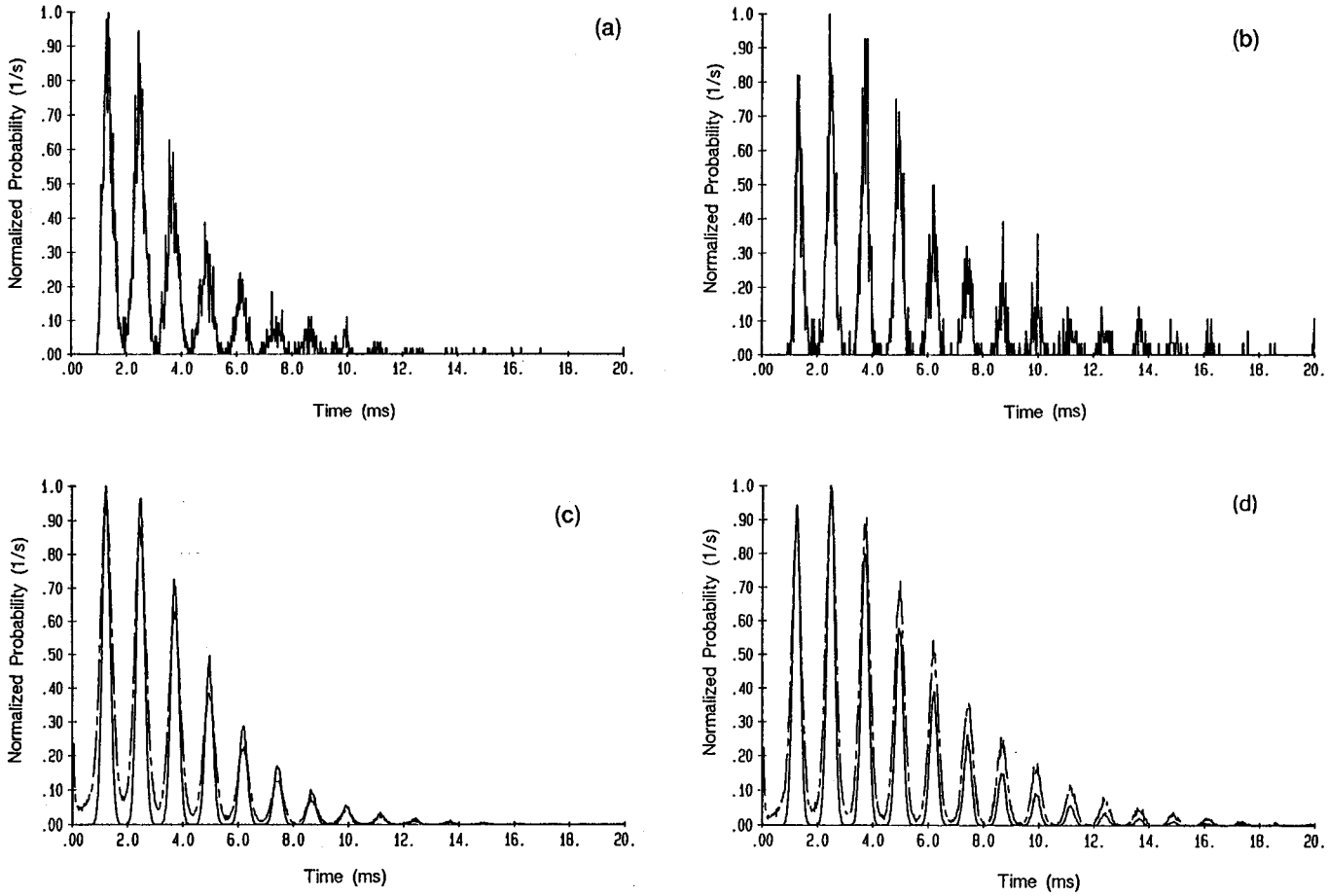

FIG. 31. Return-time distributions for a sinusoidally stimulated auditory nerve: (a), (b) experimental interspike-interval histogram data from a cat primary auditory nerve with an 800-Hz stimulus. The amplitude of the stimulus is 60 dB in (a) and 30 dB in (b). The full curves in (c) and (d) are results obtained from analog simulation of the standard quartic model of Eqs. (5.21)–(5.23). The parameters A_0 and τ_c have been chosen fixed, while D has been fitted to yield best agreement with the interspike-interval histograms in (a) and (b). The best fit in (c) is obtained at a smaller noise level D than in (d). The ratio of driving and noise level in (c) is thus higher than in (d). This is in agreement with the higher stimulus in (a) than in (b). After Longtin, Bulsara, Pierson, and Moss (1994).

noise level had to be changed. To change the intrinsic noise level is not straightforward and requires some more involved experimental procedures (Pei *et al.*, 1996). Douglass, Wilkens, Pantazelou, and Moss (1993) chose to change the noise level by adding noise externally, i.e., by applying to the neuron a sum of a single tone and some noise. The spectral properties of the series of action potentials were analyzed, yielding a power spectrum typified by background noise plus sharp peaks at multiples of the frequency of the stimulus. The signal-to-noise ratio is shown in Fig. 32. The shape of the curve *indicates* stochastic resonance in a living neuron. An alternative way of describing stochastic resonance is the dependence of the peak height of the peaks in the interspike interval histograms on the noise level (Zhou *et al.*, 1990). The height of the first histogram peak at the period of the stimulus runs as a function of the noise strength through a maximum at a value of the noise that is very close to the peak of the signal-to-noise ratio (see Fig. 32).

The experiments provide evidence that the firing of periodically stimulated neurons actually exhibits stochastic resonance. These results, obtained as *in situ* experimental results, are quite satisfactory. The present theory, however, based on bistable dynamics [Eqs. (5.21) and (5.22)], does not describe neuronal dynamics very well. This is because the firing state of a neuron is not a stable state. After a neuron has fired, it becomes automatically quiescent after a refractory time. For a more realistic modeling of stochastic resonance in neuronal processes it is therefore necessary to study different, nonlinear (nonbistable) systems.

3. Neuron firing and Poissonian spike trains

Wiesenfeld, Pierson, Pantazelou, Dames, and Moss (1994) proposed a very elegant approximate theory for modeling neuron firing in the presence of noise and a periodic stimulus. The neuron emits uncorrelated, sharp spikes (δ spikes with weights normalized to unity) at random times t_n. The spiking rate, however, is inhomogeneous, i.e., sinusoidally modulated. This sort of pro-

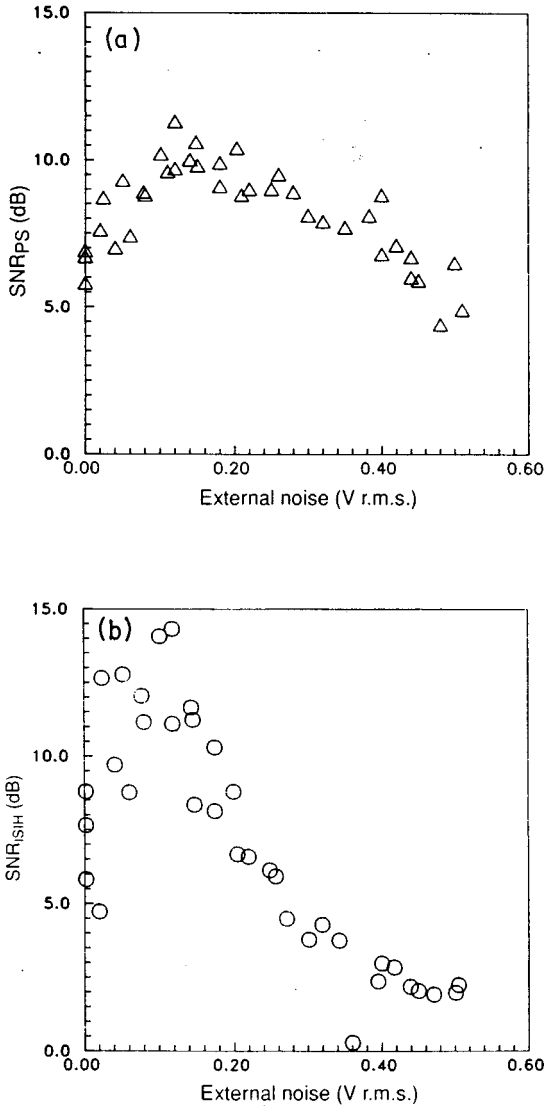

FIG. 32. Stochastic resonance in mechanoreceptor cells of the tail fan of a crayfish: (a) The signal-to-noise ratio obtained from power spectra and (b) from the peak height of the first peak in the interspike-interval histogram as a function of the externally applied noise level.

cess is described by the theory of inhomogeneous Poissonian point processes—see, for example, chapter 6 of Stratonovich (1963). Given the time-dependent spiking rate $r(t)$, the probability to find s events in the time interval T is given by [cf. Eq. (6.33) in Stratonovich (1963)]

$$P_s=\frac{1}{s!}\left[\int_0^T r(t)dt\right]^s \exp\left\{-\int_0^T r(t)dt\right\}. \tag{5.24}$$

The (phase-averaged) spectral density of the spike train consists of a frequency-independent term (white shot noise), given by the time-averaged spiking rate $\bar{r}$, and a sum of δ peaks at multiples of the stimulus frequency, where the intensities of the peaks are given by the Fourier coefficients α_n of the periodic spiking rate $r(t)$, i.e.,

$$S(\omega)=\bar{r}+2\pi\sum_{n=1}^{\infty}|r_n|^2\delta(\omega-n\Omega),$$

$$r_n=\frac{1}{T}\int_0^T r(t)\exp(-in\Omega t)dt. \tag{5.25}$$

At this point, the only assumption made is that there are no correlations between the spikes. It is remarkable that spike-spike correlations yield only an additional term to the spectral density (Jung, 1995), but otherwise leave the result [Eq. (5.25)] invariant. To analyze further the expression (5.25), some approximations need to be made. For $r(t)$, an expression has been chosen, motivated by the rate theory for noise-induced barrier crossing in the presence of periodic external forces, i.e. [cf. Eq. (4.60)],

$$r(t)=\nu\,\exp\left[-\frac{\Delta V}{D}-\frac{A_0x_m}{D}\cos(\Omega t)\right], \tag{5.26}$$

where ΔV is the barrier height in the absence of the forcing, D is the noise strength, A_0 is the amplitude and Ω is the frequency of the periodic forcing, x_m is a scale factor, and the prefactor ν depends on details of the rate process. The expression (5.26) is limited to slow and weak periodic forcing, i.e., Ω is small compared to the local (intrawell) relaxation rate and A_0 is small enough that its effect on the rate can be treated as a perturbation, i.e., A_0x_m/D has to be small. In leading order $(A_0x_m/D)^2$, the signal-to-noise ratio (SNR) is given by the ratio of the intensity of the δ peak of $S(\omega)$ at Ω, i.e.,

$$r_1=\nu I_1(A_0x_m/D)\exp\left(-\frac{\Delta V}{D}\right)\approx\nu\frac{A_0x_m}{2D}\times\exp\left(-\frac{\Delta V}{D}\right)\quad\text{for } A_0x_m/D\ll 1, \tag{5.27}$$

to the noise background in the absence of the periodic driving

$$S_N^0(\Omega)=\bar{r}=\nu\,\exp\left(-\frac{\Delta V}{D}\right), \tag{5.28}$$

yielding

$$SNR=\frac{4\pi|r_1|^2}{\bar{r}}\approx\frac{\pi x_m^2A_0^2}{D^2}\exp\left(-\frac{\Delta V}{D}\right). \tag{5.29}$$

Note that corresponding expression in Wiesenfeld, Pierson, Pantazelou, Dames, and Moss (1994) differs in the prefactor, because they used a different definition of the spectral density.

The signal-to-noise ratio shows the characteristic feature of stochastic resonance, i.e., a peak as a function of the noise strength D. Comparison with data obtained from spike sequences of a mechanically modulated mechanoreceptor of a crayfish (see Fig. 33) shows qualitative agreement. The decrease of the *SNR* at large noise levels, however, is overestimated by this theory. A nonadiabatic theory based on threshold crossing dynamics (see Sec. V.C.5) predicts a slower decrease. Stochastic resonance was also demonstrated in an experiment that uses a sensory hair cell of a cricket (Levin and Miller, 1996).

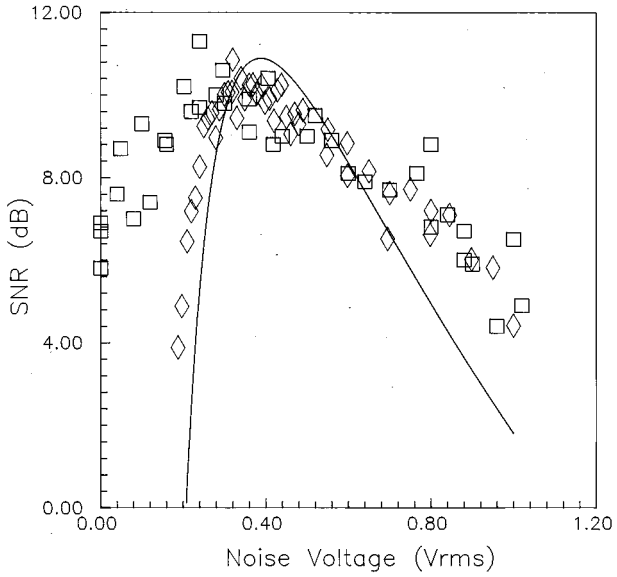

FIG. 33. Signal-to-noise ratio in crayfish mechanoreceptors (squares) compared to the electronic Fitzhugh-Nagumo simulation (diamonds) (Wiesenfeld *et al.*, 1994) and the theory of Sec. V.C.3 (solid curve). The horizontal axis represents the intensity of externally applied noise: hydrodynamic noise in the case of the mechanoreceptors, and electronic noise in the case of neuron models. The crayfish data do not decrease rapidly for small noise because of the residual internal noise of the neuron. Figure provided by Professor Moss.

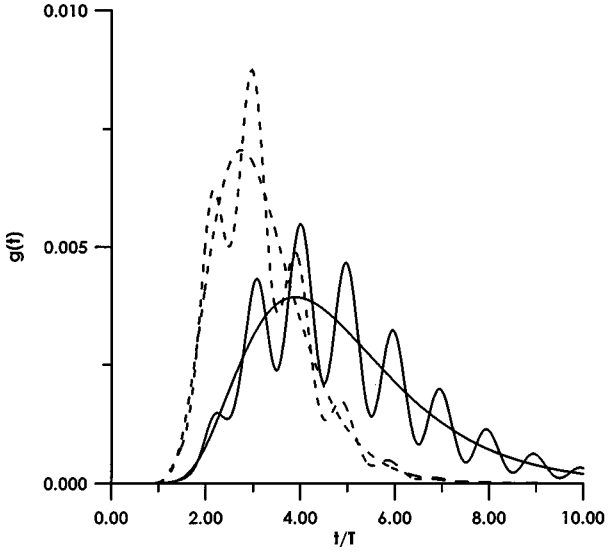

FIG. 34. The first-passage time distribution function $g(t)$ vs time measured in units of the normalized time t/T_Ω (note that in the figure t denotes the first passage time, and $T=T_\Omega$ is the forcing period). The figure contains two sets of curves, one with solid lines and another with dashed lines. The set with solid lines corresponds to a current $i_0=0.065$ A_0. The smooth solid curve (without multiple peaks) represents the distribution function without periodic stimulus ($A_0=0$) while the solid curve with the peaks corresponds to $A_0=0.03$. The smooth dashed curve corresponds to $A_0=0$ and the multipeaked dashed curve corresponds to $A_0=0.03$. The other parameters (for all curves) are $b=20$, $\Omega=0.1$, $D=0.2$.

4. Integrate-and-fire models

A very common model for neuronal dynamics is the so-called integrate-and-fire model. The model works as follows: the input $i(t)$ of the neuron consists of a spike train (cortical neurons) or a continuous signal (sensory neurons). The membrane voltage $u(t)$ is obtained by integrating the input $i(t)$. A capacitance C together with an ohmic resistance R across the membrane leads to an exponential decay of the membrane voltage. With additional noise $\xi(t)$, the equation of motion for the membrane voltage u reads

$$\dot{u}=-\frac{1}{\tau_{RC}}u+i(t)+\xi(t), \tag{5.30}$$

where $\tau_{RC}=RC$. Due to the linearity of Eq. (5.30), the noise $\xi(t)$ can consist of a sum of two contributions stemming from inherent (correlated) fluctuations of the membrane potential and noise in the input. Here, we consider only noisy input and assume that $\xi(t)$ is Gaussian white noise, i.e.,

$$\langle \xi(t)\xi(t')\rangle = 2D\,\delta(t-t'),$$

$$\langle \xi(t)\rangle = 0. \tag{5.31}$$

When the membrane voltage reaches a critical value u_0 (the threshold), the neuron fires, then is reset, and the whole procedure can start all over again.

Denoting by t_n the times at which the neuron fires, the neuron exhibits a spike train of the form

$$y(t)=\sum_n h(t-t_n)=\int_{-\infty}^{\infty} y_d(t-s)h(s)ds,$$

$$y_d(t)=\sum_n \delta(t-t_n), \tag{5.32}$$

where $h(t)$ describes the (fixed) shape of a neuronal spike. Given the distribution function of the times t_n, or equivalently that of the interspike intervals $\Delta_n=t_n-t_{n-1}$, the spectral properties of the spike train can be computed by means of the theory of random point processes [see, for example, Stratonovich (1963)].

In the case of a "perfect" integrator $[1/(RC)=0]$, the Fokker-Planck equation for the membrane voltage, equivalent to Eq. (5.30), reads for a sinusoidal input $i(t)=i_0+A_0\cos(\Omega t)$

$$\frac{\partial P(u,t)}{\partial t}=-[i_0+A_0\cos(\Omega t)]\frac{\partial P(u,t)}{\partial u} + D\frac{\partial^2 P(u,t)}{\partial u^2}. \tag{5.33}$$

The distribution function of the interspike intervals $t=\Delta$ is given by the mean-first-passage time distribution $\rho_{\mathrm{MFPT}}(t)$ [see, for example, Hänggi *et al.* (1990)], which is obtained by solving Eq. (5.33) with absorbing boundary conditions at the threshold b, i.e., $P(u=b,t)=0$, and

subsequent differentiation with respect to time. This task was carried out first analytically in the absence of the periodic stimulus $A_0=0$ [see also the corresponding solution for a finite leakage rate $1/(RC)$ in Goel and Richter-Dyn (1974)], and then numerically in the presence of the stimulus by Gerstein and Mandelbrot (1964). More recently, Bulsara, Lowen, and Rees (1994) and Bulsara, Elston, Doering, Lowen, and Lindenberg (1996) used an approximate image-source method to solve the Fokker-Planck equation in the presence of a weak and slowly varying sinusoidal stimulus. The features of their result follow:

(1) The first-passage time distribution shows in the presence of the periodic stimulus a multipeaked structure (see Fig. 34). For sufficiently large stimulus, the peaks are located at $t^n_{\max}=nT_\Omega$, with $T_\Omega=2\pi/\Omega$ being the period of the stimulus [see also Gerstein and Mandelbrot (1964)].
(2) The peak heights decay exponentially for increasing intervals t.
(3) The peak heights run through a maximum as a function of the noise strength D.

This behavior resembles very closely the behavior of return-time distribution of the bistable models described in Sec. V.C.2. As yet, the theory above is based on a number of unrealistic assumptions; moreover, it contains technical difficulties that have yet to be overcome:

(1) The phase of the sinusoidal stimulus has been reset after each firing event to the same initial value. This approximation is unrealistic from a physiological point of view, since a large amount of information about the coherence of the stimulus is eliminated. A theory of first-passage time distributions in the presence of a periodic forcing that explicitly avoids this assumption has not yet been put forward.
(2) Since the resting voltage of the membrane of a neuron is very close to the potassium voltage, being a lower bound for the variation of the membrane voltage, an originally sinusoidal stimulus becomes strongly rectified. It is therefore not realistic simply to add the sinusoidal stimulus to the membrane voltage in the integrate-and-fire model without taking into account rectification.
(3) Strictly speaking, the method of image sources is applicable only to diffusion processes that are homogeneous in space and time variables. The error made by using this method (as an approximation) in time-inhomogeneous equations such as Eq. (5.33) has not been estimated mathematically.

5. Neuron firing and threshold crossing

The threshold-crossing model for neuronal spiking is motivated from the *leaky* integrate-and-fire model as follows: the input $i(t)$ consists of a constant i_0 and a sinusoidal modulation $A_0\sin(\Omega t)$. In the absence of noise, the solution of Eq. (5.30) reads for large times

$$u_\infty(t)=i_0\tau_{RC}+\frac{A_0\tau_{RC}}{\sqrt{1+\Omega^2\tau_{RC}^2}}\sin(\Omega t-\varphi_{RC}), \qquad (5.34)$$

where $\tan(\varphi_{RC})=\Omega/\tau_{RC}$. The threshold is larger than the maximum of $u_\infty(t)$, i.e., we assume a subthreshold stimulus. In the presence of the noise $\xi(t)$, the membrane voltage $u(t)$ will randomly cross the threshold. In contrast to the integrate-and-fire model, the membrane voltage is *not* reset after a threshold crossing in the models being discussed here. The threshold-crossing models are relying on a stochastic self-resetting due to the noise itself.

The simple picture we are drawing is the following: the input of our threshold trigger consists of the sum of a sinusoidal signal with amplitude $A_0\to A_0\tau_{RC}/\sqrt{1+\Omega^2\tau_{RC}^2}$ and random noise $\xi(t)$ which occasionally crosses the reduced threshold $b\to b-i_0\tau_{RC}$. Whenever the threshold b is being crossed (at times t_n), a spike is created. This yields a stochastic spike train given in Eq. (5.32). To keep things simple, we assume a δ-shaped spike with area normalized to unity, i.e., $h(t)=\delta(t)$ in Eq. (5.32). In specific terms, we assume Gaussian-colored noise $\xi(t)$ with a zero mean and the correlation function

$$\langle\xi(t)\xi(0)\rangle=\frac{D}{\tau_2^2-\tau_1^2}\left[\tau_2\exp(-t/\tau_2)-\tau_1\exp(-t/\tau_1)\right], \qquad (5.35)$$

where τ_1 and τ_2 are characteristic time scales. Using the fundamental work of Rice (1948), one finds for the threshold crossing rate the central result (Jung, 1995)

$$\begin{aligned} r(t)&=\frac{1}{2\pi\sqrt{\tau_1\tau_2}}\exp\left(-\frac{(1-\bar{A}\sin(\Omega t))^2}{2\bar{\sigma}^2}\right)\\ &\quad\times\left[\exp\left(-\frac{\bar{A}^2\epsilon^2\cos^2(\Omega t)}{2\bar{\sigma}^2}\right)\right.\\ &\quad\left.+\frac{1}{2}\bar{A}\epsilon\sqrt{\frac{2\pi}{\bar{\sigma}^2}}\cos(\Omega t)\operatorname{erfc}\left(-\frac{\bar{A}\epsilon\cos(\Omega t)}{\sqrt{2\bar{\sigma}^2}}\right)\right]\\ &\equiv\frac{1}{\sqrt{\tau_1\tau_2}}f(\bar{A},\bar{\sigma},\epsilon), \end{aligned} \qquad (5.36)$$

with the scaled parameters $\bar{A}=A_0/b$, $\bar{\sigma}^2=\sigma^2/b^2$, $\epsilon^2=\Omega^2\tau_1\tau_2$. The periodicity reflects the encoding of the periodic input signal in the spike train. The power spectrum of the spike train has the same form as in Eq. (5.25) but has an additional term describing the spike-spike correlation function. Computing the Fourier coefficient r_1 of the periodic threshold crossing rate $r(t)$, one finds for the spectral amplification

$$\eta=\frac{4|r_1|^2}{A_0^2}=\frac{1}{\tau_1\tau_2}\,\bar{\eta}(\bar{A},\bar{\sigma}^2,\epsilon). \qquad (5.37)$$

The spectral amplification η describes the encoding gain of the periodicity of the input signal in the stochastic

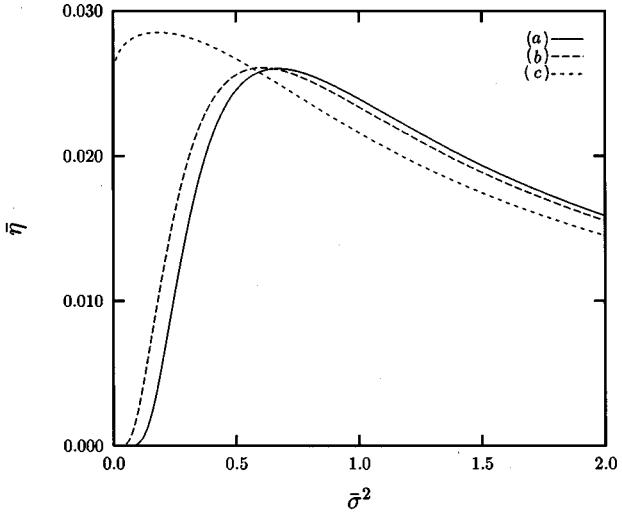

FIG. 35. The scaled spectral amplification $\bar{\eta}$, of Eq. (5.37), is shown as a function of the variance of the noise (a) for $\bar{A}=0.1$, (b) $\bar{A}=0.5$, and (c) $\bar{A}=1$. The time-scale ratio ϵ was chosen as $\epsilon=1$. Note that due to the scaling relation for η in Eq. (5.37), the actual spectral amplification can become much larger than unity (real spectral amplification) if the cutoff frequencies $1/\tau_1$ and/or $1/\tau_2$ are chosen large enough.

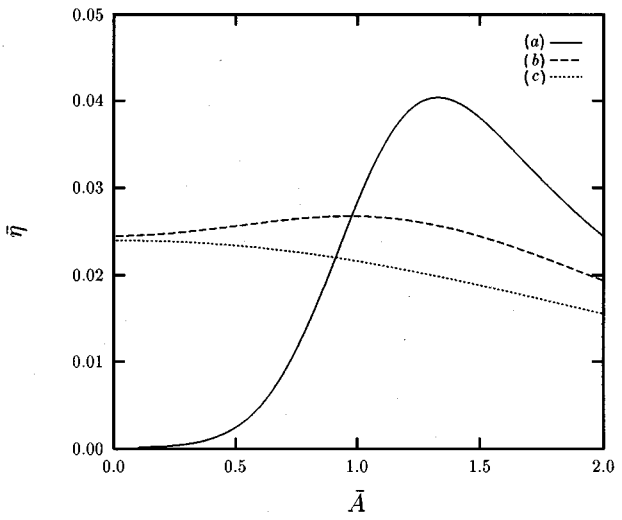

FIG. 36. The scaled spectral amplification $\bar{\eta}$ shown as a function of the amplitude of the sinusoidal signal $\bar{A}$ (a) for $\bar{\sigma}^2=0.1$,(b) $\bar{\sigma}^2=0.5$, and (c) $\bar{\sigma}^2=1$. The time-scale ratio ϵ was chosen as $\epsilon=1$.

spike train. The scaled spectral amplification $\bar{\eta}$ is shown as a function of the variance of the noise in Fig. 35. For $A_0/b<1$, i.e., in the subthreshold regime, the spectral amplification first increases with increasing noise, reaches a maximum at $\bar{\sigma}^2_{\max}\approx 1/2$, and then decreases again. For small time scales $\tau_{1,2}$, the spectral amplification becomes large and describes a real encoding gain *facilitated by random noise*. The position of the maximum is obtained from Eq. (5.36) by expanding for $A_0\tau_{RC}/D\ll 1$, i.e.,

$$\eta=\frac{1}{2}r^2(A_0=0)\left(\frac{1}{\bar{\sigma}^4}+\epsilon^2\frac{\pi}{2\bar{\sigma}^2}\right). \tag{5.38}$$

The first term on the right-hand side of Eq. (5.38) has been obtained within the adiabatic theory of Gingl, Kiss, and Moss (1995), and also by the approach of Wiesenfeld *et al.* (1994) (see Sec. V.C.3), while the other term represents nonadiabatic corrections (Jung, 1995). For large variances of the noise, the nonadiabatic corrections become very important; they yield a decrease of the spectral amplification proportional to $1/\bar{\sigma}^2$ instead of $1/\bar{\sigma}^4$ in the adiabatic limit. The position of the peak deviates significantly from that in a driven symmetric bistable system. In the limit of vanishing frequency Ω, the spectral amplification approaches a limit curve with the maximum at approximately $\bar{\sigma}^2_{\max}=\frac{1}{2}$. Increasing the frequency, the peak increases due to periodic jittering back and forth across the threshold, and shifts towards larger values of the variance $\bar{\sigma}^2$.

In Fig. 36, the scaled spectral amplification $\bar{\eta}$ is shown as a function of the amplitude $\bar{A}$. For $\bar{\sigma}^2<\bar{\sigma}^2_{\max}$, the spectral amplification shows a maximum as a function of the amplitude, as in the quartic double-well system (Sec. IV).

In conclusion, stochastic resonance has been demonstrated experimentally in neuronal systems although these systems are not bistable. In the course of developing a theoretical understanding of these experimental results, the notion of stochastic resonance has been generalized to include excitable systems with threshold dynamics. In this latter context we refer also to related work of Collins and collaborators on aperiodic stochastic resonance (Collins *et al.*, 1995a, 1995b, Collins, Chow, *et al.*, 1996; Collins, Imhoff, and Grigg, 1996; Heneghan *et al.*, 1996), and the recent developments aimed at detecting stochastic resonance in nondynamical systems with no intrinsic sharp thresholds (Fuliński, 1995; Barzykin and Seki, 1997; Bezrukov and Vodyanoy, 1997; Jung, 1997; Jung and Wiesenfeld, 1997).

VI. STOCHASTIC RESONANCE—CARRIED ON

A. Quantum stochastic resonance

Recently, the question has been posed whether stochastic resonance manifests itself on a quantum scale. In particular, recent experiments in a macroscopic quantum system, such as a superconducting quantum interference device (SQUID), established the mechanism of stochastic resonance in the classical regime of thermal activation (Rouse *et al.*, 1995; Hibbs *et al.*, 1995). The experimental work of Rouse, Han, and Lukens (1995) also addressed nonlinear stochastic resonance, such as the noise-induced resonances, which are elucidated in Sec. VII.D.1 below. Because quantum noise persists even at absolute zero temperature, the transport of quantum information should naturally be aided by quantum fluctuations as well. Indeed, quantum mechanics

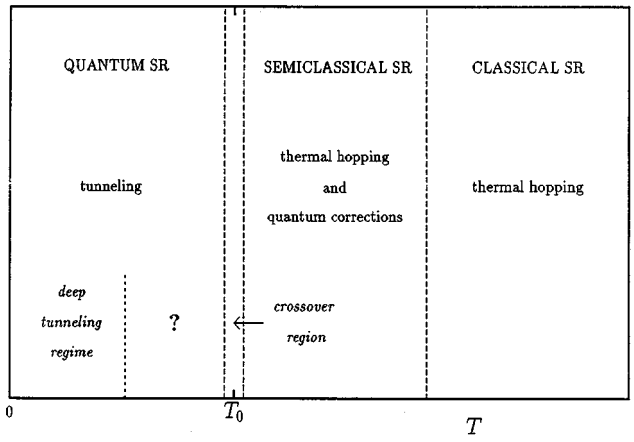

FIG. 37. The dominant escape mechanisms out of a metastable potential, and corresponding regimes for stochastic resonance depicted vs temperature T. T_0 denotes the crossover temperature below which quantum tunneling dominates over thermally activated hopping events. We note that T_0 depends on the potential shape and also on the dissipative mechanism (Hänggi *et al.*, 1985). The relative size of the corresponding stochastic resonance regions hence vary with the dissipation strength. In the region marked by a question mark, quantum stochastic resonance has presently not yet been investigated analytically; a two-level approximation is no longer adequate in that temperature regime.

provides the nonlinear system with an additional channel to overcome a threshold. This additional channel is provided by quantum tunneling, i.e., a particle can tunnel through a barrier without ever going over it. As a matter of fact, we shall see that the classical stochastic resonance effect can be assisted by quantum tunneling contributions even at finite temperatures. For strongly damped systems, such contributions can enhance the classical stochastic resonance effect up to two orders of magnitude. With decreasing temperature, quantum transitions thus start to dominate over thermally activated transitions below a crossover temperature T_0 (Hänggi *et al.*, 1985), which characterizes the temperature at which activated hopping and quantum tunneling become equally important. Its value depends both on the potenial barrier shape and the dissipative mechanism. It is interesting to note that this crossover temperature can be quite large, reaching in some physical and chemical systems values larger than 100 K (Hänggi *et al.*, 1990; Hänggi, 1993). On the other hand, in Josephson systems (Schwartz *et al.*, 1985; Clarke *et al.*, 1988; Hänggi, 1993) and in mesoscopic, disordered metals (Golding *et al.*, 1992; Chun and Birge, 1993) tunneling dominates in the cold mK region only. The various escape mechanisms that predominate the physics of stochastic resonance as a function of temperature T are depicted in Fig. 37.

1. Quantum corrections to stochastic resonance

Let us first focus on the regime $T \gtrsim T_0$, where quantum tunneling is not the dominant escape path, but nevertheless leads to significant quantum corrections. The role of quantum tunneling in this regime has been investigated only recently by Grifoni *et al.* (1996). These authors investigated the dissipative inertial bistable quantum dynamics $x(t)$ at thermal temperature T in a double-well configuration which is modulated by the periodic force $A_0 \cos(\Omega t)$. The asymptotic power spectrum $S_{as}(\omega) = \int_{-\infty}^{\infty} \exp(-i\omega\tau)\overline{K_{as}}(\tau)d\tau$, cf. Eq. (4.24), of the time-averaged, symmetrized autocorrelation function of $x(t)$ is given by

$$S_{as}(\omega) = 2\pi \sum_{n=-\infty}^{\infty} |M_n(\Omega, A_0)|^2 \delta(\omega - n\Omega). \tag{6.1}$$

Hereby, we introduced the notation $M_n(\Omega, A_0)$ for the complex-valued Fourier amplitude to explicitly indicate the dependence on the relevant parameters. The two quantities to exhibit quantum stochastic resonance are the power amplitude η in the first frequency component of $S_{as}(\omega)$ and the ratio of η to the unperturbed, equilibrium power spectrum $S_N^0(\omega)$ of $x(t)$ in the absence of driving, evaluated at the external modulation frequency Ω, i.e. the so-called signal-to-noise ratio (SNR):

$$\eta = 4\pi |M_1(\Omega, A_0)|^2,$$
$$SNR = 4\pi |M_1(\Omega, A_0)|^2 / S_N^0(\Omega). \tag{6.2}$$

By definition, η has the dimension of a length squared, while SNR has the dimension of a frequency. Thus to investigate the interplay between noise and the coherent driving input, giving rise to the phenomenon of stochastic resonance, we shall consider two dimensionless quantities: The scaled spectral amplification $\tilde{\eta}$, and the scaled signal-to-noise ratio $\widetilde{SNR}$. They read

$$\tilde{\eta} = \frac{4\pi |M_1(\Omega, A_0)|^2}{(A_0 x_m^2 / V_b)^2},$$
$$\widetilde{SNR} = \frac{[4\pi |M_1(\Omega, A_0)|^2 / S_N^0(\Omega)]/\omega_b}{(A_0 x_m / V_b)^2}. \tag{6.3}$$

Here, V_b is the barrier height at the barrier position $x_b = 0$, ω_b denotes the corresponding angular barrier frequency, and $\pm x_m$ are the positions of the two minima of the bistable potential. These two quantities that characterize stochastic resonance can be evaluated within quantum linear-response theory to give for the scaled spectral amplification

$$\tilde{\eta} = \pi \left(\frac{V_b}{k_B T} \right)^2 \frac{1}{\cosh^4(\epsilon_0 / 2k_B T)} \frac{\lambda^2}{\Omega^2 + \lambda^2}. \tag{6.4}$$

Here, k_B is the Boltzmann constant, and $\lambda = r_+ + r_-$ is the sum of the forward and backward quantum rates r_+ and r_-, respectively. These unperturbed quantum rates have been evaluated previously in the literature—see Sec. IX in the review of Hänggi, Talkner, and Borkovec (1990). A possible difference between the left and the right potential minimum is accounted for by the bias energy ϵ_0. The backward and forward rates are related by the detailed-balance condition $r_- = r_+ \exp(-\epsilon_0 / k_B T)$. Note that information about the detailed form of the potential, and the dissipative mechanism as well, is still

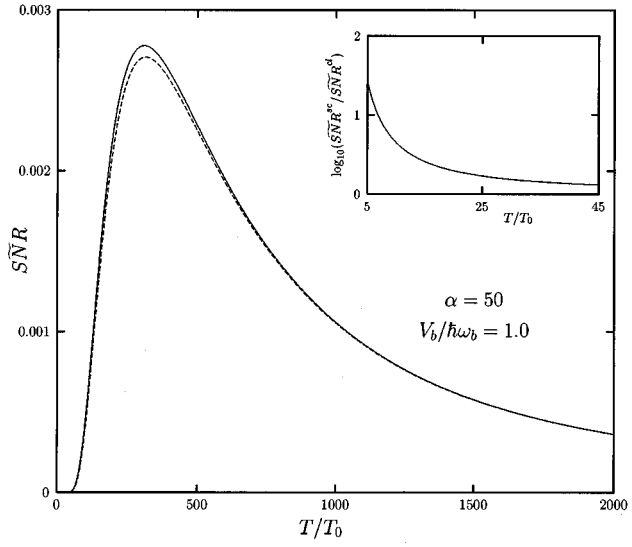

FIG. 38. The scaled signal-to-noise ratio [within linear response; see Eq. (6.5)] $\widetilde{SNR}$ of semiclassical, inertial dynamics in a symmetric double well vs the dimensionless temperature T/T_0, with T_0 denoting the crossover temperature (see text), for ohmic friction γ of strength $\alpha=\gamma/2\omega_b=50$. The solid line gives the dimensionless semiclassical signal-to-noise ratio with tunneling corrections. The dashed line gives the corresponding classical result without quantum corrections. The ratio between semiclassical quantum signal-to-noise ratio, $\widetilde{SNR}$, and the corresponding classical result, $\widetilde{SNR}^{cl}$, is depicted in the inset. Note that the tunneling contribution can enhance stochastic resonance up to two orders of magnitude. From Grifoni *et al.* (1996).

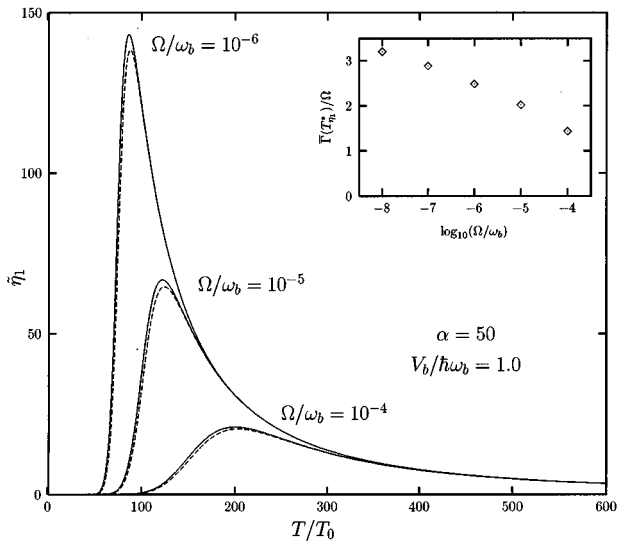

FIG. 39. Scaled spectral amplification $\tilde{\eta}$ [see Eq. (6.4)] in a symmetric double well vs dimensionless temperature (cf. Fig. 38) for different driving frequencies Ω (solid lines). For comparison, the dashed lines give the results for the classical stochastic resonance spectral amplification. The dimensionless ohmic friction strength is $\alpha=\gamma/2\omega_b=50$. The inset depicts the ratio between the total (forward and backward) rate $\overline{\Gamma}\equiv\lambda$ and Ω at the temperature T_η^* where $\tilde{\eta}$ assumes its maximum. The stochastic resonance maximum is thus approximately determined by the condition that twice the escape rate, i.e. $\overline{\Gamma}(T_\eta^*)$, approximately equals the external driving frequency Ω. After Grifoni *et al.* (1996).

contained in the total quantum rate λ. Likewise, one finds the result for the scaled $\widetilde{SNR}$, i.e.,

$$\widetilde{SNR}=\frac{\pi}{2}\left(\frac{V_b}{k_BT}\right)^2\frac{\lambda/\omega_b}{\cosh^2(\epsilon_0/2k_BT)}. \tag{6.5}$$

Both the zero-point energy fluctuations and the dissipative tunneling across the barrier near the barrier top result in a characteristic enhancement of the $\widetilde{SNR}$, or the scaled spectral amplification $\tilde{\eta}$. The enhancement can reach values up to two orders of magnitude as compared to a prediction based solely on a classical analysis. In Fig. 38 we depict the quantum-tunneling-corrected, scaled SNR for zero bias, i.e., $\epsilon_0=0$, together with the enhancement over the corresponding classical study (see the inset).

The temperature dependence at different driving frequencies Ω of the scaled spectral amplification is depicted in Fig. 39 for quantum stochastic resonance in a symmetric ($\epsilon_0=0$) double well subjected to ohmic quantum friction. In presence of tunneling, the role of both temperature and dissipation must be treated simultaneously in a manner consistent with the fluctuation-dissipation theorem (Grifoni *et al.*, 1996). In particular, with strong damping the effects of quantum fluctuations on stochastic resonance can extend well above the crossover temperature T_0. As depicted in the inset of Fig. 39, the stochastic resonance peak is dominated by the two competing effects of an increasing Arrhenius factor and a decreasing factor $(k_BT)^2$ with increasing noise temperature. These two quantities characteristically rule the stochastic resonance effects—see Eqs. (4.51) and (4.54).

2. Quantum stochastic resonance in the deep cold

The situation changes drastically when we proceed towards the extreme cold. Here, we shall focus on the deep quantum regime, where tunneling is the only channel for barrier crossing. In this low-temperature regime, periodic driving induces several new interesting, counterintuitive physical phenomena, such as "coherent destruction of tunneling" (Grossmann *et al.*, 1991), the "stabilization of dissipative coherence" with increasing temperature (Dittrich *et al.*, 1993; Oelschlägel *et al.*, 1993), or the effect of driving-induced quantum coherence (Grifoni *et al.*, 1995). Quantum stochastic resonance within the regime of incoherent tunneling transitions at adiabatic driving frequencies has been investigated first by Löfstedt and Coppersmith (1994a, 1994b) in the context of impurity tunneling in ac-driven mesoscopic metals (Golding *et al.*, 1992; Chun and Birge, 1993; Coppinger *et al.*, 1995). Linear response for quantum stochastic resonance as well as nonlinear quantum stochastic resonance has been investigated in the whole parameter range by Grifoni and Hänggi (1996a, 1996b); their studies encompass adiabatic and nonadiabatic driving frequencies, as well as the role of both an

incoherent (i.e., rate-dominated relaxation) and coherent (i.e., oscillatory-dominated damped relaxation) tunneling dynamics.

In the regime below the crossover regime, i.e., the regime marked by a question mark (?) in Fig. 37, there exist at present no analytical studies of quantum stochastic resonance. This is due mainly to the fact that in this regime the dissipation-driven tunneling dynamics involve many states. At very low temperatures, however, the dynamics are ruled mainly by two tunnel-split levels only. Thus in the deep quantum regime the investigation of quantum stochastic resonance reduces to the study of the dynamics of the spin-boson system in the presence of ohmic dissipation which, in addition, is subjected to periodic driving (Grifoni *et al.*, 1993, 1995; Dakhnovskii and Coalson, 1995; Makarov and Makri, 1995; Goychuk, Petrov, and May, 1996; Makri, 1997). More explicitly, let us consider the driven spin-boson Hamiltonian $H=H_{\rm TLS}(t)+H_B$, i.e.,

$$H_{\rm TLS}(t)=-\frac{\hbar}{2}(\Delta\sigma_x+\epsilon_0\sigma_z)-\frac{\hbar\hat{\epsilon}}{2}\cos(\Omega t)\sigma_z \qquad (6.6)$$

represents the driven bistable system in a two-level-system approximation with $(\hbar\hat{\epsilon}/a)\cos(\Omega t)$ being the applied harmonic force. The σ's are Pauli matrices, and the eigenstates of σ_z are the basis states in a localized representation, while $a\equiv 2x_m$ is the tunneling distance. The tunneling splitting energy of the symmetric two-level system is given by $\hbar\Delta$ while the bias energy is again $\hbar\epsilon_0$. Within the spin-boson model (Leggett *et al.*, 1987; Weiss, 1993), the environment is modeled by a term H_B describing an ensemble at thermal temperature T of harmonic oscillators. The term H_B in addition includes the interaction between the two-level system and the bath via a bilinear coupling in the two-level system-bath coordinates. The effects of the bath are captured by the spectral density $J(\omega)$ of the environment coupling. We make the specific choice of ohmic dissipation $J(\omega)=(2\pi\hbar/a^2)\alpha\omega e^{-\omega/\omega_c}$, where α denotes the dimensionless ohmic coupling strength and $\omega_c\gg\omega_0$ is a cutoff frequency. Insightful exact numerical path-integral studies of this driven, dissipative spin-boson system have been carried out recently by Makri (1997).

The relevant theoretical quantity describing the dissipative dynamics under the external perturbation is the expectation value $P(t)=\langle\sigma_z(t)\rangle$. On the other hand, the quantity of experimental interest for quantum stochastic resonance is the time-averaged power spectrum $S(\omega)$, defined as the Fourier transform of the correlation function

$$K(\tau)=\frac{\Omega}{2\pi}\int_0^{2\pi/\Omega}dt\,\frac{1}{2}\langle\sigma_z(t+\tau)\sigma_z(t)+\sigma_z(t)\sigma_z(t+\tau)\rangle.$$

The combined influence of dissipative and driving forces renders an evaluation of the full correlation function $K(\tau)$ extremely difficult (and hence of the power spectrum). Matters simplify for times t,τ large compared to the time scale of the transient dynamics, where $P(t)$ and

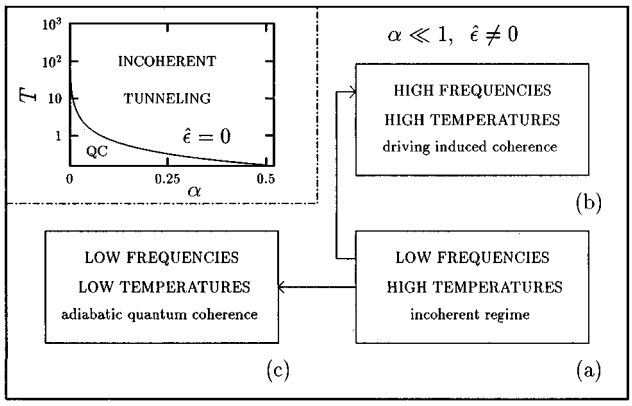

FIG. 40. Sketch of the different regimes for the driven $[(\hbar\hat{\epsilon}/a)\cos\Omega t]$ dissipative tunneling dynamics for a two-level system subject to weak ohmic coupling $\alpha\equiv\gamma(a^2/2\pi\hbar)$ (a denotes the tunneling distance and γ denotes the Ohmic viscous strength). As the temperature T or the driving angular frequency Ω are varied in the parameter space of "TEMPERATURE" and "FREQUENCY" [see the boxes labeled (a), (b), (c)], different novel tunneling regimes are encountered. For strong dimensionless ohmic coupling α, the regimes (a) and (b) extend down to the lowest temperatures. For comparison we also depict the static situation, i.e., $\hat{\epsilon}=0$, in the upper left panel: in it, we sketch the dissipative tunneling behavior in the (T,α) parameter space for quantum *incoherent* and quantum *coherent* (QC) tunneling.

$K(\tau)$ acquire in the asymptotic regime the periodicity of the external perturbation. Upon expanding the asymptotic expectation $P_{as}(t)=\lim_{t\to\infty}P(t)$ into a Fourier series, i.e.,

$$P_{as}(t)=\sum_{n=-\infty}^{\infty}M_n(\Omega,\hat{\epsilon})\exp(-in\Omega t), \qquad (6.7)$$

it is readily seen that the amplitudes $|M_n(\Omega,\hat{\epsilon})|$ determine the weights of the δ spikes of the power spectrum in the asymptotic state $S_{as}(\omega)$ via the relation $S_{as}(\omega)=2\pi\Sigma_{n=-\infty}^{\infty}|M_n(\Omega,\hat{\epsilon})|^2\delta(\omega-n\Omega)$. In particular, to investigate nonlinear quantum stochastic resonance, we shall examine the newly scaled power amplitude η_n in the nth frequency component of $S_{as}(\omega)$, i.e.,

$$\eta_n=4\pi|M_n(\Omega,\hat{\epsilon})/\hbar\hat{\epsilon}|^2. \qquad (6.8)$$

For a quantitative study of quantum stochastic resonance, it is necessary to solve the asymptotic dynamics of the nonlinearly driven dissipative bistable system. In doing so, we shall take advantage of novel results for the driven dynamics obtained by use of a real-time path-integral approach (Grifoni *et al.*, 1993; 1995). At weak and strong ohmic coupling, driving distinctly alters the qualitative tunneling dynamics: see Fig. 40. The incoherent dynamics can still be modeled by rate equations, however. At low driving frequencies, these rate equations are intrinsically Markovian—see region (a) in Fig. 40. As the external frequency Ω is increased and/or when the temperature is lowered, quantum coherence and/or driving-induced correlations render the

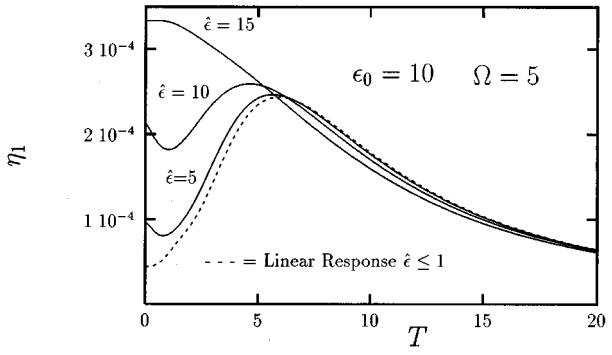

FIG. 41. The spectral amplification η_1, Eq. (6.8), for the periodically driven (driving strength $\hat{\epsilon}$), ohmic damped spin-boson system depicted vs temperatures T at a fixed bias energy $\hbar\epsilon_0=10$ and at an angular driving frequency $\Omega=5$. The dimensionless parameters are defined in the text. For the smallest driving strength $\hat{\epsilon}=5$ we additionally depict the linear-response theory approximation (dashed line). The solid lines give the nonlinear quantum stochastic resonance for the exactly solvable case of ohmic coupling strength at $\alpha=1/2$ (cf. Fig. 40). The data are taken from Grifoni and Hänggi (1996b).

asymptotic dynamics intrinsically non-Markovian—note regions (b) and (c) in Fig. 40.

Let us focus first on some characteristics of quantum stochastic resonance as they emerge from the study of the case $\alpha=1/2$ of the ohmic strength. For the special value $\alpha=\frac{1}{2}$, exact analytical solutions for quantum stochastic resonance are possible (Grifoni and Hänggi, 1996a, 1996b). The resulting fundamental power amplitude $\eta_1\equiv\eta$ is plotted in Fig. 41 as a function of the temperature for different driving strengths $\hat{\epsilon}$. There, and in Fig. 42, frequencies are in units of the bath-renormalized tunneling splitting $\Delta_e=\Delta(\Delta/\omega_c)^{\alpha/(1-\alpha)}[\cos(\pi\alpha)\Gamma(1-2\alpha)]^{1/(2-2\alpha)}$, $\alpha<1$. For $\alpha=\frac{1}{2}$, Δ_e reduces to $\pi\Delta^2/2\omega_c$. For $\alpha>1$, relevant energy scale is set by $\Delta_{\rm ren}$, which equals the previous expression Δ_e without the term in the square brackets (Legget *et al.*, 1987; Weiss, 1993; Löfstedt and Coppersmith, 1994a). The temperatures are in units of $\hbar\Delta_e/k_B$. Note that the spectral amplification is measured in units of $(\hbar\Delta_e)^{-2}$. For highly nonlinear driving fields $\hat{\epsilon}>\epsilon_0$, the power amplitude decreases monotonically as the temperature increases (uppermost curve). As the driving strength $\hat{\epsilon}$ of the periodic signal is decreased, a shallow minimum, followed by a maximum, appears when the static asymmetry ϵ_0 equals, or slightly overcomes, the strength $\hat{\epsilon}$ (intermediate curves). For even smaller external amplitudes, quantum stochastic resonance can be studied within the quantum linear-response theory (dashed curve in Fig. 41). In the linear-response region the shallow minimum is washed out, and only the principal maximum survives. It is now interesting to observe that—because the undriven two-level system dynamics (which comprises linear-response theory) for $\alpha=\frac{1}{2}$ is always incoherent down to $T=0$—the principal maximum arises at the temperature T at which the relaxation process towards thermal equilibrium is maximal. On the other hand, the minimum in η appears in the temperature region where driving-induced coherent processes are of importance. This latter feature is a nonlinear quantum stochastic resonance effect, which linear-response theory clearly cannot describe. In addition, this implies that the power amplitude η plotted versus frequency shows resonances when $\Omega\approx\epsilon_0/n$ $(n=1,2,\ldots)$; correspondingly, the driven dissipative dynamics are intrinsically non-Markovian! For arbitrary values of the ohmic coupling strength, one has to resort to approximate solutions of the dissipative dynamics. For strong coupling $\alpha>1$, or weak coupling $\alpha<1$ and high enough temperatures, the bath-induced correlations between tunneling transitions may be treated within the noninteracting blip approximation (Leggett *et al.*, 1987; Weiss, 1993). A set of coupled equations for the Fourier coefficients M_n can then be derived for any strength and frequency of the driving force. In particular, driving-induced correlations may result in an highly coherent dynamics, leading to resonances in the power spectrum. In this coherent regime, quantum stochastic resonance never occurs: the power amplitudes η_n always show a monotonic decay as the temperature is increased (Grifoni and Hänggi, 1996a, 1996b). It is only in the low-frequency regime $\hbar\Omega\ll\alpha k_BT$ that—to leading order—driving-induced non-Markovian correlations do not contribute. The asymptotic dynamics, within the noninteracting blip approximation, are intrinsically incoherent and governed by the rate equation $\dot{P}_{as}(t)=-\lambda(t)\times[P_{as}(t)-P_{eq}(t)]$, with time-dependent rate $\lambda(t)=\mathrm{Re}\,\Sigma[\varepsilon(t)]$ and equilibrium value $P_{eq}(t)=\tanh[\hbar\varepsilon(t)/2kT]$. Here, $\varepsilon(t)=\epsilon_0+\hat{\epsilon}\cos\Omega t$ plays the role of a time-dependent adiabatic asymmetry, and the rate $\lambda(t)$ $(\alpha<1)$ is obtained as the real part of

$$\Sigma[\varepsilon(t)]=\frac{\Delta_e}{\pi}\left(\frac{\beta\Delta_e}{2\pi}\right)^{1-2\alpha}\frac{\Gamma(\alpha+i\hbar\beta\varepsilon(t)/2\pi)}{\Gamma(1-\alpha+i\hbar\beta\varepsilon(t)/2\pi)}, \tag{6.9}$$

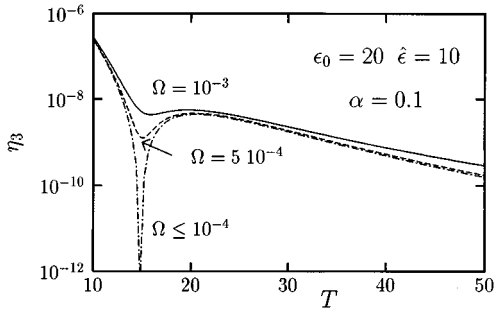

FIG. 42. Quantum noise-induced resonances for the third-order amplitude $\eta_3=4\pi|M_3(\Omega,\hat{\epsilon})/\hbar\hat{\epsilon}|^2$ vs temperature T in the regime of adiabatic incoherent tunneling. The different lines are for three different driving frequencies Ω. The noise-induced suppression which characterizes the "resonance" sharpens with decreasing driving frequency Ω. The results are for a bias energy $\epsilon_0=20$, driving strength $\hat{\epsilon}=10$, and a coupling strength of $\alpha=0.1$. Data are from Grifoni and Hänggi (1996b).

where $\Gamma(z)$ denotes the gamma function, and β is the inverse temperature $(1/k_BT)$.

The rate equation can then be solved in terms of quadratures, and the nonlinear low-frequency power spectrum can be investigated. Quantum stochastic resonance indeed occurs in this incoherent tunneling regime. As for the case $\alpha=\frac{1}{2}$, the quantum stochastic resonance maximum appears only when the static asymmetry ϵ_0 overcomes the external strength $\hat{\epsilon}$. Moreover, Fig. 42, which shows the behavior of the third scaled spectral amplification η_3 versus temperature, reveals another striking effect: As the driving frequency is decreased, a noise-induced suppression of higher harmonics occurs in correspondence to the stochastic resonance maximum in the fundamental harmonic. In this regime one finds the quantum analogue of noise-induced resonances that characterize classical nonlinear stochastic resonance (see Sec. IV.A). A numerical evaluation shows that the noise-induced suppression indeed appears when $\Omega \ll \min\lambda(t)$, so that the quasistatic expression holds, i.e.,

$$M_n=\frac{1}{2\pi}\int_0^{2\pi} dx\ \tanh[\hbar\beta(\epsilon_0+\hat{\epsilon}\cos x)/2]\cos(mx). \tag{6.10}$$

In contrast to classical stochastic resonance, where the enhancement is maximal for symmetric bistable systems, we find that a nonzero bias is necessary for quantum stochastic resonance. To understand this behavior, one can investigate the predictions for quantum stochastic resonance within a linear-response approach. In this case, only the harmonics $0,\pm1$ of $P_{as}(t)$ in Eq. (6.7) are different from zero. In particular, P_0 becomes the thermal equilibrium value P_{eq} of the operator σ_z in the absence of driving, and $M_{\pm1}=\hbar\hat{\epsilon}\chi(\pm\Omega)$ is related by Kubo's formula to the linear susceptibility $\tilde{\chi}_{xx}(\Omega)=a^2\chi(\Omega)$ for the particle position $x=(a/2)\sigma_z$, where

$$\tilde{\chi}_{xx}(\Omega)=\frac{i}{\hbar}\int_{-\infty}^{+\infty} d\tau\ \exp(-i\Omega\tau)H(\tau) \times\langle[x(\tau),x(0)]\rangle_\beta. \tag{6.11}$$

Here, $H(\tau)$ is the Heaviside function, $[\ldots,\ldots]$ denotes the commutator, and $\langle\ldots\rangle_\beta$ the thermal statistical average of the full system in the absence of the external periodic force $(\hat{\epsilon}=0)$. In the regime where incoherent transitions dominate, the dynamical susceptibility is explicitly obtained in the form

$$\chi(\Omega)=\frac{1}{4k_BT}\frac{1}{\cosh^2(\epsilon_0/2k_BT)}\frac{\lambda}{\lambda-i\Omega}. \tag{6.12}$$

The quantity $\lambda=\mathrm{Re}\Sigma(\epsilon_0)$, $\alpha<1$ [for $\alpha>1$, see Hänggi, Talkner, and Borkovec (1990), or Weiss (1993)] is the sum of the forward and backward (static) quantum rates out of the metastable states, r_+ and r_-, respectively. The factor $1/\cosh^2(\hbar\epsilon_0/2k_BT)$ expresses the fact that the two rates are related by the detailed balance condition $r_+=e^{\beta\hbar\epsilon_0}r_-$. It is now interesting to note that formally the *same* expression for the incoherent susceptibility (and hence for η) holds true for the classical case, with r_+ and r_- denoting the corresponding classical forward and backward Kramers rates. Thus in classical stochastic resonance, the maximum arises because of competition between the thermal Arrhenius dependence of these rates and the algebraic factor $(k_BT)^{-1}$ that enters the linear susceptibility, and this maximum occurs (roughly) at a temperature that follows from the matching between the frequency scales of the thermal hopping rate and the driving frequency. Detailed investigation reveals that quantum stochastic resonance characteristically occurs when incoherent tunneling contributions dominate over coherent tunneling transitions. Moreover, in clear contrast to classical stochastic resonance, and also to semiclassical stochastic resonance near and above T_0 (see above), quantum stochastic resonance in the deep cold occurs only in the presence of a finite asymmetry $\epsilon_0\neq0$ between forward and backward escape paths. Thus while classical and semiclassical stochastic resonance is maximal for zero bias [see Eqs. (4.55), (4.56)] the quantum stochastic resonance phenomenon vanishes in the deep quantum regime when the symmetry between forward and backward dissipative tunneling transitions is approached. What is the physics that governs this behavior? Clearly, with decreasing temperature the thermal, exponential-like Arrhenius factor no longer dominates the escape rates; rather, its role is taken over by the action of the tunneling paths that govern adiabatic and nonadiabatic tunneling—see Sec. IX in Hänggi, Talkner, and Borkovec (1990). This non-Arrhenius action term possesses a rather weak temperature dependence as compared to the Arrhenius dependence. Hence the crucial factor in quantum stochastic resonance is not this exponential action part governing the quantum rate behavior but rather the Arrhenius-like detailed balance factor relating the forward rate to the backward rate [see below Eq. (6.12)]. This exponential detailed balance factor contains the energy scale $(\hbar\epsilon_0/k_BT)$; thus it is this exponential dependence that crucially competes with the algebraic factor $(k_BT)^{-1}$ that enters the linear susceptibility. Whenever $\hbar\epsilon_0\ll k_BT$, the energy levels are essentially equally occupied; hence with $\epsilon_0=0$ no quantum stochastic resonance peaks occur!

The second consequence is that over a wide range of driving frequencies the stochastic resonance maximum arises at a temperature obeying $k_BT\simeq\hbar\epsilon_0$. Similar qualitative results, together with the occurrence of noise-induced suppression are obtained also in the parameter region of low temperatures $kT\ll\hbar\Delta$ and weak coupling $\alpha\ll1$, where overdamped quantum coherence occurs. In this regime, the noninteracting blip approximation fails to predict the correct long-time behavior. This is so because the neglected bath-induced correlations contribute to the dissipative effects to first order in the coupling strength. Nevertheless, a perturbative treatment allows an investigation of quantum stochastic resonance even in this regime.

In conclusion, quantum noise in the presence of periodic driving can substantially enhance or suppress quantum stochastic resonance. Note also that all of this discussion of quantum stochastic resonance constitutes a situation where inertial effects in stochastic resonance (i.e., finite ohmic friction strengths α) are always implicitly accounted for. Of particular relevance is the occurrence of noise-induced suppression within nonlinear quantum stochastic resonance. This phenomenon of signal suppression at higher harmonics can be used for a distortion-free spectral amplification of information in quantum systems. Experimental candidates to observe these novel quantum stochastic resonance effects are the above-mentioned mesoscopic metals (Golding *et al.*, 1992; Chun and Birge, 1993; Löfstedt and Coppersmith, 1994a, 1994b; Coppinger *et al.*, 1995), ac-driven SQUID systems (Hibbs *et al.*, 1995; Rouse *et al.*, 1995), as well as ac-driven atomic force microscopy (Eigler and Schweitzer, 1990; Louis and Sethna, 1995), or ac-modulated proton tunneling (Grabert and Wipf, 1990; Benderskii *et al.*, 1994).

B. Stochastic resonance in spatially extended systems

So far we mainly investigated stochastic resonance in systems with only one degree of freedom, such as a particle moving in a potential under the influence of an external driving force and noise. In this section we describe how stochastic resonance manifests itself in spatially extended systems such as a string moving in a bistable potential under the influence of noise and external forcing, or in a two-dimensional medium forming spatiotemporal patterns in the presence of noise.

1. Global synchronization of a bistable string

In this section, we consider a one-dimensional bistable medium in the presence of noise and isotropic periodic forcing. The model is described by the one-dimensional Ginzburg-Landau equation (Benzi *et al.*, 1985):

$$\frac{\partial\Phi(x,t)}{\partial t}=m\Phi(x,t)-\Phi^3(x,t)+\kappa\frac{\partial^2\Phi(x,t)}{\partial x^2}+A_0\cos(\Omega t)+\xi(x,t), \tag{6.13}$$

where $\xi(x,t)$ is white Gaussian noise in both time and space, i.e.,

$$\langle\xi(x,t)\xi(x',t')\rangle=2D\,\delta(t-t')\,\delta(x-x')$$
$$\langle\xi(x,t)\rangle=0. \tag{6.14}$$

In the absence of driving, Eq. (6.13) can be cast in the form

$$\frac{\partial\Phi(x,t)}{\partial t}=-\frac{\delta V[\Phi]}{\delta\Phi}+\xi(x,t), \tag{6.15}$$

with the functional $V[\Phi]$ (Rajaraman, 1982)

$$V[\Phi]=\int_0^L\left[\frac{1}{4}\Phi^4-\frac{1}{2}m\Phi^2+\frac{\kappa}{2}\left(\frac{\partial\Phi}{\partial x}\right)^2\right]dx. \tag{6.16}$$

The stationary solutions $\Phi(x)$ in the absence of the noise, obeying

$$m\Phi-\Phi^3+\kappa\frac{d^2\Phi}{dx^2}=0, \tag{6.17}$$

with von Neumann boundary conditions

$$\frac{d\Phi(0)}{dx}=\frac{d\Phi(L)}{dx}=0, \tag{6.18}$$

extremalize the functional $V[\Phi]$. Equation (6.17) can be interpreted as a Newtonian equation of motion in the inverse double-well potential $U_N(\Phi)=-\frac{1}{4}\Phi^4+\frac{1}{2}m\Phi^2$ with x as the time variable. The relevant homogeneous stationary solutions (stationary solution in the Newtonian picture) with boundary conditions (6.18) are given by

$$\Phi_\pm=\pm\sqrt{m},$$
$$\Phi_0=0, \tag{6.19}$$

with

$$V[\Phi_+]=V[\Phi_-]=-\frac{1}{4}m^2L,$$
$$V[\Phi_0]=0. \tag{6.20}$$

The first two solutions (the whole string is sitting in one of the potential minima) are stable and the third one (the whole string is sitting on the barrier top) is unstable. There is also a class of stable inhomogeneous solutions, the multi-instanton solutions $\Phi^{(k)}$, that obey the boundary conditions (6.18) and have k zeros in the interval $[0,L]$. For the potential energies $V[\Phi^{(k)}]$ one finds the inequalities

$$V[\Phi^{(0)}]<V[\Phi^{(1)}]<V[\Phi^{(2)}]\ldots, \tag{6.21}$$

with $\Phi^{(0)}=\Phi_\pm$. In the presence of noise, the string can escape out of the stable homogeneous states $\Phi_\pm$. A generalization of Ventsel and Freidlin's theory (Benzi *et al.*, 1985) yields for the mean exit times in the weak-noise limit $D\ll\Delta V$

$$T_\pm=C\,\exp\left(\frac{2\Delta V}{D}\right), \tag{6.22}$$

with C independent of D. Here, $\Delta V=V[\Phi^{(2)}]-V[\Phi_\pm]$ denotes the smallest $V[\Phi]$ barrier that separates the two stable states $\Phi_\pm$. This conclusion was verified numerically by solving the discretized version of Eq. (6.13) (see below). In the presence of a weak and slow homogeneous external forcing ($A=A_0\ll m^{3/2}$), Benzi *et al.* (1985) derived analytical expressions for the mean exit times T_+^a and T_+^b, relevant to the transition $\Phi_+\to\Phi_-$ in the potential configurations with $\cos(\Omega t)=\pm1$, i.e.,

$$T_+^a=C\,\exp[2(\Delta V-A_0L\sqrt{m})/D],$$
$$T_+^b=C\,\exp[2(\Delta V+A_0L\sqrt{m})/D]. \tag{6.23}$$

The system shows stochastic resonance if one of the exit times of Eq. (6.23) is shorter than the half driving

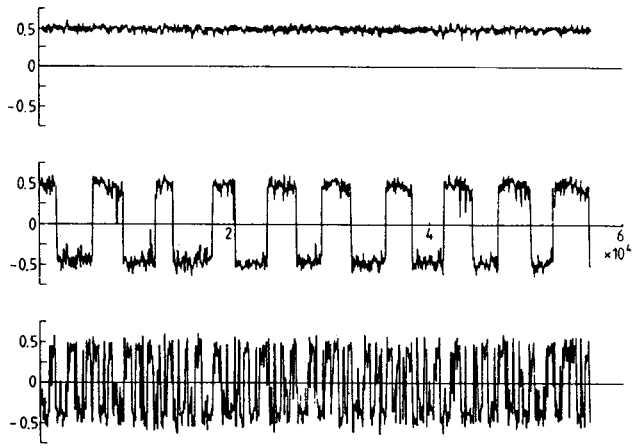

FIG. 43. The collective coordinate $u = \int \phi(x,t)dx/L$ plotted against time for $D/\Delta x = 0.002$ (upper plot), $D/\Delta_x = 0.07$ (middle plot), and $D/\Delta x = 0.11$ (lower plot). The parameters are $L=1$, $N=20$, $m=0.25$, $A=0.0125$, $\omega = 0.01\pi/3$, and $B=1/64$. These parameters imply a barrier height of 1/64 and an Arrhenius factor of 4.457.

period and the other is longer, so that on average the exit times are of the order the half driving period (the factor of 2 stems from the fact that the string has to escape twice within one period of the driving). This yields an upper and a lower bound for the optimal noise strength with arithmetic mean

$$D_{SR} = \frac{2\Delta V}{\ln(\pi/C\Omega)}. \tag{6.24}$$

A more refined analysis of stochastic resonance in a modulated string has been derived recently by Marchesoni, Gammaitoni, and Bulsara (1996) within the framework of the theory of thermal nucleation in one-dimensional chains (Hänggi, Marchesoni, and Sodano, 1988). The ensuing theoretical predictions have been verified experimentally by Löcher, Johnson, and Hunt (1996).

A full numerical investigation of the discretized Ginzburg-Landau equation has been carried out by Benzi *et al.* (1985). The discretized Ginzburg-Landau equation [Eq. (6.13)] reads

$$\dot{\psi}_n(t) = m\psi_n - \psi_n^3 + \frac{\kappa}{(\Delta x)^2}[\psi_{n+1}(t) + \psi_{n-1}(t) - 2\psi_n(t)] + A_0\cos(\Omega t) + \sqrt{D/\Delta x}\,\xi_n(t), \tag{6.25}$$

with discretization step Δx, string sites $\psi_n(t) = \Phi(x_n,t)$, and

$$\langle \xi_n(t)\xi_m(t')\rangle = 2\delta_{nm}\delta(t-t'),$$
$$\langle \xi_n(t)\rangle = 0. \tag{6.26}$$

In Fig. 43, the string collective coordinate $u = (1/L)\int_0^L \Phi(x)dx$ is shown as a function of time at three different levels of the homogeneous noise intensity. For a properly chosen value of the noise level D_{SR} (second plot), the collective coordinate switches almost periodically between $\sqrt{m}$ and $-\sqrt{m}$, i.e., between states where the entire string is either in the right or in the left potential well—the noise has globally synchronized the hopping along the bistable string. A similar conclusion has been reached recently by Lindner *et al.* (1995), who simulated numerically the same discretized Ginzburg-Landau equation [Eq. (6.13)]. Here, the different notation $\kappa/(\Delta x)^2 \to g$ and $D/\Delta x \to \epsilon$ hides the underlying Ginzburg-Landau equation. Using $L = N\Delta x$, the scaling relations $g \propto N^2$ and $\epsilon \propto N$, which were derived in Marchesoni, Gammaitoni, and Bulsara (1996), follow immediately. These authors also noticed that, while jumping back and forth between the stable configurations $\Phi_\pm$, a long string develops a remarkable spatial periodicity, which attains its maximum at resonance. The relevant spatial correlation length can be easily estimated within the thermal nucleation theory. Related to these studies of stochastic resonance in extended systems is the recent study by Wio (1996) on stochastic resonance in a bistable reaction-diffusion system, or the investigation of stochastic resonance in weakly perturbed Ising models (Néda, 1995a, 1995b; Brey and Prados, 1996; Schimansky-Geier and Siewert, 1997).

2. Spatiotemporal stochastic resonance in excitable media

Pattern formation in excitable media is an important paradigm with many applications in biology and medicine such as contraction waves in cardiac muscle, slime mold aggregation patterns, and cortical depression waves, to name only a few (for an overview, see Murray, 1989). While most theoretical and experimental work on excitable media focuses on the propagation of spiral waves, the role of fluctuations for pattern selection and propagation has been studied only recently (Jung and Mayer-Kress, 1995) by using a stochastic cellular model. One of the many interesting features of noisy media is that spatiotemporal structures and coherence can strongly vary with the noise level. Spatiotemporal stochastic resonance describes the enhancement of a spatiotemporal pattern (externally applied or intrinsic) by an optimal dose of noise.

The model of Jung and Mayer-Kress consists of a square array of excitable threshold elements with lattice constant a. Each element e_{ij} can assume three states: the quiescent state, the excited state, and a subsequent refractory state. The state of each element e_{ij} is controlled by an input $x_{ij}(t)$. If the input $x_{ij}(t)$ is below a threshold b, the element is quiescent. If $x_{ij}(t)$ is crossing a threshold from below, the element switches into the excited state, i.e., it fires. The inputs $x_{ij}(t)$ are coupled to a homogeneous thermal environment, i.e., the time dependence is described by the Langevin equation

$$\dot{x}_{ij} = -\gamma x_{ij} + \sqrt{\gamma\sigma^2}\,\xi_{ij}(t), \tag{6.27}$$

with $\langle x_{ij}^2\rangle = \sigma^2$ and zero-mean, uncorrelated noise in space and time $\langle \xi_{ij}(t)\xi_{kl}(t')\rangle = 2\delta_{(ij),(kl)}\delta(t-t')$. The excitable elements communicate via pulse coupling. When an element e_{kl} fires, it emits a spike that is re-

ceived by an element e_{ij} with an intensity depending on the distance $r_{(ij),(kl)}$ between e_{kl} and e_{ij}. Element e_{ij} integrates the incoming spikes from all firing elements yielding after one time step Δt (the smallest time scale of our system) the additional input f_{ij}

$$f_{ij}=K\sum_{kl}\ \exp\left(-\lambda\frac{r^2_{(ij),(kl)}}{a^2}\right), \tag{6.28}$$

which is added to x_{ij}. The parameter λ describes the inverse range of the interaction and the parameter K the coupling strength. The medium is updated synchronously in time steps of the smallest time scale Δt, the time interval of firing. All other time scales are measured in units of Δt. The proper normalization of this model is given by $\bar{\sigma}^2=\sigma^2/b^2$, $\bar{\gamma}=\gamma\Delta t$, $\bar{K}=K/b$. The time step and the threshold are therefore normalized to unity. The dissipation constant $\bar{\gamma}$ defines the typical time scale of the temporal evolution of a single element. For large dissipation ($\bar{\gamma}>1$), the element forgets its prehistory within one time step of temporal evolution, while for small dissipation $\bar{\gamma}\ll 1$, the system—as a whole—can build up a long memory.

It has been demonstrated that this model shows for large coupling K (in the absence of noise) the typical excitation patterns of excitable media, i.e., rotating spiral waves or target waves, usually described in terms of reaction diffusion equations with two species (Murray, 1989). In the presence of noise, the typical excitation patterns can still be observed, but they exhibit rough wave fronts and—depending on the noise level—more serious imperfections such as breakup of wave fronts and collisions with noise-nucleated waves. The overall picture in the strong-coupling regime is the coexistence of multiple finite-sized cells with coherent patterns.

For weak coupling K, however, the discrete nature of the model becomes important and different phenomena can be observed. To maintain a firing pattern, the coupling K has to exceed a critical value K_0, which is estimated for small λ and negligible curvature effects as follows: an infinite front of firing elements reduces the firing threshold of an element next to the front by an amount S_0 which is the sum of the contributions from all firing elements along the front. The element, however, is precharged by the sum of the contributions $\bar{S}_{pre}$ of firing elements of the front at earlier times (and larger spatial distances). At the critical coupling, the sum of the precharge $\bar{S}_{pre}$ and $\bar{S}_0$ of an element right before the front is unity (the normalized threshold), i.e.,

$$K_0(\gamma)\approx\sqrt{\frac{\lambda}{\pi}}\frac{1}{\exp(-\lambda)+\exp(\gamma)\Sigma_{n=2}^{\infty}\exp(-\lambda n^2-n\gamma)}. \tag{6.29}$$

Spatiotemporal stochastic resonance can be observed for coupling strengths below the critical coupling, which we define as the subthreshold regime. The excitable medium (in the subthreshold regime) is driven by a single wave front (a line in the array) from bottom to top,

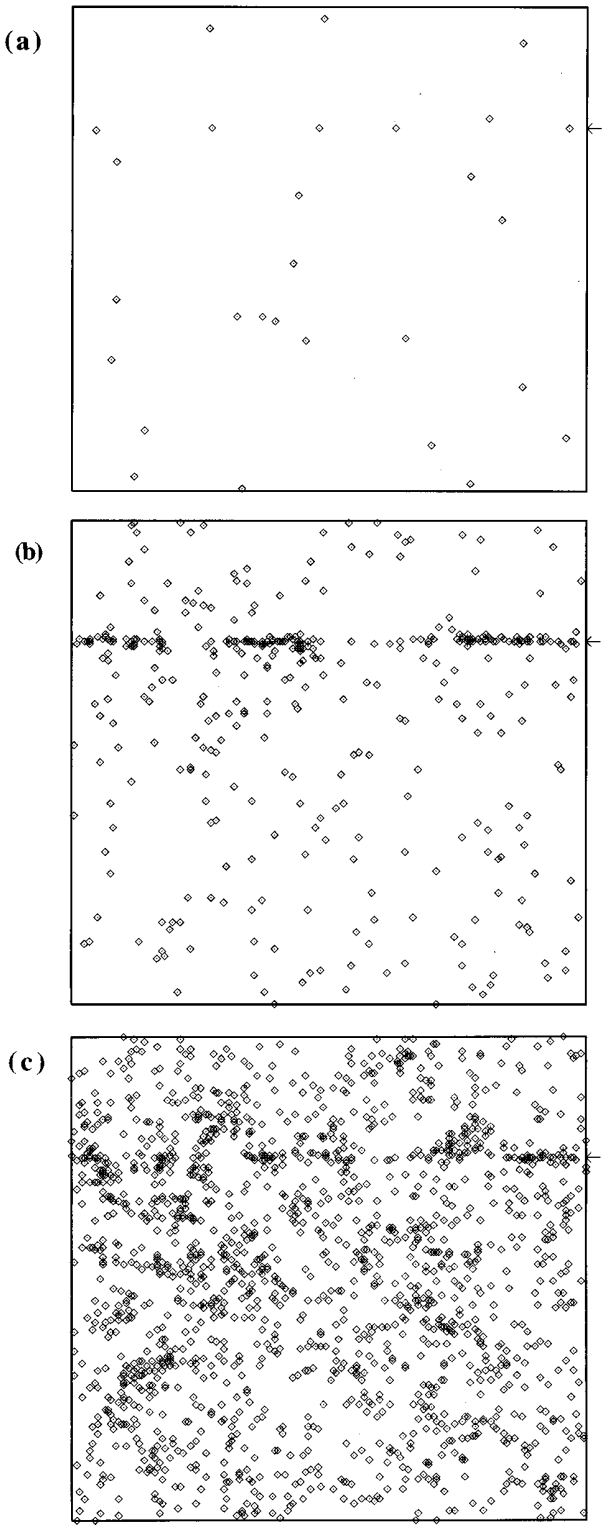

FIG. 44. The excitable medium (200×200 elements) driven by a single wave front of slightly increased excitability, $A_0 = 0.3$. The wave front is a single horizontal line in our array moving from bottom to top. The position of the wave front at the instant of time we took a snapshot is marked by a pointer on the right margin. The diamonds denote firing elements. We show three snapshots at three different noise levels; (a) $\bar{\sigma}^2=0.1$, (b) $\bar{\sigma}^2=0.16$, and (c) $\bar{\sigma}^2=0.2$. The other parameters are $K=0.121$, $\lambda=0.1$, $\bar{\gamma}=0.5$.

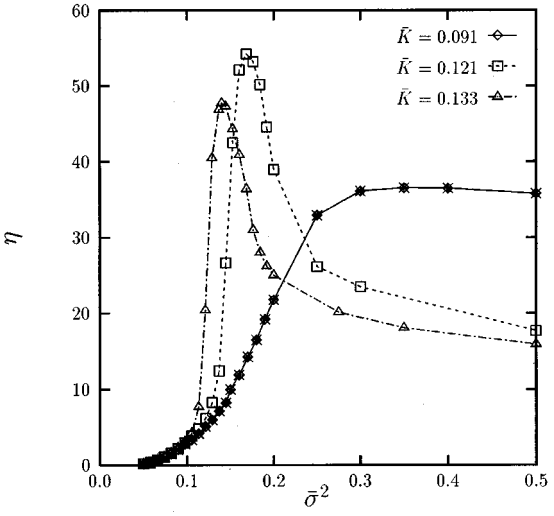

FIG. 45. The mean excess firing rate shown a function of the variance of the noise $\bar{\sigma}^2$ for $\lambda=0.1$, $\bar{\gamma}=0.5$, and $A_0=0.3$ at three different values of the coupling K.

along which the excitability is slightly increased; i.e., the threshold b is reduced: $b \to b - A_0$. In Fig. 45, the response of the medium, characterized by the correlation between the driving pattern and the firing pattern (see Fig. 44), is shown. The correlation is defined here as the mean excess firing rate along the front of the driving wave, i.e., the number of excess firing events along the front in comparison to the average number of firing events along all other lines (a small layer around the front had been excluded). For vanishing coupling $K=0$, one finds the maximum correlation according to the results for single thresholds at $\bar{\sigma}^2=1/2$. For increasing coupling, the effective threshold that has to be overcome with the help of noise is reduced. Therefore, the maximum correlation is shifted to smaller values of the noise. The peak also becomes more pronounced since the firing activity is synchronized in an area determined by the interaction range $1/\lambda$.

A rough estimate of the optimal value of the variance for the enhancement of spatiotemporal patterns has been given in Jung and Mayer-Kress (1995) in terms of a mean-field type approximation.

The firing elements along the front generate a stochastic field acting on the elements the front is approaching. The main contributions to the field acting on the element e_{ij} stem from firing elements along the front close to e_{ij}. Assuming that all of these elements are actually firing, we approximate the sum of these contributions (for small λ) by a Gaussian integral and obtain for the mean field

$$\bar{f}=K\sqrt{\pi/\lambda}\exp(-\lambda). \tag{6.30}$$

The firing threshold is reduced by the mean field, i.e., $\bar{b}_{eff}=1-\bar{f}$, leading to a renormalized condition for spatiotemporal stochastic resonance

$$\bar{\sigma}^2_{opt}=\frac{1}{2}\,\bar{b}^2_{eff}=\frac{1}{2}\,[1-K\sqrt{\pi/\lambda}\,\exp(-\lambda)]^2. \tag{6.31}$$

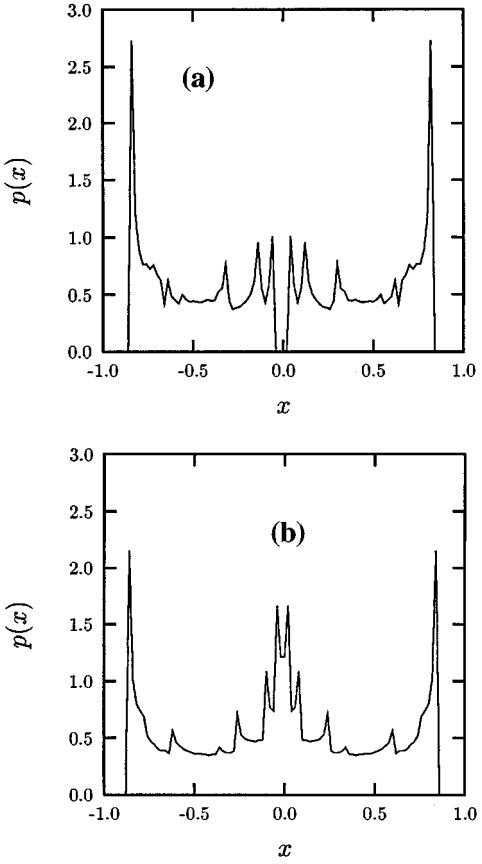

FIG. 46. The probability density $p(x)$ of 10^6 iterates x_n shown in the absence of modulation ($A_0=0$) (a) below the crisis at $a=3.57$, and (b) above the crisis at $a=3.62$.

The effect of improving an image by using stochastic resonance has been demonstrated very nicely in a recent work by Simonotto, Riani, Seife, Roberts, Twitty, and Moss (1997) for an array of uncoupled threshold detectors (in the model above, this corresponds to the case $K=0$).

C. Stochastic resonance, chaos, and crisis

It is well known that deterministic chaos resembles the features of noise on a coarse-grained time scale. It is therefore a natural question to ask whether stochastic resonance can be observed in dynamical systems in the absence of noise. Two different approaches to this problem have been put forward in the recent literature. Carroll and Pecora (1993a, 1993b) substitute the stochastic noise by a chaotic source. The chaotic source is applied to a periodically driven Duffing oscillator in a regime where it produces a period-doubled periodic response. The chaotic source yields switching between the attractors corresponding to the two phase-shifted responses of the Duffing oscillator, separated by an unstable period-1 orbit. The switching happens at some preferred locations along the orbits, which are being visited periodically. It is therefore synchronized with the orbit. This situation resembles the conventional setup for stochastic

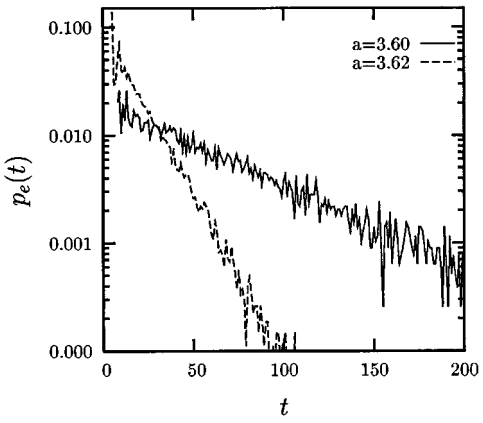

FIG. 47. The distribution of residence times t shown in the absence of forcing ($A_0=0$) at $a=3.6$ and $a=3.62$, both above the crisis $a_0=3.59$.

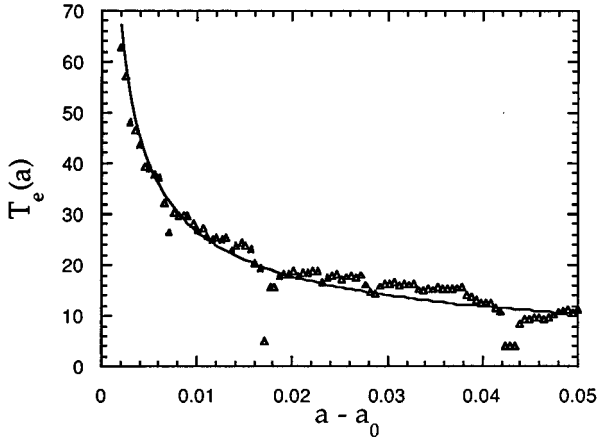

FIG. 48. The mean residence time shown in the absence of the driving as a function of the control parameter $a-a_0$, where a_0 is the value of the control parameter at which the crisis occurs. The triangles represent results from a numerical calculation. Apart from the resonances (the dips) the mean residence time can be fitted very well by a power law $T_e \propto (a-a_0)^{\gamma}$, with $\gamma=0.576$ (solid line).

resonance and yields stochastic resonance as expected. A similar study has been published by Kapitaniak (1994) and by Yang, Ding, and Hu (1995). For the Lorentz system with a time-periodic variation of the control parameter operating near the threshold to chaos, stochastic resonance has been observed by Crisanti, Falcioni, Paladin, and Vulpiani (1994).

A conceptually different approach has been put forward by Anishchenko, Neiman, and Safanova (1993). They use the intrinsic chaotic dynamics of a nonlinear map in the vicinity of a band-merging crisis to generate a sort of activated hopping process which is then synchronized by a small periodic signal. No external source is necessary to provide the randomness. They use the nonlinear periodically driven map

$$x_{n+1}=(a-1)x_n-ax_n^3+A_0\sin(2\pi f_0 n). \tag{6.32}$$

The complete description of the period-doubling scenario towards chaos is described in Anishchenko, Neimann, and Safanova (1993). Most important for the following discussion is a crisis due to the merging of two chaotic bands ($x>0$ and $x<0$) at $a\approx 3.598\equiv a_0$. This is demonstrated in Fig. 46 by the invariant measures of the undriven map $A_0=0$ at $a=3.57$ (a) and $a=3.62$ (b). The fixed point $x_1=0$ is stable for $0<a<2$ and unstable for $a>2$. Two chaotic bands emerge out of two disjoint Feigenbaum-type period-doubling scenarios at $a\geq 3.3$. For $a<a_0$, these bands are separated by the unstable fixed point $x_1=0$. At $a=a_0$ the bands merge. The unstable fixed point $x_1=0$ acts in the vicinity of the band-merging point a_0 as a repellor allowing the trajectory to traverse between the formerly separated chaotic bands only very rarely, yielding activation-type behavior of the trajectory. The statistical distribution $p_e(t)$ of times between two exits, i.e., the residence-time distribution, is shown in Fig. 47. It shows for not too small times the typical exponential decay

$$p_e(t)=\frac{1}{T_e}\exp(-t/T_e), \tag{6.33}$$

with the mean residence time

$$T_e=\int_0^{\infty} t p_e(t)dt. \tag{6.34}$$

The power-law scaling of the mean residence time T_e with the distance to the crisis $a-a_0$, i.e.,

$$T_e(a)\propto(a-a_0)^{-\gamma}, \tag{6.35}$$

(see Fig. 48), is—according to Grebogi, Ott, and Yorke (1987)—characteristic of a *crisis*. There are some dips in $T_e(a)$, e.g., at $a=0.36405$, that correspond to periodic windows in the map.

The decrease (at least in the average) of the mean residence time for increasing $a-a_0$ implies an increasing level of stochasticity, i.e., the level of stochasticity can be controlled by varying $a-a_0$.

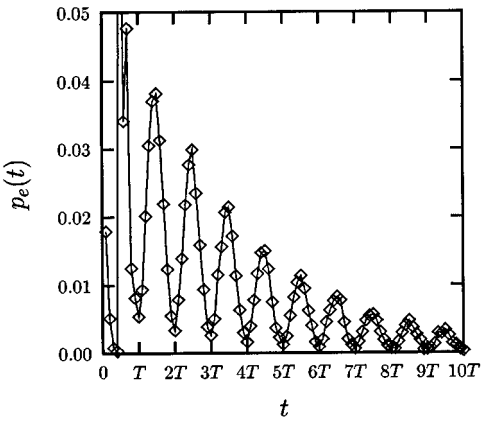

FIG. 49. The distribution of residence times t shown in the presence of the driving at $a=3.60$, $A_0=0.01$, and $f_0=0.1$. The carets show actual data points, while the solid line has been added to guide the eye. The locations of the sequence of exponentially decaying peaks are given by $t_n=(1/2)f_0^{-1},(3/2)f_0^{-1},(5/2)f_0^{-1},\ldots$.

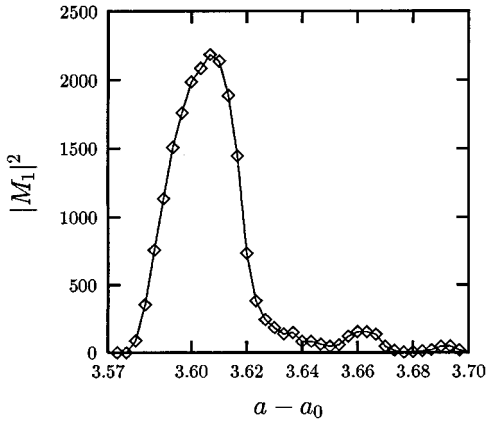

FIG. 50. The response to the periodic forcing (more precisely, the intensity of the line in the power spectrum at the driving frequency) shown as a function of the control parameter $a-a_0$ for $A_0=0.01$ and $f_0=0.01$.

In the presence of a periodic forcing, i.e., for $A_0\neq 0$, the residence-time distribution exhibits a series of exponentially decaying peaks, located at odd multiples of the half period of the driving (see Fig. 49). In order to identify stochastic resonance, one has to vary the stochasticity in the presence of the periodic driving and compute the intensity of the spike (the signal strength) in the power spectrum of $x(t)$. To single out contributions to the response from forced periodic motion or resonances within the chaotic bands, we apply a binary filter process to monitor whether the system is in the right band $(+1)$ or left band (-1). The response of the binary variable $y\equiv x/|x|$ measured in terms of the intensity of the line in its power spectrum at the driving frequency is shown in Fig. 50. Starting at the crisis, i.e., at $a=a_0$, one observes that the signal strength increases until it reaches a maximum, and then decreases again.

The differences to stochastic resonance in a noisy bistable system follow:

(i) There are several peaks plus additional resonances where the driving frequency f_0 and the switching frequency $f_s=1/T_e$ are commensurable, i.e., $f_0/f_s=m/n$, with $m,n=1,2,3,\ldots$.

(ii) Changing $a-a_0$ does not change the stochasticity (noise strength) in a systematic way. To systematically compare with stochastic resonance in a noisy bistable system, one should first find a mapping between the noise strength and $a-a_0$.

(iii) The periodic windows of period M of the unperturbed map yield resonances with the external driving whenever their periods agree, i.e., $f_0=1/M$.

Similar results have been obtained by Nicolis *et al.* (1993) by studying a one-dimensional intermittent map.

D. Effects of noise color

In many practical situations the finite time scale τ_c characterizing the relaxation of the autocorrelation of the noise (i.e., colored noise) is much shorter than the characteristic time scale of the system. Hence as we did in Sec. IV for the driven bistable dynamics, it often is appropriate to model the noise source by a (white) random force $\xi(t)$. In the physical world, however, such an idealization is never exactly realized. In order to investigate the importance of corrections to white noise, approximate techniques were introduced to compute the effects of small to moderate to arbitrarily large noise correlation times τ_c (Hänggi *et al.*, 1984, 1989; Hänggi and Jung, 1995). Strong color (i.e., a large τ_c value) is not unrealistic for many physical applications. Usually, a strongly correlated noise emerges as the result of coarse graining over a hidden set of slowly varying variables (Kubo *et al.*, 1985), or colored noise is simply applied and monitored externally by the experimenter.

The effect of color on stochastic resonance may be nontrivial, as suggested by the very characterization of stochastic resonance as a synchronization mechanism. The noise correlation time τ_c may compete with T_Ω and T_K to determine the realization and the magnitude of the resonance phenomenon. We anticipate that stochastic resonance in overdamped systems driven by an additive exponentially correlated Gaussian noise $\xi(t)$ is generally reduced compared to the case of white noise $\tau_c=0$ of equal strength D. The stochastic resonance peak is shifted to larger noise intensities due to the fact that colored noise exponentially suppresses the switching rate with increasing τ_c (Gammaitoni, Menichella-Saetta, Santucci, Marchesoni, and Presilla, 1989; Hänggi *et al.*, 1993).

Following the approach developed by Hänggi *et al.* (1993), we treat here the archetypal case of a periodically perturbed double well in the presence of exponentially colored Gaussian noise (Ornstein-Uhlenbeck noise). In scaled, dimensionless variables, the dynamics reads explicitly

$$\dot{x}=-V'(x)+A_0\cos(\Omega t)+\xi(t), \tag{6.36a}$$

$$\dot{\xi}=-\frac{1}{\tau_c}\xi+\frac{1}{\tau_c}\epsilon(t), \tag{6.36b}$$

where $V(x)$ is the standard quartic double-well potential of Sec. IV.A, i.e., $V(x)=-x^2/2+x^4/4$, and $\xi(t)$ is an Ornstein-Uhlenbeck stochastic process driven by the Gaussian white noise $\epsilon(t)$ with $\langle\epsilon(t)\rangle=0$ and $\langle\epsilon(t)\epsilon(0)\rangle=2D\,\delta(t)$. The stationary autocorrelation function of $\epsilon(t)$ is an exponential function with time constant τ_c,

$$\langle\xi(t)\xi(0)\rangle=(D/\tau_c)\exp(-|t|/\tau_c). \tag{6.37}$$

In the limit of zero correlation time $\tau_c\to 0$, Eq. (6.37) reproduces the white-noise source of Secs. II and IV. Within the framework of the linear-response theory of Sec. IV.B for small forcing amplitudes, the relevant response function [Eq. (4.30)] assumes the form of a fluctuation theorem; i.e., it is given in terms of a stationary correlation of two fluctuations of the unperturbed process

$$\chi(t)=-H(t)\frac{d}{dt}\langle x(t)\zeta(x(0))\rangle_0, \tag{6.38}$$

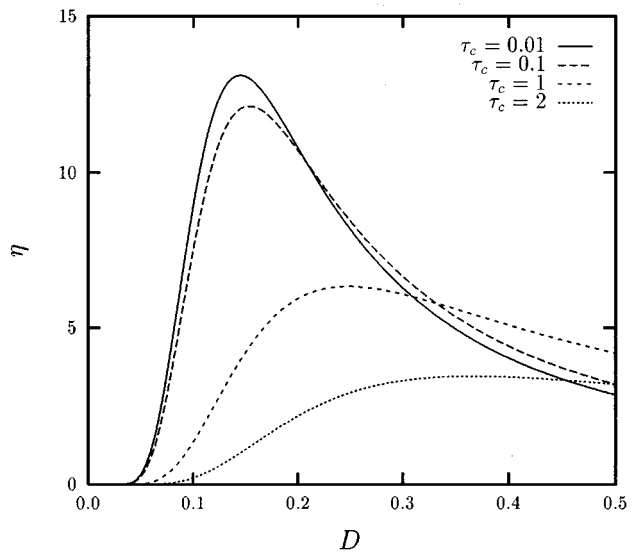

FIG. 51. The spectral amplification η (in linear response), as predicted by Eqs. (6.43) and (6.44) for the quartic double-well potential $V(x) = -x^2/2 + x^4/4$, shown for increasing values of the dimensionless noise correlation time τ_c at $\Omega = 0.1$.

where $H(t)$ denotes a Heaviside step function. In the opposite limits $\tau_c \ll 1$ (i.e., weak color) and $\tau_c \gg 1$ (i.e., strong color), $\zeta(x(t))$ may be approximated to read

$$\zeta(x(t)) = \frac{1}{D}[x + \tau_c V'(x)], \tag{6.39}$$

whereas the unperturbed averages $\langle \cdots \rangle_0$ in Eq. (6.38) must be taken over the relevant (approximate) probability density

$$p_{st}(x,\tau_c) = \frac{\mathcal{N}_1}{|1-\tau_c V''(x)|} \exp\left[-\frac{V(x)}{D} - \frac{\tau_c}{2D} V'^2(x) \right] \tag{6.40a}$$

for $\tau_c \ll 1$, and

$$p_{st}(x,\tau_c) = \mathcal{N}_2 |1 + \tau_c V''(x)| \times \exp\left[-\frac{V(x)}{D} - \frac{\tau_c}{2D} V'^2(x) \right] \tag{6.40b}$$

for $\tau_c \gg 1$. Here, $\mathcal{N}_1$ and $\mathcal{N}_2$ denote the appropriate normalization constants.

Within the long-time approximation, the correlation function $\langle x(t)\zeta(x(0)) \rangle$ (see Sec. IV.B) can in leading order be estimated as

$$\langle x(t)\zeta(x(0)) \rangle_0 \sim \langle x\zeta \rangle_0 \exp[-2r_K(\tau_c)t] \tag{6.41}$$

with the colored noise-driven escape rate given as

$$r_K(\tau_c) = r_K(1 - 3\tau_c/2) \tag{6.42a}$$

for weakly colored noise $\tau_c \ll 1$, and

$$r_K(\tau_c) = r_K \exp[-(8/27)\tau_c(\Delta V/D)] \tag{6.42b}$$

for strongly colored noise, i.e., $\tau_c \gg 1$. Upon inserting Eqs. (6.41) and (6.39) into the expression for the susceptibility in Eq. (6.38) we finally obtain for the spectral amplification η

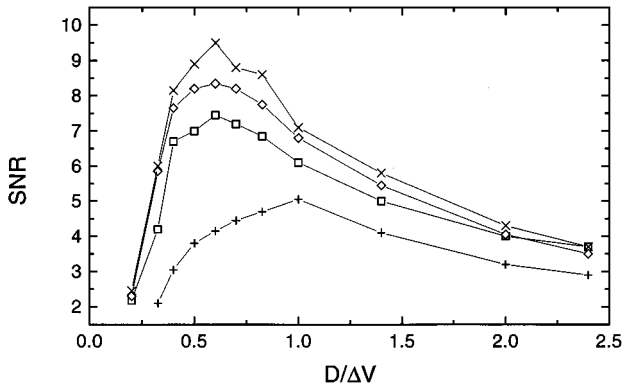

FIG. 52. Signal-to-noise ratio (SNR) vs D for different values of τ_c: $\tau_c = 30$ μs (crosses); $\tau_c = 50$ μs (diamonds); $\tau_c = 100$ μs (squares); $\tau_c = 200$ μs (pluses). Other simulation parameters are $\nu_\Omega = 30$ Hz, $Ax_m = 0.5\Delta V$, $x_m = 7.3$ V, and $a = 6850$ Hz.

$$\eta = \frac{\langle x^2 \rangle_0 + \tau_c \langle x V'(x) \rangle_0}{D^2} \frac{4r_K^2(\tau_c)}{4r_K^2(\tau_c) + \Omega^2}, \tag{6.43}$$

with $r_K(\tau_c)$ and $\langle \cdots \rangle_0$ computed in the appropriate limits of Eqs. (6.42) and (6.40), respectively.

Prediction (6.43) for both color regimes suggests that noise color degrades the observability of stochastic resonance. Indeed, upon increasing τ_c, the relaxation rate $r_K(\tau_c)$ gets exponentially depressed with respect to $r_K(\tau_c = 0)$. For Ω fixed, we therefore must increase D to match the stochastic resonance condition, which consists of maximizing η (see Sec. IV.B). This results in a shift of the stochastic resonance peak towards higher D values and a corresponding reduction of the peak height.

We note that the limiting expressions (6.42) for $r_K(\tau_c)$ stem from one unified approximation scheme (Hänggi and Jung, 1995), that is

$$r_K(\tau_c) = \frac{1}{\sqrt{2}\pi}(1 + 3\tau_c)^{-1/2} \times \exp\left[-\frac{\Delta V}{D} \left(\frac{1 + \frac{27}{16}\tau_c + \frac{1}{2}(\tau_c)^2}{1 + \frac{27}{16}\tau_c} \right) \right]. \tag{6.44}$$

Correspondingly, the analytical expression obtained by replacing $r_K(\tau_c)$ of Eq. (6.43) with Eq. (6.44) bridges the two limiting expressions of η for $\tau_c \ll 1$ and $\tau_c \gg 1$. In Fig. 51 we display four such curves for η versus D, for increasing values of noise color τ. As expected, noise color suppresses stochastic resonance monotonically with τ_c. This feature is in accordance with the early analog simulations by Gammaitoni, Menichella-Saetta, Santucci, Marchesoni, and Presilla (1989), as depicted in Fig. 52. The suppression of stochastic resonance with increasing noise color has recently been demonstrated experimentally in a tunnel diode (Mantegna and Spagnolo, 1995), and by use of Monte Carlo simulations by Berghaus *et al.* (1996).

Inertial effects, which result in (non-Markovian) memory effects for the spatial coordinate $x(t)$ have been addressed theoretically for the spectral amplifica-

tion η by Hänggi *et al.* (1993), and experimentally for the signal-to-noise ratio by Gammaitoni, Menichella-Saetta, Santucci, Marchesoni, and Presilla (1989). Likewise, the role of memory friction, which relates—via the fluctuation-dissipation theorem—to internal colored noise, has been studied for overdamped dynamics by Neiman and Sung (1996). The result that inertial effects, or equivalently, decreasing finite friction strengths tend to enhance stochastic resonance can similarly be induced with strong color for the memory friction (Neiman and Sung, 1996).

VII. SUNDRY TOPICS

In this section we present several topics relating to the physics of stochastic resonance that have not been featured in detail in the previous sections. In doing so, we have confined ourselves to particular examples determined only by our knowledge and personal taste; thus this selection is necessarily incomplete.

A. Devices

1. Stochastic resonance and the dithering effect

A *Schmitt trigger*, see Sec. V.B.1, operating in the limiting case when its two threshold voltages coincide, provides an example of a two-state system, namely a *threshold device*. There are many examples of this kind of electronic device, the more common class being represented by the analog-to-digital converters (ADC). The basic (1-bit) ADC device consists of a signal comparator (an operational amplifier followed by a resistor and two back-to-back *Zener diodes*), the output voltage of which switches between V and $-V$ when the input v_i crosses a reference voltage. Multibit ADCs, realized by a proper combination of comparators (see, e.g., Millman, 1983), are of common use in digital signal processing (Oppenheim and Schaffer, 1975), where analog signals are sampled at discrete times and converted into a sequence of numbers. Since the register length is finite, the conversion procedure, termed signal *quantization*, results in distortion and loss of signal detail. In order to avoid distortion and recover the signal detail, it has become a common practice, since the 1960s, to add a small amount of noise to the analog signal prior to quantization—a technique termed *dithering* (Bennet, 1948). To understand how the addition of a proper quantity of noise can improve the performances of an ADC, we note that the conversion from a continuous (analog) to a digital signal consists of two different operations: time discretization and amplitude quantization. Time discretization, if properly applied, can be shown to be error free. The effects of amplitude quantization (finite word length) are instead always present and manifest themselves in a number of different ways. First, due to the presence of a nonlinear-response characteristic, signal quantization leads to an unavoidable distortion, i.e., the presence of spurious signals in a frequency band other than the original one. There is also a loss of signal detail that is small compared to the quantization step. The effects of the amplitude quantization can be quantified by introducing a proper *quantization error*, $\zeta = y - x$, where x is the analog signal before quantization and y is the quantized signal. It is clear from this definition that if we had a linear-response characteristic (apart from amplification factors) ζ would be zero and there would be no distortion at all. A number of studies were performed over the last thirty years in order to find a way of reducing ζ. The main conclusions follow:

(1) The addition of a proper external signal (called *dither*) to the input x can statistically reduce ζ.

(2) The best choice for the dither signal is a random dither uniformly distributed.

(3) There exists an optimal value of the random dither amplitude, which coincides with the amplitude of the quantization step.

Hence the quantization error ζ is minimized and, correspondingly, the ADC performances maximized, when a noise of a proper intensity is added to the input signal. The similarity with stochastic resonance, where an optimal strength of the added noise maximizes the output signal-to-noise ratio, is apparent. As a matter of fact, stochastic resonance in this class of threshold systems is equivalent to the dithering effect, as demonstrated by Gammaitoni (1995a, 1995b).

B. Stochastic resonance in coupled systems

In this section we discuss the impact of noise and periodic forcing on an ensemble of coupled bistable systems. In view of a possible collective response of the system (especially close to a phase transition), one can expect that the stochastic resonance effect will be even more pronounced than in a single system (Jung *et al.*, 1992).

1. Two coupled bistable systems

The simplest way to study stochastic resonance in coupled systems is to consider two coupled overdamped bistable elements in the presence of noise and periodic forcing (Neiman and Schimansky-Geier, 1995):

$$\dot{x} = \alpha x - x^3 + \gamma(y - x) + \xi_x(t) + A_0 \cos(\Omega t),$$

$$\dot{y} = \beta y - y^3 + \gamma(x - y) + \xi_y(t) + A_0 \cos(\Omega t), \tag{7.1}$$

with independent Gaussian white noise terms, but identical periodic forcing, i.e.,

$$\langle \xi_x(t)\xi_y(t') \rangle = 2D\,\delta_{xy}\delta(t - t'). \tag{7.2}$$

As in the bistable string (see Sec. VI.B.1), stochastic resonance in the coupled system has been quantified by the linear response for the sum $s(t)$ of the two degrees of freedom $s(t) = x(t) + y(t)$ due to small periodic modulations. With the help of digital simulations and approximation theory, the following results have been obtained:

(1) At a given coupling constant, the signal-to-noise ratio goes through a maximum as a function of the noise strength.

(2) Starting from zero coupling (which corresponds to two independent systems), the signal-to-noise ratio vs coupling first increases (i.e., the collective response is indeed higher than that of two uncoupled systems), runs through a maximum, and decreases again for large coupling towards an asymptotic (finite) value.

2. Collective response in globally coupled bistable systems

An early study dealing with stochastic resonance for systems with many degrees of freedom (Jung *et al.*, 1992) focused on a large number N of identical, linearly and homogeneously coupled bistable systems in the presence of periodic forcing. The coupled equations of motion are given by

$$\dot{x}_n(t)=x_n-x_n^3+\frac{1}{N}\sum_{m=1}^{N} g(x_m-x_n)+\xi_n(t) + A_0\cos(\Omega t), \tag{7.3}$$

with Gaussian, mutually independent and uncorrelated fluctuations

$$\langle \xi_n(t)\xi_m(t')\rangle = 2D\,\delta_{nm}\delta(t-t')$$
$$\langle \xi_n(t)\rangle = 0. \tag{7.4}$$

The coupling constant is denoted by g. Systems such as this exhibit spontaneous-ordering transitions (Bruce, 1980; Amit, 1984; Dewel *et al.*, 1985; Valls and Mazenko, 1986). Analytical studies of these phase transitions are possible within a mean-field approximation (Mansour and Nicolis, 1975; Desai and Zwanzig, 1978; Bruce, 1980; Shiino, 1987; Van den Broeck *et al.*, 1994; Drozdov and Morillo, 1996; Hu, Haken, and Xie, 1996). The stationary solution of the Fokker-Planck equation in mean-field approximation is not unique below a critical noise strength. There are three solutions: two stable solutions with spontaneous symmetry breaking, which represent ferromagnetic ordered states, and an unstable one with zero magnetization m; here the order parameter m is given by the averaged population difference in the potential wells. At the critical point $D=D_c$, the system undergoes a phase transition of second order.

Within the mean-field approximation and a two-state description, the response of the order parameter $\langle x\rangle \equiv m$ to the periodic forcing and thus the spectral amplification η of the order parameter has been obtained as

$$\eta=\left(\frac{2r_K}{D}\right)^2\frac{1-m^2}{\Omega^2+\Lambda^2}, \tag{7.5}$$

with the collective relaxation rate given by

$$\Lambda=2r_K\sqrt{1-m^2}\left(\frac{1}{1-m^2}-\frac{g}{D}\right). \tag{7.6}$$

The mean value m determined by the transcendental equation $m=\tanh[(g/D)m]$.

The spectral amplification strongly increases with the coupling to exhibit a peak at the critical point $D=D_c=g$. The maximum spectral amplification attains a maximum at $g=\Delta V$, a phenomenon that has been observed for two coupled bistable systems (cf. Sec. VII.B.1) and for coupled-neuron models in Sec. VII.B.3. These results have also been confirmed in later studies by Morillo *et al.* (1995), and Hu, Haken, and Xie (1996).

3. Globally coupled neuron models

Another approach to describe the response of globally coupled bistable systems to periodic forcing is the application of adiabatic elimination of all but one degree of freedom (Bulsara and Schmera, 1993; Inchiosa and Bulsara, 1995a, 1995b,1995c; Inchiosa and Bulsara, 1996). The model used is motivated by the dynamics of artificial neural networks (Amit, 1989; Krogh and Palmer, 1991), namely

$$C_i\dot{u}_i=-\frac{u_i}{R_i}+\sum_{j=1}^{N} J_{ij}\tanh(u_j)+\xi(t)+A_0\cos(\Omega t), \tag{7.7}$$

with C_i and R_i denoting capacitances and resistances of the membranes. The zero-mean Gaussian noise and the periodic signal are assumed to be identical for all elements. The coupling constants J_{ij} can be chosen arbitrarily. The correlation function of the noise is given by

$$\langle \xi(t)\xi(t')\rangle = 2D\,\delta(t-t'). \tag{7.8}$$

The globally coupled system of Eq. (7.7) has been solved numerically and analytically by assuming a separation of time scales of one neuron vs the rest of the neurons acting as a linearized bath, thus allowing for adiabatic elimination of the bath neurons. The most important result of these studies is that, as above, the maximal signal-to-noise ratio goes through a maximum as a function of the coupling strength (the $J's$); moreover, the signal-to-noise ratio between the incoming periodic signal $A_0\cos(\Omega t)$ and the noise strength D has been shown to provide an upper bound to the signal-to-noise ratio of the output $u_i(t)$.

C. Miscellaneous topics on stochastic resonance

1. Multiplicative stochastic resonance

There exist many cases of physical interest where the role of fluctuating control parameters is mimicked by *multiplicative* noise (Fox, 1978; Schenzle and Brand, 1979; Faetti *et al.*, 1982; Graham and Schenzle, 1982). Gammaitoni, Marchesoni, Menichella-Saetta, and Santucci (1994) have analogously simulated the phenomenon of stochastic resonance in the overdamped bistable system described by the stochastic differential equation

$$\dot{x}=-V'(x)+x\xi_M(t)+\xi_A(t)+A(t), \tag{7.9}$$

where $V(x)$ is the standard quartic double-well potential and $A(t)=A_0\cos(\Omega t)$, with $A_0 x_m \ll \Delta V$. The fluctuating parameters $\xi_i(t)$, with $i=A,M$, are stationary zero-mean valued, Gaussian random processes with autocorrelation functions

$$\langle \xi_i(t)\xi_j(0)\rangle = 2Q_i\delta_{ij}\delta(t). \tag{7.10}$$

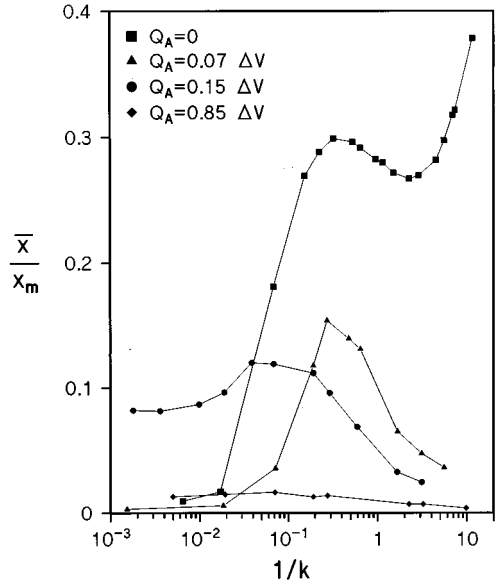

FIG. 53. The normalized response amplitude x/x_m depicted vs the dimensionless multiplicative noise strength $k^{-1}\equiv 2Q_M/a$ for $A_0=0.1ax_m$ and different values of Q_A. The potential parameters are $x_m=2.2$ V and $a=10^4$ s^{-1}. After Gammaitoni, Marchesoni, Menichella-Saetta, and Santucci (1994).

The main conclusion of their investigation is that the process $x(t)$ develops a periodic component $\langle x(t)\rangle_{as}$ according to the approximate law (2.6); the amplitude $\bar{x}$ and the phase $\bar{\phi}$ of $\langle x(t)\rangle_{as}$ depend on A_0, Q_A, and Q_M. Most notably, $\bar{x}$ shows typical stochastic resonance behavior with increasing Q_M while keeping Q_A fixed (multiplicative stochastic resonance). In Fig. 53, the dependence of $\bar{x}_1$ on Q_M is plotted for the most remarkable case of a purely multiplicative bistable process $Q_A=0$.

To interpret the outcome of the analog simulation of Eq. (7.9), one should solve the relevant time-dependent Fokker-Planck equation

$$\frac{\partial}{\partial t}p=\frac{\partial}{\partial x}\left[V'(x)-Q_M x-A_0\cos\Omega t+\frac{\partial}{\partial x}(Q_A+Q_M x^2)\right]p \tag{7.11}$$

for the probability density $p=p(x,t;A_0)$. In the presence of a static tilting, i.e., for $A_0\neq 0$ and $\Omega=0$, the stationary solution of Eq. (7.11) reads

$$p_0(x;A_0)=\mathcal{N}_0(A_0)\left(x^2+\frac{Q_A}{Q_M}\right)^{-1/2+k[1+(k/2)(Q_A/\Delta V)]}\times\exp\left(-k\frac{x^2}{x_m^2}-\frac{A_0}{Q_M|x|}\right), \tag{7.12}$$

where $k\equiv a/2Q_M$ and $\mathcal{N}_0(A_0)$ is a suitable normalization constant. In the presence of a periodic tilting; i.e., for $\Omega>0$, the process $x(t)$ is no longer stationary and a time-dependent probability density $p_{as}(x,t;A_0)$ is required to describe its asymptotic state. However, in the limit of low forcing frequency Ω, the adiabatic approximation $p_{as}(x,t;A_0)\simeq p_0(x;A(t))$ suffices to shed light on the nonstationary dynamics underlying the phenomenon of multiplicative stochastic resonance.

In the purely multiplicative case $Q_A=0$ (Fig. 53), the forcing term alone is responsible for $x(t)$ switching back and forth between the positive and the negative half axis. Should the adiabatic approximation hold true for any value of Q_M, the process $x(t)$ would approach instantaneously its most probable value in the vicinity of the peak of $p_0(x;A(t))$. Therefore, the amplitude $\bar{x}$ of $\langle x(t)\rangle_{as}$ would be of the order of $\bar{x}_m$, which is a monotonic decreasing function of Q_M. However, Fig. 53 shows a dramatic drop of $\bar{x}$ as Q_M tends to zero. Such a deviation from the prediction of the adiabatic approximation is due to the fact that, with decreasing Q_M, the switch time of $x(t)$ between positive and negative values, controlled by $A(t)$ with periodically reversing sign, grows much larger than the forcing period $T_\Omega=2\pi/\Omega$. For instance, assuming that at $t=0$ the variable x is confined to the unstable axis $x<x_A\simeq A_0/a$ with $A_0>0$, the mean-first-passage time T_A required by x to escape through x_A onto the stable half axis $x>x_A$ diverges strongly for $x_A/x_m\to 0$. On increasing Q_M close to a, such a divergence is substantially weakened, so that the adiabatic approximation $T_A\ll T_\Omega$ applies. In this regime the relaxation process is controlled mainly by the modulated interwell dynamics of $x(t)$ described by $p_0(x;A(t))$ and, as stated above, $\bar{x}$ approaches $\bar{x}_m$. In the opposite limit, $T_A\gg T_\Omega$ (i.e., $Q_M\ll a$), the steady-state distribution of $x(t)$ spreads over the entire x axis with oscillating local maxima at $\pm x_m+A(t)/2(a-Q_M)$ (modulated intrawell dynamics). It follows immediately that for $Q_M=0+$ the amplitude $\bar{x}$ is of the order $A_0/2a$, which is much smaller than the value of $\bar{x}_m$ at $k=1$, whence the appearance of the stochastic resonance peaks of Fig. 53 for $\Omega T_A\sim 1$. Accordingly, the stochastic resonance peaks shift to the left with increasing A_0. In conclusion, the crossover from intrawell to interwell modulated dynamics is the basic mechanism responsible for multiplicative stochastic resonance.

2. Resonant crossing

In this section, we report on an intricate colored-noise effect for the residence-time distributions, which takes place when the correlation time of the noise is large (Gammaitoni, Marchesoni, *et al.*, 1993). In such a situation, the system dynamics are characterized by four time scales: the local relaxation rate a within a potential well, the correlation time of the noise τ_c, the forcing frequency Ω, and the transition rate r_K. The residence-time distribution (at small amplitudes of the driving A_0) consists—as shown repeatedly in figures throughout this review—of a series of peaks located at odd multiples of the half period of the driving $T_\Omega=2\pi/\Omega$, superimposed on an exponential backbone. The periodic part can be extracted from the exponential backbone by a fitting procedure.

It has been demonstrated that the amplitude of the periodic part evolves as a function of the driving frequency Ω through a maximum if the correlation time τ_c of the noise is large, i.e., $a\tau_c \gg 1$. The location of the maximum has been estimated by $\Omega^2_{\max} \sim a/\tau_c$. In contrast to the time-scale matching condition for stochastic resonance, i.e., $\Omega \sim \pi r_K$, this new condition describes a matching between the intrawell time scale and the driving frequency Ω.

3. Aperiodic stochastic resonance

Since most of the studies on stochastic resonance assume periodic external forcing, it is interesting to ask whether noise can also amplify small aperiodic signals. To this end several different studies (in scope and technique) have been put forward.

Jung and Hänggi (1991a) considered noise due to the phase diffusion of the external force. This is a realistic assumption, for instance, if the external field is provided by a laser where spontaneous emission generates phase diffusion (Haken, 1970). Instead of a deterministic phase Ωt, they proposed the use of a stochastic phase θ, i.e., $\dot{\theta} = \Omega + (1/\tau_d)\,\xi_\theta(t)$, with $\xi_\theta(t)$ the derivative of a Wiener process. The finite coherence time of the phase dynamics leads to a broadening of the peaks in the power spectrum and a suppression of the stochastic resonance effect.

Neiman and Schimansky-Geier (1994) considered the overdamped motion of a particle in a bistable potential $V(x) = \frac{1}{4}x^4 - \frac{1}{2}x^2$, driven by white Gaussian noise and harmonic noise (Schimansky-Geier and Zülicke, 1990; Dykman, Mannella, McClintock, Stein, and Stocks, 1993b). Harmonic noise $y(t)$ is generated by applying white Gaussian noise on a second-order linear filter. The spectral density of the harmonic noise has a peak at a nonzero frequency ω_p and thus mimics a certain degree of periodicity. The power spectrum of $x(t)$ exhibits a maximum at $\omega_{\max}$, which is located close to ω_p, but with a small variation as a function of the noise. As in the case of phase diffusion, the peaks have a finite width. The signal-to-noise ratio shows a relative maximum at a finite noise strength typical of stochastic resonance.

In recent years, we witness a prosperous period for aperiodic stochastic resonance, which was ushered in by addressing the problem of optimizing information transfer in excitable systems (Collins *et al.*, 1995a, 1995b; De Weese and Bialek, 1995; Collins, Chow, *et al.*, 1996; Collins, Imhoff, and Grigg, 1996; Heneghan *et al.*, 1996; Levin and Miller, 1996; Nieman *et al.*, 1997). The abovenamed authors considered the Fitzhugh-Nagumo equations driven by white noise and an arbitrary aperiodic signal. This system was operated below threshold and the aperiodic signal was not large enough to induce excitation. Together with the noise, however, excitations were possible. Stochastic resonance has been demonstrated for the correlation of the aperiodic signal with the excitation rate (the number of excitation events per unit time).

This area has stimulated an interesting ongoing discussion: Do there exist suitable measures quantifying stochastic resonance—and what are they—that can be based solely on information theory considerations? A promising approach has been put forward by Heneghan *et al.* (1996) who consider the so-termed *transinformation* that quantifies the rate of information transfer from stimulus to response. They demonstrated that the presence of noise optimizes, via aperiodic stochastic resonance, the information-transfer rate. An attempt to characterize conventional stochastic resonance by means of information theory tools has been put forward by Schimansky-Geier and co-workers (Neiman *et al.*, 1996; Schimansky-Geier *et al.*, 1998), by Bulsara and Zador (1996), and by Chapeau-Blondeau (1997). Considering conditional entropies and Kullback measures, Schimansky-Geier *et al.* (1998) demonstrated with a Schmitt trigger system, driven periodically at strong, but still subthreshold amplitude strengths, that information measures do exhibit characteristic extrema. These extrema, however, do *not* decribe the conventional regime of stochastic resonance for the signal-to-noise ratio, but they rather seem to mimic the stochastic resonance behavior in a regime that is in accordance with stochastic resonance for the spectral amplification η.

D. Stochastic resonance—related topics

1. Noise-induced resonances

In studying stochastic resonance, one looks at the periodic contribution of the output at the same frequency as the input. More recently, the general question of the generation of higher harmonics in the presence of noise has been addressed in a number of studies (Bartussek *et al.*, 1993; Dykman, Mannella, McClintock, Stein, and Stocks, 1993a; Bartussek, Hänggi, and Jung, 1994; Dykman *et al.*, 1994; Jung and Talkner, 1995; Bulsara, Inchiosa, and Gammaitoni, 1996; Jung and Bartussek, 1996). In this section we focus on a novel effect (Bartussek, Hänggi, and Jung, 1994), namely the noise-selective resonance-like suppression of higher harmonics. These "noise-induced resonances" have been observed using numerical solutions of the Fokker-Planck equation in bistable systems (Bartussek, Hänggi, and Jung, 1994) as well as in monostable systems (Jung and Bartussek, 1996). Noise-induced resonances have already been observed in experiments with a periodically driven SQUID by Rouse, Han, and Lukens (1995). Recently, similar resonances have been predicted for quantum stochastic resonance by Grifoni and Hänggi (1996a, 1996b).

Apart from numerical, adiabatic studies (Bartussek, Hänggi, and Jung, 1994; Rouse *et al.*, 1995), an analytical theory allowing one to predict whether or not a particular system would exhibit noise-induced resonance has been put forward by Jung and Talkner (1995). Their approach is sketched as follows: we consider here a general overdamped system subject to additive white noise and periodic forcing, i.e.,

$$\dot{x} = f(x) + A_0 \cos(\Omega t) + \xi(t), \tag{7.13}$$

where $\xi(t)$ is as usual white Gaussian noise with zero mean and strength D, and $f(x)$ is the forcing function.

As shown in Sec. IV.A, the spectral density consists of a broad background and δ spikes at multiples of the driving frequency. The weights of the δ spikes are given by $g_n = 2\pi|M_n|^2$, where M_n are the complex Fourier coefficients of the asymptotic (large times) mean value $\langle x(t)\rangle_{as}$. Since the nth harmonic is in leading order proportional to A_0^n (see Jung and Bartussek, 1996), the intensities g_n are proportional to A_0^{2n}. We therefore define the characteristic coefficients

$$\gamma_n \equiv \frac{4\pi|M_n|^2}{n!^2 A_0^{2n}}, \tag{7.14}$$

to describe the intensities of the harmonics. In the adiabatic approximation, the characteristic coefficients γ_n have been obtained by Jung and Talkner (1995) in their respective leading order A_0^{2n} as

$$\gamma_n = \frac{4\pi|M_n|^2}{n!^2 A_0^{2n}} \approx \frac{4\pi}{(2D)^{2n}}\left(\frac{K_{n+1}}{n!}\right)^2, \tag{7.15}$$

where K_n are the *cumulants* of the stationary probability density of the unperturbed process ($A_0 = 0$). The intensity of the basic harmonic γ_1 cannot exhibit noise-induced resonance for any system, because the second order cumulant is strictly positive. The sign of the cumulants $K_{n>2}$ can change, for example, as a function of the noise strength D, giving rise to zeros of the intensities γ_n of the higher harmonics, i.e., to noise-induced resonances.

Decomposing the complex amplitude M_n into the product $M_n = |M_n|\sin\phi_n$, it can be seen that whenever a noise-induced resonance occurs, the phase ϕ_n exhibits a jump of magnitude π. Several concrete systems (single well, double well, two-state system, etc.) have been discussed by Jung and Talkner (1995).

2. Periodically rocked molecular motors

It is generally appreciated that useful work cannot be extracted from thermal equilibrium fluctuations. Such a device would violate the second law of thermodynamics. Feynman *et al.* (1966) discussed this issue by means of a model of a mechanical ratchet—a scheme that was originally devised and elucidated during the heyday of early Brownian motion by M. V. Smoluchowski (1912, 1914). In his articles, which these days still provide delightful reading, Smoluchowski (1912, 1914) shows that in the absence of an intelligent creature, such as a Maxwell demon, no net currents will occur. In the presence of nonequilibrium forces the situation changes drastically: now a thermal ratchet system, that is, a periodic structure with spatial asymmetry subjected to noise, can rectify symmetric, unbiased nonequilibrium fluctuations into a fluctuation-induced directed current (Ajdari and Prost, 1992; Magnasco, 1993; Astumian and Bier, 1994; Bartussek, Hänggi, and Kissner, 1994; Doering *et al.*, 1994; Leibler, 1994; for a comprehensive reviews see Hänggi and Bartussek, 1996; Astumian, 1997; Jülicher *et al.*, 1997). Put differently, by a ratchet we mean a system that is able to move particles with finite macroscopic velocity in the absence of any macroscopic bias forces

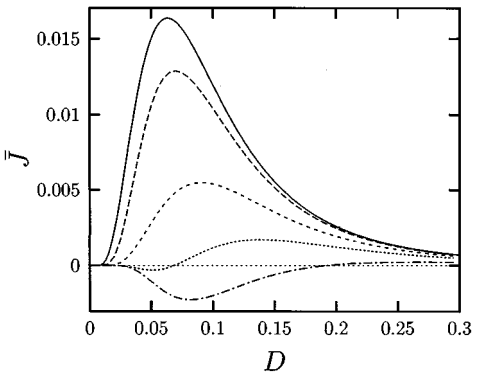

FIG. 54. Unidirectional probability current J vs noise strength D at fixed driving amplitude $A_0 = 0.5$ in a rocking ratchet with asymmetric periodic potential $V_R(x) = -[\sin(2\pi x) + \frac{1}{4}\sin(4\pi x)]/2\pi$. The various lines correspond to different driving angular frequencies Ω: adiabatic driving: $\Omega = 0.01$ (solid line); and nonadiabatic driving: $\Omega = 1$ (dashed), $\Omega = 2.5$ (short-dashed), $\Omega = 4$ (dotted), and $\Omega = 7$ (dashed-dotted). With the period L of the ratchet potential equal to unity, the average particle drift $\langle \dot{x}\rangle = LJ$ equals in this case the probability current J. A characteristic current reversal (with J passing through zero) occurs in the regime of nonadiabatic driving! The adiabatic theory, see Eq. (7.17), falls on to the line with $\Omega = 0.01$. After Bartussek, Hänggi, and Kissner (1994).

such as static external force fields, field gradients of thermal, chemical, or other origin. Hence the acting nonequilibrium forces of zero ensemble average are spatially uniform, and generally are statistically symmetric. The same principle applies if the stationary nonequilibrium forces are substituted by a spatially uniform, coherent periodic signal $F(t)$ of zero temporal average (Magnasco, 1993; Ajdari *et al.*, 1994; Bartussek, Hänggi, and Kissner, 1994). These systems are thus closely related in spirit to the stochastic resonance phenomenon: Fluctuation-induced escape among neighboring states in a periodic, multistable potential supported by weak deterministic periodic signals is responsible for moving particles forward noisily. In short, a deterministic driving alone, which exceeds a lower threshold is sufficient to create an induced current. Increasing at fixed angular frequency Ω the driving strength in overdamped, deterministic ratchet dynamics reveals numerous interesting features such as a devil's staircase behavior of current vs driving strength, current-quantization phenomena, and further peculiar features. In the presence of thermal Nyquist noise $\zeta(t)$, with $\langle\zeta(t)\rangle = 0$ and correlation $\langle\zeta(t)\zeta(t')\rangle = 2D\,\delta(t-t')$ the noisy, periodically driven, overdamped rocking ratchet dynamics reads

$$\dot{x} = -\frac{d}{dx}V_R(x) + A_0\cos(\Omega t) + \zeta(t). \tag{7.16}$$

Herein $V_R(x)$ is the periodic (period L) sawtooth-like ratchet potential $V_R(x) = V_R(x+L)$ possessing no reflection symmetry $V_R(x) \neq V_R(-x)$. In Fig. 54 we depict the noise-induced current versus the thermal intensity D. Noteworthy in Fig. 54 is the stochastic-

resonance-like feature of the probability current J vs D characteristics, as well as the phenomenon of *current reversal* (Bartussek, Hänggi, and Kissner, 1994) that occurs for nonadiabatic driving frequencies Ω. The mean velocity of the particle position is given by $\langle \dot{x} \rangle = LJ$, where J is the time-averaged probability current. Within an adiabatic approximation, i.e., for slow driving $(\Omega \to 0)$ the current J reads explicitly

$$J = \frac{D}{2\pi/\Omega} \int_0^{2\pi/\Omega} dt \Bigg\{ \{1 - \exp[\Phi(L,t)]\}^{-1} \times \int_0^L dx \int_0^L dy \, \exp[\Phi(y,t) - \Phi(x,t)] - \int_0^L dx \int_0^x dy \, \exp[\Phi(y,t) - \Phi(x,t)] \Bigg\}^{-1}, \quad (7.17)$$

where $\Phi(x,t) = [V_R(x) - xA_0 \cos(\Omega t)]/D$.

In Fig. 54 this approximation for the smallest frequency $\Omega = 0.01$ coincides within line thickness with the exact Floquet-theory result (solid line). The effects of inertia and/or weak friction are also intriguing: In the absence of thermal noise, the characteristic chaotic motion is sufficient to induce a directed current J, which exhibits multiple current reversals vs the driving amplitude A_0 (Jung *et al.*, 1996).

Another ratchet type that is related closely to the rocking ratchet in Eq. (7.16) is obtained if one substitutes the external coherent driving by an oscillating temperature, i.e.,

$$A_0 \cos(\Omega t) \to \zeta(t)[1 + A_0 \cos(\Omega t)]. \quad (7.18)$$

This defines a *diffusion ratchet* (Reimann *et al.*, 1996), which tends to resist carrying a finite current in the asymptotic limits of fast and slow driving. In this case the current starts only proportional to Ω^2, as $\Omega \to 0$ (i.e., a zero net current in the leading-order adiabatic approximation) and vanishes again proportional to Ω^{-2}, as $\Omega \to \infty$.

3. Escape rates in periodically driven systems

The problem of activated rates in threshold systems that are exposed to noise and periodic perturbations is nontrivial. The phase $\Omega t \equiv \theta$ of the periodic driving constitutes an additional dimension that can be used to define the escape rate out of a basin of attraction in extended space (Jung and Hänggi, 1991b). The basin of attraction is then shown to be separated by an unstable periodic orbit in extended x-θ space. For a bistable potential, this rate is related to the smallest nonzero Floquet eigenvalue μ. Note that this very quantity rules the long-time relaxation of general statistical quantities such as time-dependent mean values or time-averaged correlations. This positive-valued, rate-determining eigenvalue, being at weak noise well separated from higher-order relaxational Floquet eigenvalues, has been investigated for a driven, symmetric double well by Jung (1989; see Figs. 4–6 therein). For the pecularities that occur in periodically driven dynamics in a periodic potential, where the rate-determining Floquet eigenvalue is related to the Floquet eigenvalue at one of the two boundaries of the first Brillouin zone, we refer the reader to the discussion given in Jung and Hänggi (1991b). A main result is that the rate (or Floquet eigenvalue), which increases proportional to A_0^2, does not exhibit any kind of resonance-like behavior! Thus, as repeatedly demonstrated in this review, the stochastic resonance phenomenon is not due to a resonance for the rate of escape in the periodically driven system. In recent studies by Reichl and her collaborators (Alpatov and Reichl, 1994; Kim and Reichl, 1996) the higher-order Floquet eigenvalues have been investigated by formally mapping the periodically driven overdamped system onto an equivalent quantum dynamics at imaginary times. As a main result they find that in the regime where the quantum system exhibits a transition to chaos the spectrum of Floquet eigenvalues shows level repulsion.

Yet another quantity related to the rate-determining Floquet eigenvalue is the diffusion coefficient in a tilted periodic potential. Here, the interplay of subthreshold static drive and thermal fluctuations results in an enhancement of the ensuing stationary current, with a maximum for a certain value of the temperature. Such an effect, not observable in the overdamped limit (Hu, 1993; Gittermann, Khalfin, and Shapiro, 1994; Casado, Mejías, and Morillo, 1995), may be important in *weakly* damped systems (Marchesoni, 1997). If the static drive is replaced by a periodic tilt with suprathreshold amplitude, novel effects can be induced such as an enhancement of the diffusion rate that even exceeds (Hu, Dafferstshofer, and Haken, 1996) the rate of free diffusion! Likewise, the role of suprathreshold driving strengths applied to stochastic resonance systems has recently been studied for the phenomenon of a noise-induced failure mechanism for driven switch transitions (Apostolico *et al.*, 1997).

VIII. CONCLUSIONS AND OUTLOOK

In this review we have shown that adding noise to a system can sometimes improve its ability to transfer information reliably. This phenomenon—known as *stochastic resonance*—was originally proposed, almost seventeen years ago, to account for the periodicity in the Earth's ice ages, but has since been shown to occur in many systems. By now, understanding of the phenomenon of stochastic resonance has reached a mature level that we have attempted to review with this long paper. Numerous contributions to stochastic resonance have appeared in most physics journals and can be found scattered through many other scientific journals (e.g., see http://www.umbrars.com/sr), particularly in the fields of biology and physiology; it thus has reached the level of what we may term an "industry."

Undoubtedly, the neurophysiological applications represent cornerstones in the field of stochastic resonance. Such applications have attracted continued inter-

est from scientists in biology, biomedical engineering, and medicine. A new interdisciplinary field beyond conventional stochastic resonance, with inputs from nonlinear dynamics, nonequilibrium statistical physics, biological and medical sciences has emerged.

The general feature of a system exhibiting stochastic resonance is its increased sensitivity to small perturbations when an appropriate dose of noise is added; see the Introduction and Sec. II. The idea that random noise can be beneficial to the formation of ''order'' sounds paradoxical, but must be taken seriously by now. Stochastic resonance simply stands for a new paradigm wherein noise represents a useful tool, rather than a nuisance. Given the basic three ingredients of stochastic resonance, which are (1) a form of threshold, (2) a source of ''noise,'' and (3) a generally weak input source, it is clear that stochastic resonance is generic enough to be observable in a large variety of systems.

For the benefit of the reader let us summarize here what we think has been achieved in the field of stochastic resonance, point out open questions, and finally share our views about future perspectives.

For simple physical systems that can be described by either one of the two generic models introduced in Sec. III (two-state model) and in Secs. IV.A and IV.B (continuous-state bistable model), the mechanism that underpins the stochastic resonance effect is by now well understood. The increased response of the system in the presence of noise is due to the *synchronization* of noise-induced hopping with the temporal profile of the weak perturbation. This response of the system is ruled by two competing aspects: starting out from the zero-noise limit, increasing noise allows—correlated with the small perturbation—excursions into the neighboring well. This causes an increased response. On the other hand, increasing the noise level counteracts the aforementioned correlation; thereby reducing the response. These two aspects are encoded mathematically by the susceptibility χ, which essentially is made up of two factors: the product of an Arrhenius factor, describing the activated hopping, and a factor proportional to the inverse noise intensity $1/D$, characterizing the degradation of the response. The result is a bell-shaped curve for the response amplitude vs noise intensity, hence the term stochastic resonance—an expression that for some may appear ill-defined. This physics in turn determines the most common quantifiers for stochastic resonance: the signal-to-noise ratio (SNR) of the output, and the spectral (power) amplification η; see Secs. II.A and IV.B. Likewise, the statistical features of the driven residence-time distributions $N(T)$ (see Sec. IV.C), reflect the synchronization between random hopping and external modulation. The multipeaked signatures exhibited by the residence-time distribution at *odd* multiples of half the driving period are nothing but the fingerprints of this synchronization process that occurs in the competition between the active driving source and the passive dissipation. It should not go unnoticed that the understanding of this very concept of driven residence-time distributions paved the way to interpreting a mass of physiological data from a new viewpoint; see Secs. IV.C and V.C.

Equipped with the basics of stochastic resonance theory, developed in some detail in Secs. III and IV, we discussed and interpreted in Sec. V several prominent applications and experiments taken from the fields of physics and neurophysiology (a more detailed list of experimental stochastic resonance demonstrations is given in Sec. II.C.3).

More recent developments in the field of stochastic resonance presently in the limelight of the activities of many research groups are discussed in Sec. VI. Both quantum stochastic resonance and spatiotemporal stochastic resonance have only just begun to be explored. Quantum tunneling assists the stochastic resonance effect in the semiclassical regime; in the deep cold, however, quantum coherence increasingly spoils the effect; see Sec. VI.A. The notion of stochastic resonance generalized to spatially extended pattern-forming systems has been the subject of Sec. VI.B: spatiotemporal patterns can be enhanced by adding the proper amount of noise. The notion of deterministic chaos, which intrinsically provides a source of disorder, has been studied by various groups, and has been reviewed in Sec. VI.C. The last section, Sec. VI.D, has been devoted to the study of the effects of finite correlation times (colored noise) of the background noise. For overdamped dynamics the role of colored noise generally results in a reduction of the efficiency of stochastic resonance. In contrast, finite inertia effects, induced by moderate friction, tend to boost the stochastic resonance response. The physics of stochastic resonance at extreme weak friction, however, still needs to be investigated in greater detail.

The field of stochastic resonance research has witnessed a remarkable flourishing during the last few years; needless to say it is no longer possible to present a detailed account on each single contribution. In Sec. VII we have discussed selected contributions that provide additional insight. Stochastic resonance and its connection with the dithering effect, globally coupled periodically modulated bistable elements, or the impact of additional multiplicative noise on stochastic resonance in the presence of additive noise (see Sec. VII.C.1) are all topics that relate closely to stochastic resonance. Recently, research on stochastic resonance in physical systems has diverged into neighboring fields such as the problem of noise-induced transport in Brownian ratchets; see Sec. VII.D.2. The modern topic of nonlinear stochastic resonance involves the impact of noise on the generation and mixing of higher harmonics; see Sec. VII.D.1. A peculiar effect, the suppression of higher harmonics at some specific noise strengths, is being reported there. This effective elimination of higher harmonics could be used to the effect of minimizing the distortion of information transfer in nonlinear systems.

In Sec. VII.C.3 on aperiodic stochastic resonance—i.e., the phenomenon being obtained in presence of a nonperiodic input signal—we touched on a still open problem. Can stochastic resonance be suitably charac-

terized by means of information theory concepts alone? In view of quantum stochastic resonance, which intrinsically avoids the notion of joint probability measures, a unifying answer seems anything but trivial.

It may be worthwhile to conclude with some speculations on what the future of stochastic resonance may look like. What is still lacking from a physics point of view is a detailed, microscopic approach to stochastic resonance that would account for the mutual interplay between the transfer of power among the system $x(t)$, the bath(s) [or sources of noise $\xi(t)$], and the external signal $A(t)$. Another promising area for fruitful further research is quantum stochastic resonance. For example, almost nothing is known about the quantum analog of stochastic resonance in threshold-crossing devices, stochastic resonance in arrays of coupled quantum systems, or—last but not least—the difficult problem of modeling quantum stochastic resonance in stationary nonequilibrium systems (i.e., the physics occurring in driven, dissipative quantum systems that are far from thermal equilibrium). The observation that classical concepts become increasingly invalid upon crossing the borderline between the classical and the quantum world, and beyond, is an indication that several surprises and novel stochastic resonance phenomena are waiting to be uncovered. The same holds true for spatiotemporal stochastic resonance, which yet has to be extended into three-dimensional structures.

Clearly, stochastic resonance constitutes an information-transmitting phenomenon that exploits the noise in a self-optimizing manner. Therefore, its promising role in complex systems such as the nervous system, or even the brain have not gone unnoticed in the communities of physiological, biological, and medical sciences; see the reviews by Moss, Pierson, and O'Gorman (1994) and Wiesenfeld and Moss (1995). For example, the question of whether extremely low-frequency electromagnetic fields actually affect biological function via the stochastic resonance phenomenon still remains open. What has been achieved so far is the successful demonstration of stochastic resonance with injected external noise in the peripheral nervous system of crayfish (Douglass *et al.*, 1993; Pei *et al.*, 1996), in crickets (Levin and Miller, 1996), in the human visual perception (Riani and Simonotto, 1995; Simonotto *et al.*, 1997), and in ion channels (Bezrukov and Vodyanoy, 1995), to name a few. Without doubt this latter area, too, is expected to prosper by providing numerous interesting new results and novel insights.

ACKNOWLEDGEMENTS

P.J. and P.H. would like to thank the Deutsche Forschungsgemeinschaft for financial support. F.M. and L.G. wish to thank the Istituto Nazionale di Fisica della Materia (INFM) and CNR for partial funding. F.M. would further like to thank B. I. Halperin for his kind hospitality at the Physical Laboratories of the Harvard University. Most of the analog simulations presented herein were carried out in collaboration with E. Menichella-Saetta and S. Santucci (Perugia). We greatly appreciate insightful discussions with Th. Anastasio, R. Bartussek, A. Bulsara, D. K. Campbell, J. Collins, Th. Dittrich, M. Dykman, W. Ebeling, J. Grohs, R. F. Fox, H. Frauenfelder, G. Hu, M. Grifoni, A. Jackson, L. Kiss, A. Kittel, A. Longtin, R. Mantegna, G. Mayer-Kress, F. Moss, J. Parisi, E. Pollak, C. Presilla, H. Risken, R. Roy, L. Schimansky-Geier, B. Spagnolo, A. Sutera, W. Sung, P. Talkner, A. Vulpiani, U. Weiss, K. Wiesenfeld, and C. Zerbe. Last but not least, we would like to thank our indispensable Mrs. Eva Seehuber for her continuous help while preparing this work.

P.H., P.J., and F.M. are deeply indebted to our friend and mentor Hannes Risken, whose wisdom and friendship we are missing deeply after his untimely death in January 1994.

APPENDIX: PERTURBATION THEORY

For weak external forcing, the time-inhomogeneous term in the Fokker-Planck equation can be treated as a small perturbation with the amplitude A_0 acting as small parameter. Perturbation theory (Presilla *et al.*, 1989; Hu *et al.*, 1990; Jung, 1993) provides explicit expressions for characteristic quantities of the driven systems, such as the Floquet eigenvalues, eigenfunctions, and mean values in terms of the eigenvalues and eigenfunctions of the unperturbed Fokker-Planck operator.

The starting point is the Floquet eigenvalue problem, obtained in Sec. IV.A by inserting the Floquet ansatz (4.9) into the Fokker-Planck equation (4.11) with $\varphi=0$

$$\left[\mathcal{L}_0 - A_0\cos(\Omega t)\frac{\partial}{\partial x} - \frac{\partial}{\partial t}\right] p_\mu(x,t;0) = -\mu p_\mu(x,t;0), \tag{A1}$$

with

$$\mathcal{L}_0 = -\frac{\partial}{\partial x} f(x) + D\frac{\partial^2}{\partial x^2}, \tag{A2}$$

and

$$f(x) = x - x^3. \tag{A3}$$

Expanding the Floquet eigenfunctions into a Fourier series

$$p_\mu(x,t;0) = \sum_{n=-\infty}^{\infty} c_n(x)\exp[in\Omega t] \tag{A4}$$

yields the hierarchy of coupled ordinary differential equations

$$(\mathcal{L}_0 - in\Omega + \mu)c_n(x) - \frac{A_0}{2}[c'_{n+1}(x) + c'_{n-1}(x)] = 0, \tag{A5}$$

with $c'_n(x) = dc_n(x)/dx$.

For strictly real-valued Floquet eigenvalues μ, the Floquet eigenfunctions are real as well, i.e.,

$$c_n(x)=c^*_{-n}(x). \tag{A6}$$

In order for the perturbation theory to be applicable to more general situations such as tilted periodic potentials, we do not make use of this assumption. The zeroth order perturbation theory for $A_0=0$

$$(\mathcal{L}_0-in\Omega+\mu^{(0)})c_n^{(0)}(x)=0 \tag{A7}$$

is solved by

$$c_n^{(0)}(x)=\psi_l(x),$$

$$\mu_{ln}^{(0)}=\lambda_l+in\Omega, \tag{A8}$$

where the index l of $\{c_n(x)\}$ has been dropped throughout for convenience. Here, $\psi_l(x)$, $\psi_l^\dagger(x)$, and λ_l are the eigenfunctions and eigenvalues of the unperturbed (adjoint) Fokker-Planck operator, i.e.,

$$\mathcal{L}_0\psi_l(x)=-\lambda_l\psi_l(x),$$

$$\mathcal{L}_0^\dagger\psi_l^\dagger(x)=-\lambda_l\psi_l^\dagger(x),$$

$$\langle l|m\rangle\equiv\int_{-\infty}^{\infty}\psi_l(x)\psi_m^\dagger(x)dx=\delta_{lm}. \tag{A9}$$

To order $(A_0)^0$, all equations with label n have the same form. The eigenvalues differ by a multiple of $i\Omega$. Without loss of generality, we can start the perturbation expansion at $n=0$, i.e.,

$$\mu_{ln=0}^{(0)}\equiv\mu_l^{(0)}=\lambda_l,$$

$$c_n^{(0)}(x)=\delta_{n0}\psi_l(x). \tag{A10}$$

The first three equations of Eq. (A5) are written down explicitly as

$$(\mathcal{L}_0+\mu)c_0(x)=\frac{A_0}{2}[c_1'(x)+c_{-1}'(x)], \tag{A11}$$

$$(\mathcal{L}_0-i\Omega+\mu)c_1(x)=\frac{A_0}{2}[c_2'(x)+c_0'(x)],$$

$$(\mathcal{L}_0+i\Omega+\mu)c_{-1}(x)=\frac{A_0}{2}[c_0'(x)+c_{-2}'(x)]. \tag{A12}$$

We now seek a solution of the latter system of differential equations in terms of the perturbation expansions

$$c_n(x)=\delta_{n0}\psi_l(x)+A_0c_n^{(1)}(x)+A_0^2c_n^{(2)}(x)+\cdots,$$

$$\mu_l=\lambda_l+A_0\mu_l^{(1)}+A_0^2\mu_l^{(2)}+\cdots. \tag{A13}$$

It follows immediately from Eq. (A11) that $\mu^{(1)}$ vanishes. Comparing terms of order A_0 and A_0^2 in Eqs. (A11) and (A12) yields

$$(\mathcal{L}_0+\lambda_l)c_0^{(2)}(x)+\mu_l^{(2)}\psi_l(x)=\frac{1}{2}[c_1'^{(1)}(x)+c_{-1}'^{(1)}(x)], \tag{A14}$$

$$(\mathcal{L}_0-i\Omega+\lambda_l)c_1^{(1)}(x)=\frac{1}{2}\psi_l'(x),$$

$$(\mathcal{L}_0+i\Omega+\lambda_l)c_{-1}^{(1)}(x)=\frac{1}{2}\psi_l'(x). \tag{A15}$$

Since $\lambda_l\pm i\Omega$ are not eigenvalues of the operator $\mathcal{L}_0$, the operators $\mathcal{L}_0+\lambda_l\pm i\Omega$ can be inverted and the functions $c_{\pm1}^{(1)}(x)$ are obtained formally as

$$c_1^{(1)}(x)=\frac{1}{2}(\mathcal{L}_0-i\Omega+\lambda_l)^{-1}\psi_l'(x),$$

$$c_{-1}^{(1)}(x)=\frac{1}{2}(\mathcal{L}_0+i\Omega+\lambda_l)^{-1}\psi_l'(x). \tag{A16}$$

Inserting Eq. (A16) into Eq. (A14), multiplying by the eigenfunction $\psi_l^\dagger$ and then integrating over x, we obtain

$$\mu_l^{(2)}=\frac{1}{4}\int_{-\infty}^{\infty}\psi_l^\dagger(x)\frac{\partial}{\partial x}\mathcal{L}_1\frac{\partial}{\partial x}\psi_l(x)dx$$

$$=\frac{1}{4}\left\langle l\left|\frac{\partial}{\partial x}\mathcal{L}_1\frac{\partial}{\partial x}\right|l\right\rangle, \tag{A17}$$

where

$$\mathcal{L}_1=\frac{1}{\mathcal{L}_0+i\Omega+\lambda_l}+\frac{1}{\mathcal{L}_0-i\Omega+\lambda_l}. \tag{A18}$$

For the Floquet eigenfunctions one obtains in leading-order perturbation theory

$$p_{\mu_l}(x,t)=\psi_l(x)+\frac{A_0}{2}\{\exp(-i\Omega t)[\mathcal{L}_0+i\Omega+\lambda_l]^{-1}$$

$$+\exp(i\Omega t)[\mathcal{L}_0-i\Omega+\lambda_l]^{-1}\}\psi_l'(x). \tag{A19}$$

In view of the identity

$$\frac{\partial}{\partial x}\psi_l(x)=\sum_{q=0}^{\infty}\psi_q(x)\int_{-\infty}^{\infty}\psi_q^\dagger(x)\frac{\partial}{\partial x}\psi_l(x)dx$$

$$=\sum_{q=0}^{\infty}\left\langle q\left|\frac{\partial}{\partial x}\right|l\right\rangle\psi_q(x), \tag{A20}$$

the Floquet eigenvalues and eigenfunctions can be expressed in terms of the eigenfunctions of the undriven Fokker-Planck operator, namely

$$\mu_l=\lambda_l+\frac{A_0^2}{2}\sum_{q=0}^{\infty}\frac{\lambda_l-\lambda_q}{(\lambda_l-\lambda_q)^2+\Omega^2}\left\langle l\left|\frac{\partial}{\partial x}\right|q\right\rangle$$

$$\times\left\langle q\left|\frac{\partial}{\partial x}\right|l\right\rangle$$

$$p_{\mu_l}(x,t)=\psi_l(x)+A_0\sum_{q=0}^{\infty}\frac{1}{\sqrt{(\lambda_l-\lambda_q)^2+\Omega^2}}$$

$$\times\left\langle q\left|\frac{\partial}{\partial x}\right|l\right\rangle\cos(\Omega t+\alpha_{ql})\psi_q(x), \tag{A21}$$

with

$$\tan(\alpha_{ql}) = \Omega/(\lambda_l - \lambda_q). \tag{A22}$$

In particular, the asymptotic probability density $p_{as}(x,t)$, corresponding to the vanishing Floquet eigenvalue $\mu_0 = \lambda_0 = 0$, reads

$$\begin{aligned} p_{as}(x,t) &= p_0(x) + A_0 \sum_{q=1}^{\infty} \left\langle q \left| \frac{\partial}{\partial x} \right| 0 \right\rangle \\ &\quad \times \psi_q(x) \frac{1}{\sqrt{\lambda_q^2 + \Omega^2}} \cos(\Omega t + \alpha_{q0}) \\ &= p_0(x) + A_s(x)\sin(\Omega t) + A_c(x)\cos(\Omega t), \end{aligned} \tag{A23}$$

with

$$A_c(x) = A_0 \sum_{q=1}^{\infty} \frac{\lambda_q}{\lambda_q^2 + \Omega^2} \left\langle q \left| \frac{\partial}{\partial x} \right| 0 \right\rangle \psi_q(x),$$

$$A_s(x) = A_0 \sum_{q=1}^{\infty} \frac{\Omega}{\lambda_q^2 + \Omega^2} \left\langle q \left| \frac{\partial}{\partial x} \right| 0 \right\rangle \psi_q(x). \tag{A24}$$

The spectral amplification [Eq. (4.21)] is obtained by inserting Eq. (A23) into the definition $\langle x(t) \rangle_{as} = \int x p_{as}(x,t)\, dx$, that is,

$$\begin{aligned} \eta = \sum_{n,m=0}^{\infty} & \frac{\lambda_n \lambda_m + \Omega^2}{(\lambda_n^2 + \Omega^2)(\lambda_m^2 + \Omega^2)} \left\langle n \left| \frac{\partial}{\partial x} \right| 0 \right\rangle \\ & \times \left\langle m \left| \frac{\partial}{\partial x} \right| 0 \right\rangle \langle 0|x|n\rangle \langle 0|x|m\rangle. \end{aligned} \tag{A25}$$

The expression (A25) is exact up to order $(A_0)^2$.

The expression for $\langle x(t) \rangle_{as}$ to leading order in A_0 coincides with the prediction of the thermal-equilibrium linear-response theory of Sec. IV.B. This last statement can be proved explicitly by inserting the completeness relation into the expression

$$\chi(t) = \int x e^{\mathcal{L}_0 t} \left(-\frac{\partial}{\partial x} \right) p_0(x)\, dx \tag{A26}$$

for the response function $\chi(t)$ of the modulated system of Eq. (A.1), whence

$$\chi(t) = -\sum_{q=1}^{\infty} e^{-\lambda_q t} \left\langle q \left| \frac{\partial}{\partial x} \right| 0 \right\rangle \langle 0|x|q\rangle. \tag{A27}$$

Note that Eq. (A26) follows immediately from the general definition (4.28) of $\chi(t)$ by substituting $\Gamma_{ext} = \delta'(y-z)$ for the perturbation kernel, and $P_0(x,t|y,0) = e^{\mathcal{L}_0 t}\delta(x-y)$ for the unperturbed conditional probability density of the system under study. On further substituting the spectral representation (A27) of $\chi(t)$ into Eq. (4.26), we eventually reproduce the perturbation theory prediction for $\langle x(t) \rangle_{as}$:

$$\begin{aligned} \langle x(t) \rangle_{as} = A_0 \sum_{q=1}^{\infty} & \left\langle q \left| \frac{\partial}{\partial x} \right| 0 \right\rangle \langle 0|x|q\rangle \frac{1}{\sqrt{\lambda_q^2 + \Omega^2}} \\ & \times \cos(\Omega t + \alpha_{q0}). \end{aligned} \tag{A28}$$

On approximating $\langle 0|x|1\rangle$ to 1 and $\langle 1|\partial/\partial x|0\rangle$ to $-\lambda_1/D$, one eventually recovers Eq. (2.7a) for $x(D)$ (Hu *et al.*, 1990).

REFERENCES

Abramowitz, M., and I. A. Stegun, 1965, *Handbook of Mathematical Functions* (Dover, New York).

Ajdari, A., D. Mukamel, L. Peliti, and J. Prost, 1994, J. Phys. I **4**, 1551.

Ajdari, A., and J. Prost, 1992, C.R. Acad. Sci. **315**, 1635.

Alpatov, P., and L. E. Reichl, 1994, Phys. Rev. E **49**, 2630.

Amit, D. J., 1984, *Field Theory, The Renormalization Group and Critical Phenomena* (World Scientific, Singapore).

Amit, D. J., 1989, *Modeling Brain Functions* (Cambridge University, Cambridge).

Anishchenko, V. S., A. B. Neimann, and M. A. Safanova, 1993, J. Stat. Phys. **70**, 183.

Anishchenko, V. S., M. A. Safonova, and L. O. Chua, 1994, Int. J. Bifurcation Chaos Appl. Sci. Eng. **4**, 441.

Apostolico, F., L. Gammaitoni, F. Marchesoni, and S. Santucci, 1997, Phys. Rev. E **55**, 36.

Arimondo, E., D. Dangoisse, E. Menchi, and F. Papoff, 1987, J. Opt. Soc. Am. B **4**, 892.

Arimondo, E., and B. M. Dinelli, 1983, Opt. Commun. **44**, 277.

Astumian, R. D., 1997, Science **276**, 917.

Astumian, R. D., and M. Bier, 1994, Phys. Rev. Lett. **72**, 1766.

Bartussek, R., P. Hänggi, and P. Jung, 1994, Phys. Rev. E **49**, 3930.

Bartussek, R., P. Hänggi, and J. G. Kissner, 1994, Europhys. Lett. **28**, 459.

Bartussek, R., P. Jung, and P. Hänggi, 1993, in Noise in Physical Systems and 1/*f* Fluctuations, edited by P. H. Handel, AIP Conf. Proc. 285, 661 (AIP, New York, 1993).

Barzykin, A. V., and K. Seki, 1997, Europhys. Lett. **40**, 117.

Benderskii, V. A., D. E. Makarov, and C. A. Wight, 1994, Adv. Chem. Phys. **85**, 1.

Bennet, W. R., 1948, Bell Syst. Tech. J. **27**, 446.

Benzi, R., G. Parisi, A. Sutera, and A. Vulpiani, 1982, Tellus **34**, 10.

Benzi, R., A. Sutera, G. Parisi, and A. Vulpiani, 1983, SIAM (Soc. Ind. Appl. Math.) J. Appl. Math. **43**, 565.

Benzi, R., A. Sutera, and A. Vulpiani, 1981, J. Phys. A **14**, L453.

Benzi, R., A. Sutera, and A. Vulpiani, 1985, J. Phys. A **18**, 2239.

Berdichevsky, V., and M. Gitterman, 1996, J. Phys. A **29**, L447.

Berghaus, C., A. Hilgers, and J. Schnakenberg, 1996, Z. Phys. B **100**, 157.

Bezrukov, S. M., and I. Vodyanoy, 1995, Nature (London) **378**, 362.

Bezrukov, S. M., and I. Vodyanoy, 1997, Nature (London) **385**, 319.

Blake, I. F., and W. C. Lindsey, 1973, IEEE Trans. Inf. Theory **IT-19**, 295.

Bonifacio, R., and L. A. Lugiato, 1978, Phys. Rev. A **18**, 1192.

Brey, J. J., and A. Prados, 1996, Phys. Lett. A **216**, 240.

Bruce, A. D., 1980, Adv. Phys. **29**, 111.
Bulsara, A., S. Chillemi, L. Kiss, P. V. E. McClintock, R. Mannella, F. Marchesoni, G. Nicolis, and K. Wiesenfeld, 1995, Eds., *International Workshop on Fluctuations in Physics and Biology: Stochastic Resonance, Signal Processing and Related Phenomena*, published in Nuovo Cimento **17D**, 653.
Bulsara, A., T. C. Elston, C. R. Doering, S. B. Lowen, and K. Lindenberg, 1996, Phys. Rev. E **53**, 3958.
Bulsara, A., and L. Gammaitoni, 1996, Phys. Today **49**, No. 3, 39.
Bulsara, A., M. Inchiosa, and L. Gammaitoni, 1996, Phys. Rev. Lett. **77**, 2162.
Bulsara, A., E. W. Jacob, T. Zhou, F. Moss, and L. Kiss, 1991, J. Theor. Biol. **152**, 531.
Bulsara, A., S. B. Lowen, and C. D. Rees, 1994, Phys. Rev. E **49**, 4989.
Bulsara, A., and G. Schmera, 1993, Phys. Rev. E **47**, 3734.
Bulsara, A., and A. Zador, 1996, Phys. Rev. E **54**, R2185.
Carroll, T. L., and L. M. Pecora, 1993a, Phys. Rev. Lett. **70**, 576.
Carroll, T. L., and L. M. Pecora, 1993b, Phys. Rev. E **47**, 3941.
Casado, J. M., J. J. Mejías, and M. Morillo, 1995, Phys. Lett. A **197**, 365.
Castelpoggi, F., and H. S. Wio, 1997, Europhys. Lett. **38**, 91.
Chapeau-Blondeau, F., 1997, Phys. Rev. E **55**, 2016.
Chialvo, D. R., and A. V. Apkarian, J. Stat. Phys. **70**, 375.
Choi, M., R. F. Fox, and P. Jung, 1998, Phys. Rev. E (in press).
Chun, K., and N. O. Birge, 1993, Phys. Rev. E **48**, 11 4500.
Claes, I., and C. Van den Broeck, 1991, Phys. Rev. A **44**, 4970.
Clarke, J., A. N. Cleland, M. H. Devoret, D. Esteve, and J. M. Martinis, 1988, Science **239**, 992.
Collins, J. J., C. C. Chow, A. C. Capela, and T. T. Imhoff, 1996, Phys. Rev. E **54**, R5575.
Collins, J. J., C. C. Chow, and T. T. Imhoff, 1995a, Phys. Rev. E **52**, R3321.
Collins, J. J., C. C. Chow, and T. T. Imhoff, 1995b, Nature (London) **376**, 236.
Collins, J. J., T. T. Imhoff, and P. Grigg, 1996, J. Neurophysiol. **76**, 642.
Coppinger, F., J. Genoe, D. K. Maude, U. Gennser, J. C. Portal, K. E. Singer, P. Rutter, T. Taskin, A. R. Peaker, and A. C. Wright, 1995, Phys. Rev. Lett. **75**, 3513.
Crisanti, A., M. Falcioni, G. Paladin, and A. Vulpiani, 1994, J. Phys. A **27**, L597.
Dakhnovskii, Yu., and R. D. Coalson, 1995, J. Chem. Phys. **103**, 2908.
Dayan, I., M. Gitterman, and G. H. Weiss, 1992, Phys. Rev. A **46**, 757.
Debnath, G., T. Zhou, and F. Moss, 1989, Phys. Rev. A **39**, 4323.
Desai, R., and R. Zwanzig, 1978, J. Stat. Phys. **19**, 1.
De Weese, M., and W. Bialek, 1995, Nuovo Cimento **17D**, 733.
Dewel, G., P. Borckmanns, D. Walgraef, 1985, Phys. Rev. A **31**, 1983.
Dittrich, T., B. Oelschlägel, and P. Hänggi, 1993, Europhys. Lett. **22**, 5.
Doering, C. R., W. Horsthemke, and J. Riordan, 1994, Phys. Rev. Lett. **72**, 2984.
Douglass, J. K., L. Wilkens, E. Pantazelou, and F. Moss, 1993, Nature (London) **365**, 337.
Drozdov, A. N., and M. Morillo, 1996, Phys. Rev. E **54**, 3304.
Dykman, M. I., G. P. Golubev, I. Kh. Kaufman, D. G. Luchinsky, P. V. E. McClintock, and E. A. Zhukov, 1995, Appl. Phys. Lett. **67**, 308.
Dykman, M. I., H. Haken, G. Hu, D. G. Luchinsky, R. Mannella, P. V. E. McClintock, C. Z. Ning, N. D. Stein, and N. G. Stocks, 1993, Phys. Lett. A **180**, 332.
Dykman, M. I., D. G. Luchinsky, R. Mannella, P. V. E. McClintock, H. E. Short, N. D. Stein, and N. G. Stocks, 1994, Phys. Rev. E **49**, 1198.
Dykman, M. I., D. G. Luchinsky, R. Mannella, P. V. E. McClintock, N. D. Stein, and N. G. Stocks, 1995, Nuovo Cimento D **17**, 661.
Dykman M. I., D. G. Luchinsky, P. V. E. McClintock, N. D. Stein, and N. G. Stocks, 1992, Phys. Rev. A **46**, R1713.
Dykman, M. I., R. Mannella, P. V. E. McClintock, N. D. Stein, and N. G. Stocks, 1993a, Phys. Rev. E **47**, 1629.
Dykman, M. I., R. Mannella, P. V. E. McClintock, N. D. Stein, and N. G. Stocks, 1993b, Phys. Rev. E **47**, 3996.
Dykman, M. I., R. Mannella, P. V. E. McClintock, and N. G. Stocks, 1990a, Phys. Rev. Lett. **65**, 48.
Dykman, M. I., R. Mannella, P. V. E. McClintock, and N. G. Stocks, 1990b, Phys. Rev. Lett. **65**, 2606.
Dykman, M. I., R. Mannella, P. V. E. McClintock, and N. G. Stocks, 1992, Phys. Rev. Lett. **68**, 2985.
Dykman, M. I., R. Mannella, P. V. E. McClintock, and N. G. Stocks, 1993, Phys. Rev. Lett. **70**, 874.
Eckmann, J-P., and L. E. Thomas, 1982, J. Phys. A **15**, L261.
Eigler, D. M., and E. K. Schweitzer, 1990, Nature (London) **344**, 523.
Faetti, S., P. Grigolini, and F. Marchesoni, 1982, Z. Phys. B **47**, 353.
Fauve, S., and F. Heslot, 1983, Phys. Lett. **97A**, 5.
Feynman, R. P., R. B. Leighton, and M. Sands, 1966, *The Feynman Lectures on Physics* (Addison-Wesley, Reading, MA), Vol. I, Chap. 46.
Fioretti, A., L. Guidoni, R. Mannella, and E. Arimondo, 1993, J. Stat. Phys. **70**, 403.
Floquet, G., 1883, Ann. de l'Ecole Norm. Suppl. **12**, 47.
Fox, R. F., 1978, Phys. Rep. **48**, 179.
Fox, R. F., 1989, Phys. Rev. A **39**, 4148.
Fox, R., and Y. Lu, 1993, Phys. Rev. E **48**, 3390.
Fronzoni, L., F. Moss, and P. V. E. McClintock, 1989, eds., *Noise in Nonlinear Dynamical Systems*, Vol. 3 (Cambridge University, Cambridge), p. 222.
Fuliński, A., 1995, Phys. Rev. E **52**, 4523.
Gage, E. C., and L. Mandel, 1988, Phys. Rev. A **38**, 5166.
Gammaitoni, L., 1995a, Phys. Rev. E **52**, 4691.
Gammaitoni, L., 1995b, Phys. Lett. A **208**, 315.
Gammaitoni, L., and F. Marchesoni, 1993, Phys. Rev. Lett. **70**, 873.
Gammaitoni, L., F. Marchesoni, M. Martinelli, L. Pardi, and S. Santucci, 1991, Phys. Lett. A **158**, 449.
Gammaitoni, L., F. Marchesoni, E. Menichella-Saetta, and S. Santucci, 1989, Phys. Rev. Lett. **62**, 349.
Gammaitoni, L., F. Marchesoni, E. Menichella-Saetta, and S. Santucci, 1990, Phys. Rev. Lett. **65**, 2607.
Gammaitoni, L., F. Marchesoni, E. Menichella-Saetta, and S. Santucci, 1993, Phys. Rev. Lett. **71**, 3625.
Gammaitoni, L., F. Marchesoni, E. Menichella-Saetta, and S. Santucci, 1994, Phys. Rev. E **49**, 4878.
Gammaitoni, L., F. Marchesoni, E. Menichella-Saetta, and S. Santucci, 1995, Phys. Rev. E **51**, R3799.

Gammaitoni, L., F. Marchesoni, and S. Santucci, 1994, Phys. Lett. A **195**, 116.
Gammaitoni, L., F. Marchesoni, and S. Santucci, 1995, Phys. Rev. Lett. **74**, 1052.
Gammaitoni, L., M. Martinelli, L. Pardi, and S. Santucci, 1991, Phys. Rev. Lett. **67**, 1799.
Gammaitoni, L., M. Martinelli, L. Pardi, and S. Santucci, 1992, Mod. Phys. Lett. B **6**, 197.
Gammaitoni, L., M. Martinelli, L. Pardi, and S. Santucci, 1993, J. Stat. Phys. **70**, 425.
Gammaitoni, L., E. Menichella-Saetta, S. Santucci, and F. Marchesoni, 1989, Phys. Lett. A **142**, 59.
Gammaitoni, L., E. Menichella-Saetta, S. Santucci, F. Marchesoni, and C. Presilla, 1989, Phys. Rev. A **40**, 2114.
Gerstein, G. L., and B. Mandelbrot, 1964, Biophys. J. **4**, 41.
Gingl, Z., L. B. Kiss, and F. Moss, 1995, Europhys. Lett. **29**, 191.
Gitterman, M., I. B. Khalfin, and B. Ya. Shapiro, 1994, Phys. Lett. A **184**, 339.
Gluckman, B. J., T. I. Netoff, E. J. Neel, W. L. Ditto, M. Spano, and S. J. Schiff, 1996, Phys. Rev. Lett. **77**, 4098.
Goel, N. S., and N. Richter-Dyn, 1974, *Stochastic Models in Biology* (Academic, New York).
Golding, B., N. M. Zimmermann, and S. N. Coppersmith, 1992, Phys. Rev. Lett. **68**, 998.
Gómez-Ordóñez, J., and M. Morillo, 1994, Phys. Rev. E **49**, 4919.
Gong, D., G. Hu, X. Wen, C. Yang, G. Qin, R. Li, and D. Ding, 1992, Phys. Rev. A **46**, 3243; Phys. Rev. E **48**, 4862 (E).
Gong, D., G. R. Qin, G. Hu, and X. D. Weng, 1991, Phys. Lett. A **159**, 147.
Goychuk, I. A., E. G. Petrov, and V. May, 1996, Chem. Phys. Lett. **353**, 428.
Grabert, H., and H. Wipf, 1990, in *Festkörperprobleme–Advances in Solid State Physics*, edited by U. Rössler (Vieweg, Braunschweig), Vol. 30, 1.
Graham, R., and A. Schenzle, 1982, Phys. Rev. A **25**, 1731.
Grebogi, C., E. Ott, and J. A. Yorke, 1987, Physica D **7**, 181.
Grifoni, M., and P. Hänggi, 1996a, Phys. Rev. Lett. **76**, 1611.
Grifoni, M., and P. Hänggi, 1996b, Phys. Rev. E **54**, 1390.
Grifoni, M., L. Hartmann, S. Berchtold, and P. Hänggi, 1996, Phys. Rev. E **53**, 5890; **56**, 6213 (E).
Grifoni, M., M. Sassetti, P. Hänggi, and U. Weiss, 1995, Phys. Rev. E **52**, 3596.
Grifoni, M., M. Sassetti, J. Stockburger, and U. Weiss, 1993, Phys. Rev. E **48**, 3497.
Grigolini, P., and F. Marchesoni, 1985, Adv. Chem. Phys. **62**, 29.
Grigorenko, A. N., V. I. Konov, and P. I. Nikitin, 1990, JETP Lett. **52**, 592.
Grigorenko, A. N., and P. I. Nikitin, 1995, IEEE Trans. Magn. **31**, 2491.
Grigorenko, A. N., P. I. Nikitin, A. N. Slavin, and P. Y. Zhou, 1994, J. Appl. Phys. **76**, 6335.
Grohs, J., S. Apanasevich, P. Jung, H. Issler, D. Burak, and C. Klingshirn, 1994, Phys. Rev. A **49**, 2199.
Grohs, J., H. Issler, and C. Klingshirn, 1991, Opt. Commun. **86**, 183.
Grohs, J., A. Schmidt, M. Kunz, C. Weber, A. Daunois, B. Schehr, A. Rupp, W. Dotter, F. Werner, and C. Klingshirn, 1989, Proc. SPIE **1127**, 39.
Grossmann, F., T. Dittrich, P. Jung, and P. Hänggi, 1991, Phys. Rev. Lett. **67**, 516.
Haken, H. 1970, *Laser Theory* (Springer, Berlin).
Hänggi, P., 1978, Helv. Phys. Acta **51**, 202.
Hänggi, P., 1993, in *Activated Barrier Crossing*, edited by G. R. Fleming and P. Hänggi (World Scientific, London), pp. 268–292.
Hänggi, P., and R. Bartussek, 1996, in *Nonlinear Physics of Complex Systems: Current Status and Future Trends*, edited by J. Parisi, S. C. Müller, and W. Zimmermann, Lecture Notes in Physics 476 (Springer, Berlin, New York), p. 294.
Hänggi, P., H. Grabert, G. L. Ingold, and U. Weiss, 1985, Phys. Rev. Lett. **55**, 761.
Hänggi, P., and P. Jung, 1995, Adv. Chem. Phys. **89**, 239.
Hänggi, P., P. Jung, and F. Marchesoni, 1989, J. Stat. Phys. **54**, 1367.
Hänggi, P., P. Jung, C. Zerbe, and F. Moss, 1993, J. Stat. Phys. **70**, 25.
Hänggi, P., F. Marchesoni, and P. Grigolini, 1984, Z. Phys. B **56**, 333.
Hänggi, P., F. Marchesoni, and P. Sodano, 1988, Phys. Rev. Lett. **60**, 2563.
Hänggi, P., P. Talkner, and M. Borkovec, 1990, Rev. Mod. Phys. **62**, 251.
Hänggi, P., and H. Thomas, 1982, Phys. Rep. **88**, 207.
Heneghan, C., C. C. Chow, J. J. Collins, T. T. Imhoff, S. B. Lowen, and M. C. Teich, 1996, Phys. Rev. E **54**, R2228.
Hibbs, A. D., A. L. Singsaas, E. W. Jacobs, A. R. Bulsara, J. J. Bekkedahl, and F. Moss, 1995, J. Appl. Phys. **77**, 2582.
Hohmann, W., J. Müller, and F. W. Schneider, 1996, J. Chem. Phys. **100**, 5388.
Hu, G., 1993, Phys. Lett. A **174**, 247.
Hu, G., A. Daffertshofer, and H. Haken, 1996, Phys. Rev. Lett. **76**, 4874.
Hu, G., T. Ditzinger, C. Z. Ning, and H. Haken, 1993, Phys. Rev. Lett. **71**, 807.
Hu, G., H. Haken, and C. Z. Ning, 1992, Phys. Lett. A **172**, 21.
Hu, G., H. Haken, and C. Z. Ning, 1993, Phys. Rev. E **47**, 2321.
Hu, G., H. Haken, and F. Xie, 1996, Phys. Rev. Lett. **77**, 1925.
Hu, G., G. Nicolis, and C. Nicolis, 1990, Phys. Rev. A **42**, 2030.
Hu, G., G. R. Qing, D. C. Gong, and X. D. Weng, 1991, Phys. Rev. A **44**, 6424.
I, L., and J.-M. Liu, 1995, Phys. Rev. Lett. **74**, 3161.
Iannelli, J. M., A. Yariv, T. R. Chen, and Y. H. Zhuang, 1994, Appl. Phys. Lett. **65**, 1983.
Imbrie, J., A. C. Mix, and D. G. Martinson, 1993, Nature (London) **363**, 531.
Inchiosa, M., and A. Bulsara, 1995a, Phys. Rev. E **52**, 327.
Inchiosa, M., and A. Bulsara, 1995b, Phys. Rev. E **53**, 327.
Inchiosa, M., and A. Bulsara, 1995c, Phys. Lett. A **200**, 283.
Inchiosa, M., and A. Bulsara, 1996, Phys. Rev. E **51**, 2021.
Ippen, E., J. Lindner, and W. Ditto, 1993, J. Stat. Phys. **70**, 148.
Jost, B., and B. Sahleh, 1996, Opt. Lett. **21**, 287.
Jülicher, F., A. Ajdari, and J. Prost, 1997, Rev. Mod. Phys. **69**, 1269.
Jung, P., 1989, Z. Phys. B **76**, 521.
Jung, P., 1993, Phys. Rep. **234**, 175.
Jung, P., 1994, Phys. Rev. E **50**, 2513.
Jung, P., 1995, Phys. Lett. A **207**, 93.
Jung, P., 1997, in *Stochastic Dynamics*, edited by L. Schimansky-Geier and T. Pöschel, Lecutre Notes in Physics No. 484 (Springer, Berlin), p. 23.
Jung, P., and R. Bartussek, 1996, in *Fluctuations and Order: The New Synthesis*, edited by M. Millonas (Springer, New York, Berlin), pp. 35–52.

Jung, P., U. Behn, E. Pantazelou, and F. Moss, 1992, Phys. Rev. A **46**, R1709.
Jung, P., G. Gray, R. Roy, and P. Mandel, 1990, Phys. Rev. Lett. **65**, 1873.
Jung, P., and P. Hänggi, 1989, Europhys. Lett. **8**, 505.
Jung, P., and P. Hänggi, 1990, Phys. Rev. A **41**, 2977.
Jung, P., and P. Hänggi, 1991a, Phys. Rev. A **44**, 8032.
Jung, P., and P. Hänggi, 1991b, Ber. Bunsenges. Phys. Chem. **95**, 311.
Jung, P., and P. Hänggi, 1993, Z. Phys. B **90**, 255.
Jung, P., J. G. Kissner, and P. Hänggi, 1996, Phys. Rev. Lett. **76**, 3436.
Jung, P., and G. Mayer-Kress, 1995, Phys. Rev. Lett. **74**, 2130.
Jung, P., and P. Talkner, 1995, Phys. Rev. E **51**, 2640.
Jung, P., and K. Wiesenfeld, 1997, Nature (London) **385**, 291.
Kapitaniak, T., 1994, Phys. Rev. E **49**, 5855.
Kim, S., and L. E. Reichl, 1996, Phys. Rev. E **53**, 3088.
Kiss, L. B., Z. Gingl, Z. Marton, J. Kertesz, F. Moss, G. Schmera, and A. Bulsara, 1993, J. Stat. Phys. **70**, 451.
Kittel, A., R. Richter, M. Hirsch, G. Flätgen, J. Peinke, and J. Parisi, 1993, Z. Naturforsch. Teil A **48**, 633.
Kramers, H., 1940, Physica (Utrecht) **7**, 284.
Krogh, A., and R. Palmer, 1991, *Introduction to the Theory of Neural Computation* (Addsion Wesley, New York), 1991.
Kubo, R., 1957, J. Phys. Soc. Jpn. **12**, 570.
Kubo, R., 1966, Rep. Prog. Phys. **29**, 255.
Kubo, R., M. Toda, and N. Hashitsume, 1985, *Statistical Physics II*, Springer Series in Solid State Sciences Vol. 31 (Springer, Berlin, New York).
Lambsdorff, M., C. Dornfeld, and C. Klingshirn, 1986, Z. Phys. B **64**, 409.
Leggett, A. J., S. Chakravarty, A. T. Dorsey, M. P. A. Fisher, A. Garg, and W. Zwerger, 1987, Rev. Mod. Phys. **59**, 1; **67**, 725(E).
Leibler, S., 1994, Nature (London) **370**, 412.
Levin, J. E., and J. P. Miller, 1996, Nature (London) **380**, 165.
Lindner, J. F., B. K. Meadows, W. L. Ditto, M. E. Inchiosa, and A. Bulsara, 1995, Phys. Rev. Lett. **75**, 3.
Löcher, M., G. A. Johnson, and E. R. Hunt, 1996, Phys. Rev. Lett. **77**, 4698.
Löfstedt, R., and S. N. Coppersmith, 1994a, Phys. Rev. Lett. **72**, 1947.
Löfstedt, R., and S. N. Coppersmith, 1994b, Phys. Rev. E **49**, 4821.
Longtin, A., 1993, J. Stat. Phys. **70**, 309.
Longtin, A., A. Bulsara, and F. Moss, 1991, Phys. Rev. Lett. **67**, 656.
Longtin, A., A. R. Bulsara, D. Pierson, and F. Moss, 1994, Biol. Cybern. **70**, 569.
Louis, A. A., and J. P. Sethna, 1995, Phys. Rev. Lett. **74**, 1363.
Magnasco, M. O., 1993, Phys. Rev. Lett. **71**, 1477.
Magnus, W., and S. Winkler, 1979, *Hill's Equation* (Dover, New York).
Mahato, M. C., and S. R. Shenoy, 1994, Phys. Rev. E **50**, 2503.
Makarov, D. E., and N. Makri, 1995, Phys. Rev. E **52**, 5863.
Makri, N., 1997, J. Chem. Phys. **106**, 2286.
Mandel, L., R. Roy, and S. Singh, 1981, in *Optical Bistability*, edited by C. M. Bowden, M. Ciftan, and H. R. Robl (Plenum, New York), p. 127.
Mannella, R., A. Fioretti, L. Fronzoni, B. Zambon, E. Arimondo, and S. Chillemi, 1995, Phys. Lett. A **197**, 25.
Mansour, M., and G. Nicolis, 1975, J. Stat. Phys. **13**, 197.
Mantegna, R. N., and B. Spagnolo, 1994, Phys. Rev. E **49**, R1792.
Mantegna, R. N., and B. Spagnolo, 1995, Nuovo Cimento D **17**, 873.
Mantegna, R. N., and B. Spagnolo, 1996, Phys. Rev. Lett. **76**, 563.
Marchesoni, F., 1997, Phys. Lett. A **231**, 61.
Marchesoni, F., L. Gammaitoni, and A. Bulsara, 1996, Phys. Rev. Lett. **76**, 2609.
Marchesoni, F., and P. Grigolini, 1983, Physica A **121**, 269.
Masoliver, J., A. Robinson, and G. H. Weiss, 1995, Phys. Rev. E **51**, 4021.
Matteucci, G., 1989, Climate Dynamics **3**, 179.
Matteucci, G., 1991, Climate Dynamics **6**, 67.
McClintock, P. V. E, and F. Moss, 1989, in *Noise in Nolinear Dynamical Systems*, Vol. 3, edited by F. Moss and P. V. E. McClintock, (Cambridge University, Cambridge), p. 243.
McNamara, B., and K. Wiesenfeld, 1989, Phys. Rev. A **39**, 4854.
McNamara, B., K. Wiesenfeld, and R. Roy, 1988, Phys. Rev. Lett. **60**, 2626.
Melnikov, V. I., 1993, Phys. Rev. E **48**, 2481.
Millman, J., 1983, *Microelectronics*, McGraw-Hill Series in Electrical Engineering, Electrons and Electronic Circuits (McGraw-Hill, New York).
Morillo, M., J. Gómez-Ordòñez, and J. M. Casado, 1995, Phys. Rev. E **52**, 316.
Moss, F., 1991, Ber. Bunsenges. Phys. Chem. **95**, 303.
Moss, F., 1994, in *Contemporary Problems in Statistical Physics*, edited by G. H. Weiss (SIAM, Philadelphia), pp. 205–253.
Moss, F., A. Bulsara, and M. F. Shlesinger, 1993, Eds., The Proceedings of the NATO Advanced Research Workshop: Stochastic Resonance in Physics and Biology, J. Stat. Phys. **70** (Plenum, New York), pp. 1–512.
Moss, F., J. K. Douglass, L. Wilkins, D. Pierson, and E. Pantazelou, 1993, Ann. (N.Y.) Acad. Sci. **706**, 26.
Moss, F., D. Pierson, and D. O'Gorman, 1994, Int. J. Bifurcation Chaos Appl. Sci. Eng. **4**, 1383.
Moss, F., and K. Wiesenfeld, 1995a, Sci. Am. **273**, 50.
Moss, F., and K. Wiesenfeld, 1995b, Spektrum der Wissenschaft, **273** (Oktober), 92.
Murray, J. D., 1989, *Mathematical Biology* (Springer, Berlin).
Néda, Z., 1995a, Phys. Lett. A **210**, 125.
Néda, Z., 1995b, Phys. Rev. E **51**, 5315.
Neiman, A., and L. Schimansky-Geier, 1994, Phys. Rev. Lett. **72**, 2988.
Neiman, A., and L. Schimansky-Geier, 1995, Phys. Lett. A **197**, 379.
Neiman, A., L. Schimansky-Geier, and F. Moss, 1997, Phys. Rev. E **56**, R9.
Neimann, A., B. Shulgin, V. Anishchenko, W. Ebeling, L. Schimansky-Geier, and J. A. Freund, 1996, Phys. Rev. Lett. **76**, 4299.
Neiman, A., and W. Sung, 1996, Phys. Lett. A **223**, 341.
Nicolis, C., 1981, Sol. Phys. **74**, 473.
Nicolis, C., 1982, Tellus **34**, 1.
Nicolis, C., 1993, J. Stat. Phys. **70**, 3.
Nicolis, C., and G. Nicolis, 1981, Tellus **33**, 225.
Nicolis, C., G. Nicolis, and G. Hu, 1990, Phys. Lett. A **151**, 139.
Nicolis, G., C. Nicolis, and D. McKernan, 1993, J. Stat. Phys. **70**, 125.
Oelschlägel, B., T. Dittrich, and P. Hänggi, 1993, Acta Phys. Pol. B **24**, 845.

Oppenheim, A. V., and R. W. Schaffer, 1975, *Digital Signal Processing* (Prentice Hall, New York).
Papoulis, A., 1965, *Probability, Random Variables, and Stochastic Processes* (McGraw-Hill, New York).
Pei, X., J. Wilkens, and F. Moss, 1996, J. Neurophysiol. **76**, 3002.
Pérez-Madrid, A., and J. M. Rubí, 1995, Phys. Rev. E **51**, 4159.
Phillips, J. C., and K. Schulten, 1995, Phys. Rev. E **52**, 2473.
Presilla, C., F. Marchesoni, and L. Gammaitoni, 1989, Phys. Rev. A **40**, 2105.
Raikher, Y. L., and V. I. Stepanov, 1994, J. Phys.: Condens. Matter **6**, 4137.
Rajaraman, R., 1982, *Solitons and Instantons* (North-Holland, Amsterdam).
Rappel, W. J., and S. H. Strogatz, 1994, Phys. Rev. E **50**, 3249.
Reibold, E., W. Just, J. Becker, and H. Benner, 1997, Phys. Rev. Lett. **78**, 3101.
Reimann, P., R. Bartussek, W. Häussler, and P. Hänggi, 1996, Phys. Lett. A **215**, 26.
Riani, M., and E. Simonotto, 1994, Phys. Rev. Lett. **72**, 3120.
Riani, M., and E. Simonotto, 1995, Nuovo Cimento D **17**, 903.
Rice, S. O., 1944, Bell Syst. Tech. J. **23**, 1; reprinted in N. Vax, 1954, *Noise and Stochastic Processes* (Dover, New York).
Rice, S. O., 1948, Bell Syst. Tech. J. **27**, 109.
Risken, H., 1984, *The Fokker-Planck Equation*, Springer Series in Synergetics Vol. 18 (Springer, Berlin, New York).
Risken, H., and H. D. Vollmer, 1989, in *Noise in Nonlinear Dynamical Systems; Theory, Experiments, Simulation*, Vol. I, edited by F. Moss and P. V. E. McClintock (Cambridge University, Cambridge), p. 191.
Rose, J. E., J. F. Brugge, D. J. Anderson, and J. E. Hind, 1967, J. Neurophysiol. **30**, 769.
Rouse, R., S. Han, and J. E. Lukens, 1995, Appl. Phys. Lett. **66**, 108.
Roy, R., P. A. Schulz, and A. Walther, 1987, Opt. Lett. **12**, 672.
Sargent III, M., M. O. Scully, and W. E. Lamb Jr., 1974, *Laser Physics* (Addison-Wesley, Reading, MA).
Schenzle, A., and H. R. Brand, 1979, Phys. Rev. A **20**, 1628.
Schimansky-Geier, L., J. A. Freund, A. B. Neiman, and B. Shulgin, 1998, "Noise Induced Order: Stochastic Resonance," Int. J. Bifurcation Chaos Appl. Sci. Eng. (in press).
Schimansky-Geier, L., and U. Siewert, 1997, in *Stochastic Dynamics*, edited by L. Schimansky-Geier, and T. Pöschel, Lecture Notes in Physics No. 484 (Springer, Berlin), p. 245.
Schimansky-Geier, L., and Ch. Zülicke, 1990, Z. Phys. B **79**, 451.
Schwartz, D. B., B. Sen, C. N. Archie, and J. E. Lukens, 1985, Phys. Rev. Lett. **55**, 1547.
Shiino, M., 1987, Phys. Rev. A **36**, 2393.
Shneidman, V. A., P. Jung, and P. Hänggi, 1994a, Phys. Rev. Lett. **72**, 2682.
Shneidman, V. A., P. Jung, and P. Hänggi, 1994b, Europhys. Lett. **26**, 571.
Shulgin, B., A. Neiman, and V. Anishchenko, 1995, Phys. Rev. Lett. **75**, 4157.
Simon, A., and A. Libchaber, 1992, Phys. Rev. Lett. **68**, 3375.
Simonotto, E., M. Riani, C. Seife, M. Roberts, J. Twitty, and F. Moss, 1997, Phys. Rev. Lett. **78**, 1186.
Smoluchowski, M. v., 1912, Phys. Z. **8**, 1069; see p. 1078.
Smoluchowski, M. v., 1914, in *Vorträge über die kinetische Theorie der Materie und der Elektrizität*, edited by M. Planck *et al.* (Teubner, Leipzig), pp. 89–121.
Spano, M. L., M. Wun-Fogle, and W. L. Ditto, 1992, Phys. Rev. A **46**, R5253.
Stocks, N. G., 1995, Nuovo Cimento D **17**, 925.
Stratonovich, R. L., 1963, *Topics in the Theory of Random Noise*, Vol. I (Gordon and Breach, New York), p. 143ff.
Teich, M. C., S. M. Khanna, and P. C. Guiney, 1993, J. Stat. Phys. **70**, 257.
Thorwart, M., and P. Jung, 1997, Phys. Rev. Lett. **78**, 2503.
Valls, O. T., and G. F. Mazenko, 1986, Phys. Rev. B **34**, 7941.
Van den Broeck, C., J. M. R. Parrando, J. Armero, and A. Hernandez-Machado, 1994, Phys. Rev. E **49**, 2639.
van Kampen, N. G., 1992, *Stochastic Processes in Physics and Chemistry*, 2nd ed. (North Holland, Amsterdam, New York).
Vemuri, G., and R. Roy, 1989, Phys. Rev. A **39**, 4668.
Vilar, J. M. G., and J. M. Rubi, 1997, Phys. Rev. Lett. **78**, 2886.
Weiss, U., 1993, *Quantum Dissipative Systems*, Series in Modern Condensed Matter Physics (World Scientific, Singapore), Vol. 2.
Wiesenfeld, K., and F. Moss, 1995, Nature (London) **373**, 33.
Wiesenfeld, K., D. Pierson, E. Pantazelou, C. Dames, and F. Moss, 1994, Phys. Rev. Lett. **72**, 2125.
Winograd, I. J., T. B. Coplen, J. M. Landwehr, A. C. Riggs, K. R. Ludwig, B. J. Szabo, P. T. Kolesar, and K. M. Revesz, 1992, Science **258**, 255.
Wio, H. S., 1996, Phys. Rev. E **54**, R3075.
Yang, W., M. Ding, and G. Hu, 1995, Phys. Rev. Lett. **74**, 3955.
Zambon, B., F. De Tomasi, D. Hennequin, and E. Arimondo, 1989, Phys. Rev. A **40**, 3782.
Zhou, T., and F. Moss, 1990, Phys. Rev. A **41**, 4255.
Zhou, T., F. Moss, and P. Jung, 1990, Phys. Rev. A **42**, 3161.